ERSITY OF HAWAII
LIBRARY
SEP 13 '51

The PHILOSOPHICAL MAGAZINE

FIRST PUBLISHED IN 1798

42 SEVENTH SERIES No. 331 August, 1951

A Journal of Theoretical Experimental and Applied Physics

EDITOR
PROFESSOR N. F. MOTT, M.A., D.Sc., F.R.S.

EDITORIAL BOARD
SIR LAWRENCE BRAGG, O.B.E., M.C., M.A., D.Sc., F.R.S.
ALLAN FERGUSON, M.A., D.Sc.
SIR GEORGE THOMSON, M.A., D.Sc., F.R.S.
PROFESSOR A. M. TYNDALL, C.B.E., D.Sc., F.R.S.

PRICE 12s. 0d.
Annual Subscription £6 0s. 0d. payable in advance.

AND PUBLISHED BY TAYLOR & FRANCIS LTD., RED LION COURT, FLEET ST., LONDON, E.C.4.

Annals of Science

A QUARTERLY REVIEW OF THE HISTORY OF SCIENCE SINCE THE RENAISSANCE

EDITORS

D. McKIE, D.Sc., Ph.D.,
University College, London.

HARCOURT BROWN, M.A., Ph.D.,
Brown University, Providence, R.I., U.S.A.

H. W. ROBINSON,
Former Librarian,
Royal Society of London.

ANNUAL SUBSCRIPTION
£2 0s. 0d.
OR
10s. 6d.
PER PART
POST FREE

ALERE FLAMMAM

Contents of Vol. 7, No. 2, June 1951

THE RISE OF THE TINPLATE INDUSTRY.—IV. AN EIGHTEENTH CENTURY TINPLATE MILL. By F. W. GIBBS, M.Sc., Ph.D.

FRIEDRICH ACCUM (1769–1838). A BIOGRAPHICAL STUDY. By R. J. COLE, B.Sc., F.R.I.C., A.M.I.Chem.E.

CHEMISTRY IN ROZIER'S JOURNAL. III. PIERRE BAYEN. By E. W. J. NEAVE, M.C., M.Sc., Ph.D.

ROBERT DOSSIE (1717–1777) AND THE SOCIETY OF ARTS. By F. W. GIBBS, M.Sc., Ph.D.

JEREMIAS BENJAMIN RICHTER AND THE LAW OF RECIPROCAL PROPORTIONS.—I. By J. R. PARTINGTON, M.B.E., D.Sc.

THE SCIENTIFIC WORK OF WILLIAM BROWNRIGG, M.D., F.R.S. (1711–1800).—III. By J. RUSSELL-WOOD, M.Sc., Ph.D.

GUERICKE AND DUFAY. By I. BERNHARD COHEN, Ph.D.

REVIEW

TAYLOR & FRANCIS, LTD., Red Lion Court, Fleet Street, LONDON, E.C.4

LXXXIII. *Crystal Dislocations.—Elementary Concepts and Definitions.*

By F. C. FRANK,
H. H. Wills Physical Laboratory, University of Bristol*.

[Received April 23, 1951.]

SUMMARY.

The elementary concepts of crystal dislocation theory—in particular the Burgers vector, perfect and imperfect dislocations, sessile dislocations, extended dislocations, twin and twinning dislocations—are defined in a manner independent of particular crystal lattices or models or special orientations of the dislocation: and it is shown how their essential properties arise, in so far as they are independent of the particular crystal in which they occur.

§1. INTRODUCTION.

DURING the past three or four years, those accustomed to deal with the theory of crystal dislocations have to some extent developed a private language and a number of special concepts, each simple enough in itself but together forming a substantial self-contained body of theory. The definitions of these concepts are to be found scattered in various papers and have been propagated in conferences and summer schools. A formal collection seems desirable. The concepts and definitions have largely originated in discussions at Bristol, in which, among others, F. R. N. Nabarro, G. Wyllie and the writer have been involved. We attribute the basis of our approach to a paper by J. M. Burgers (1939). We have also made use of important contributions by W. Shockley.

§2. THE IDEAL CRYSTAL.

The ideal crystal is built on a mathematical lattice, such that ions of the pth kind are to be found at the points

$$\mathbf{r}_{\mathrm{p}}=l\mathbf{a}+m\mathbf{b}+n\mathbf{c}+\mathbf{r}_{\mathrm{p,\,q}}\,,$$

where l, m, n, are all positive or negative integers, including zero ; p takes the values 1, 2, . . . up to u which is the number of kinds of ion in the ideal chemical formula of the substance ; and q takes the values 1, 2 . . . up to v_{p}, which is the number of ions of the pth kind per unit cell. The unit cell is the parallelipiped whose three contiguous edges are the lattice vectors **a**, **b**, **c**. Any three independent linear combinations of **a**, **b** and **c** make alternative lattice vectors. When **a**, **b** and **c** are so chosen that the v_p are as small as possible, they are said to be primitive lattice vectors, and the lattice ($l\mathbf{a}+m\mathbf{b}+n\mathbf{c}$) is called the Bravais lattice of the crystal. The choice is not unique, and all vectors which are members of a set of three satisfying this condition will be called primitive vectors of the lattice. It is these which determine the perfect dislocations (to be defined below) of which the lattice is capable. Classified according to symmetry, there are fourteen different Bravais lattices. For example, if **a**, **b** and **c** are equal in length and make equal angles with each other, the lattice is in general rhombohedral: if the angles are 60°, 90° or $109\frac{1}{2}°$ the lattice has cubic symmetry, these three being the face-centred cubic (f.c.c.), simple cubic (s.c.) and the body-centred cubic (b.c.c.) lattices. Sodium chloride and aluminium have the same (f.c.c.) Bravais lattice and are equivalent in respect of their perfect dislocations.

---

* Communicated by the Author.

The further classifications by symmetry which depend on the vectors $\mathbf{r}_{p,q,}$ and which give 32 crystal classes and 230 space-groups, do not appear to be useful in classifying the further possibilities for dislocations : the latter are associated more with the twinning possibilities of the lattices, which have never been brought into a formal framework in an entirely successful way.

The conventional unit cell of a crystal is one displaying the symmetry properties, which is not necessarily the primitive cell. Thus, for the three members of the cubic system mentioned above, one uses cubic cells containing respectively 4, 1 and 2 lattice points of the Bravais lattice.

§ 3. ACTUAL CRYSTALS : GOOD AND BAD REGIONS.

The ions in actual crystals have thermal vibrations, and quantum-mechanical uncertainty of position which may be described as " zero-point vibrations ". Both of these may be eliminated by taking a time average. There may also be vacant lattice points, interstitial ions, and wrong ions substituted for the right ones at lattice points : all these atomic defects may be notionally rectified, unless present to an excessive extent (*e. g.*, when there are so many interstitial ions that it becomes impossible to recognize which is the principal lattice and which the interstitial one). Finally, the crystal may be continuously deformed, *e. g.* elastically, and yet retain an unmistakable *local* correspondence to the ideal lattice, provided the strains are not too large. Following an admirably simple use of words suggested by Slater at the request of Shockley (private communication), we call all regions in which the strains, and density of atomic defects, are small enough to allow this unmistakable correspondence, regions of good crystal : otherwise, regions of bad crystal. We shall sharpen the definition of good and bad crystal regions presently.

§ 4. Associated Paths.

Consider a good region of real crystal, with its vibrations and atomic defects notionally eliminated, and let a tetrahedron of four neighbouring ions ABCD in this region be associated, one for one, with four corresponding ions A′B′C′D′ of an ideal " reference lattice ", forming an almost congruent tetrahedron. A fifth neighbouring ion, E, in the real crystal can then be associated unambiguously with one, E′, in the reference lattice, the angles AEB and A′E′B′, BEC and B′E′C′, etc., taken in corresponding pairs, being almost equal or, at the worst, more nearly equal (say, in the sense of least squares) than if any alternative ion of the reference lattice is taken for the associated ion E′. Continuing this process, using angles made with BCD and E to fix a sixth ion F, and so on, we may extend a path from ion to ion through any region of good crystal, with an unambiguously associated path in the reference lattice. Moreover, a path may be displaced to a neighbouring path between the same end points, with an unambiguous corresponding displacement of the associated path. The whole region within which such displacements can be made will now be called " good ".

Fig. 1.

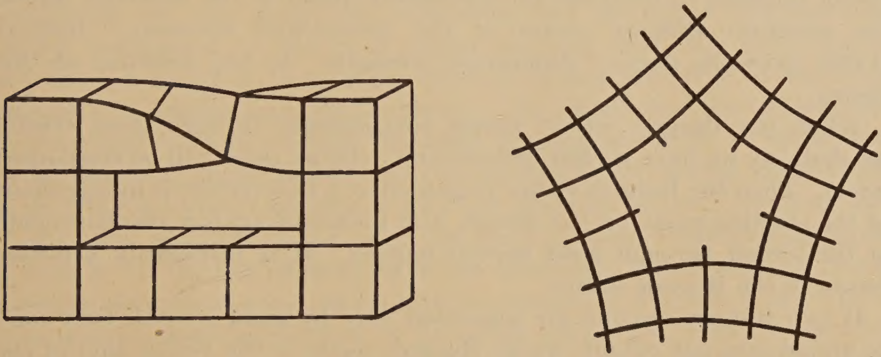

" Moebius Crystals "

§ 5. The Burgers Circuit.

A path which closes on itself in the real crystal will be called a Burgers circuit. A Burgers circuit which lies in a simply connected region of good crystal may be formed by expansion from the initial tetrahedron : hence its associated path is also a closed circuit. The associated path of a Burgers circuit which links a topological torus (or infinite rod) of bad crystal does not necessarily close on itself. In this case the continuity of good crystal round the Burgers circuit ensures only that the associated path closes within a lattice vector.

§ 6. EXCLUDED CASES.

We shall extend the definition of bad crystal so as to avoid certain topological oddities, exemplified by fig. (1), which may be termed " Moebius crystals " by analogy with " Moebius strips ". Such geometrical situations may possibly occur in pathological crystals like chrysotile. If unlimited strains are impossible, they necessarily have relatively large cores of emptiness, or of bad crystal in the sense already defined, and are of limited extension in at least one direction. A region extending from the core to a boundary is declared " bad " so that the core cannot be encircled by a Burgers circuit. We do this wherever, otherwise, we should fail to have a single-valued correspondence between *directions* in the real crystal and the reference lattice.

§ 7. CRYSTAL DISLOCATIONS.

If the closed Burgers circuit in the real crystal has an associated path which fails to close on itself, the circuit is said to encircle one or more lines of crystal dislocation (or, briefly, dislocations). We shall call the vector required to complete the associated circuit in the reference lattice the resultant Burgers vector of the dislocations enclosed. Burgers (1939) gave the name " dislocation strength " to the modulus of this vector.

When the Burgers circuit passes continuously through good crystal we shall say we have perfect dislocations. (Other cases will be considered later). Then the Burgers vector (regarded as a free vector) is independent of the starting point on the circuit, and invariant against displacements of the circuit through good crystal regions. It is necessarily a lattice vector of the Bravais lattice.

If two Burgers circuits are separated only by good crystal, they may be united into one circuit, whose Burgers vector is the vector sum of the Burgers vectors of its component circuits. Conversely, one circuit may be dissected into two, the sum of whose Burgers vectors is that of the one, by making a path through good crystal connecting two points on its circumference. When the circuit cannot be further dissected in this way, it may be shrunk on to its central core of bad crystal, which contains a single dislocation.

Since the Burgers circuit can be continuously displaced along the dislocation line, without change in its Burgers vector, a dislocation cannot terminate within the crystal.

§ 8. DISLOCATION NODES.

A dislocation line may branch. The Burgers circuit enclosing the one line may be displaced so that it encloses the two (or more) dislocation lines into which it divides : hence the sum of their Burgers vectors must equal that of the first line. A more symmetrical statement of the situation is that if the Burgers vectors of all dislocation lines meeting at a node are defined by right-handed circuits, when looking outwards from the node, the sum of these Burgers vectors is zero. This corresponds to a vectorial version of Kirchhoff's law.

§9. THE KINEMATIC PROPERTIES OF PERFECT DISLOCATIONS.

Dislocations can move in many types of crystal. Indeed, the principal role of the dislocation concept in the theory of plastic deformation is to describe briefly the main essentials of the collective atomic motions involved in crystal slip. The possible motions of dislocations include those which do and those which do not involve the production or disappearance of lattice vacancies or interstitial atoms. Consider a Burgers circuit described anywhere in the crystal and let a dislocation line move from outside the circuit to inside it, passing between two adjacent ions P and Q on the circuit. The closure residue of the associated path is thereby changed by the Burgers vector, $\mathbf{b}$, of the dislocation. Hence the ion P is moved relative to Q by a distance, and in a direction, which locally corresponds to $\mathbf{b}$ in the reference lattice. If the real crystal is, locally, nearly perfect apart from the dislocation considered, we may make the orientation and spacing of the reference lattice correspond to the local region and say that the displacement of P relative to Q is $\mathbf{b}$, to an approximation of the same order as is usually involved in small-strain elastic theory. In order that our statements may remain valid in severely distorted crystals, however, let us denote by $\mathbf{b}'$ the local vector in the real crystal which corresponds to $\mathbf{b}$ which is an invariant vector associated with the reference lattice. We may call $\mathbf{b}'$ the local Burgers vector when we need a name which distinguishes it from $\mathbf{b}$. If the line element $d\sigma$ of the dislocation moves so as to sweep a planar element of area, the unit vector normal to which is $\mathbf{n}$, and there is an elastic stress represented by the stress tensor $\mathbf{P}$ so that the traction on the element of area is $\mathbf{nP}$, the work done by the elastic field in this motion of the dislocation, per unit area swept, is $(\mathbf{nP}).\mathbf{b}'$. By virtue of the symmetry of the stress tensor this may also be written $(\mathbf{b}'\mathbf{P}).\mathbf{n}$. Either of these expressions therefore gives the magnitude of the force, due to an elastic field, per unit length of dislocation line, tending to move the dislocation in the specified plane. This corresponds simply to the existence of a force $(\mathbf{b}'\mathbf{P})\times d\sigma$ on each element of the dislocation line. Fuller derivations of these formulae have been given by Peach and Koehler (1950) and Nabarro (1951) (though $\mathbf{n}$ has a less general significance in Nabarro's derivation).

There is a change of volume $(\mathbf{b}'.\mathbf{n})$ per unit area when the dislocation moves in the plane specified by $\mathbf{n}$. When this is positive, it must occur by production of lattice vacancies, or transfer of ions from interstitial sites to lattice sites : when it is negative it must occur by removal of lattice vacancies, or transfer of ions to interstitial sites.

Such motions are accompanied by a change in free energy if the local concentration of atomic defects differs from its equilibrium value. In the case, probably appropriate to metals in a suitable temperature range, that the only diffusing atomic defects we need consider are vacancies, of one kind of ion only, each occupying a lattice volume v', and their concentration exceeds the equilibrium value by a factor α, this change in free energy per unit area swept in the plane whose normal is **n** is equal to $(\mathbf{b}'.\mathbf{n}/v')k\mathrm{T}\ln\alpha$. This may be expressed by saying that there is an osmotic force $(\mathbf{b}'\times d\boldsymbol{\sigma}/v')k\mathrm{T}\ln\alpha$ on the dislocation.

The change of volume is zero if, and only if $(\mathbf{b}'.\mathbf{n})$ is zero : *i. e.* if the dislocation line moves in a surface containing itself and its Burgers vector. This is called the glide surface of the dislocation. The only motions (if any) of a dislocation which can occur rapidly under small stresses are glide motions.

In the special case that the dislocation line is parallel to its Burgers vector, all motions are glide motions. A dislocation in this orientation is called a screw dislocation.

Fig. 2.

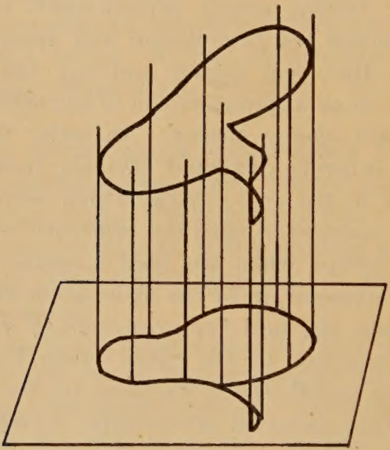

The glide surface of a dislocation.

Disregarding local changes of **b**′ we may say that a dislocation is free to glide on the cylinder generated by lines parallel to its Burgers vector, passing through all points along an instantaneous position of the dislocation line, and also, whenever it becomes coincident with one of these generators, on any surface formed by moving the generator parallel to itself : so that its projection, along the direction of the Burgers vector, on to a fixed plane, is invariant in area and in shape, but may acquire any line extensions enclosing no area (fig. 2).

Motion of a dislocation (other than a screw dislocation) normal to its glide surface, by removal or generation of vacancies (alternatively, by generation or removal of interstitialcies) will be called positive or negative climb.

A node of three or more dislocation lines cannot move by glide alone unless their glide surfaces have at least a line in common. In general, they have only a common point. For example, at a triple node the Burgers vectors necessarily have a common plane : unless all three dislocation lines also lie in this plane the node cannot move without climb.

The motion of a dislocation node, changing the lengths of the dislocation lines which meet at it, can effect the progressive union of two or more dislocations into one, or the dissociation of one into a larger number.

§ 10. EDGE AND SCREW DISLOCATIONS.

The screw dislocation is one parallel to its Burgers vector, and is so called because lattice planes normal to this vector are transformed by the presence of the dislocation into one or more helicoidal surfaces. A dislocation lying normal to its Burgers vector is called an edge dislocation, since it may be thought of as lying at the edge of an extra plane inserted into the lattice. It provides a second case whose elastic field is relatively easy to calculate (Burgers 1939), and the elastic field of any straight dislocation may be found by superposing the fields of screw and edge dislocation, in proportion to the cosine and sine of the angle between the Burgers vector and the dislocation line.

§ 11. TRANSLATION TWINS.

It occurs commonly that two like or mirror-image crystals differing in orientation by a particular rotation or reflection will fit on to each other on a particular plane, crystallographically the same for each, with an energy very little greater than the continuing single crystal. This is ordinary twinning*. When two crystal lattices which are parallel, and differ only by a translation, will fit together on a particular plane with low energy, we shall call the situation " translation-twinning ". It is not recognized in classical crystallography because it cannot be detected with a goniometer ; nor is it visible by X-ray diffraction unless it repeats at short intervals in the specimen. The best-known examples of translation twinning are " stacking faults " in the sphere-packing lattices, *i. e.* breaches of the stacking rules which lead to face-centred cubic or hexagonal close-packing. But other examples should exist. For example, in the crystal of a long-chain paraffin it is probable that a displacement of one-half crystal parallel to the long axis of the molecules will lead to a number of positions at which the energy shows subsidiary minima, not much higher than the absolute minimum characteristic of the perfect crystal.

---

* The converse of this statement is not necessarily true. It probably is true for growth-twins and solid recrystallization twins : but the composition plane of some deformation twins may not be a surface of particularly low energy.

We may distinguish two types of translation twin : type I., or intrinsic, in which the two different lattice patterns are followed right up to the twinning surface (irrespective of whether this occurs on a plane of atoms or no) ; and type II., or extrinsic, in which a layer is sandwiched in between, not belonging to the continuing patterns of either.

§ 12. Imperfect Dislocations.

Unlike an ordinary twin-boundary, a translation-twin-boundary need not go right through the crystal. When it does not, its edge in the interior of the crystal is a dislocation. Assuming that there is no appreciable singularity of elastic properties at the translation-twin surface, it has the same stress-field as an ordinary dislocation. It will be called an imperfect dislocation (alternatively, a partial dislocation) in contrast with perfect dislocations which are surrounded entirely by good crystal.

Fig. 3.

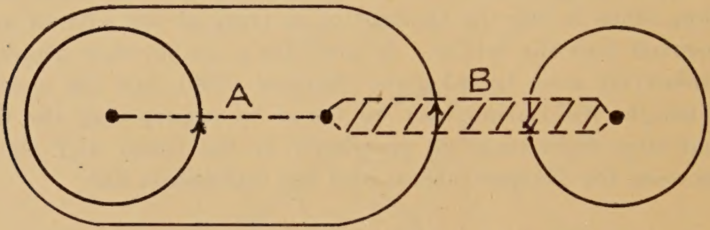

Burgers circuits for imperfect dislocations.

The Burgers vector of the imperfect dislocation bounding a translation twinning surface of type I may be defined in just the same way as that of a perfect dislocation, except that the Burgers circuit must start and finish on the twinning surface instead of at a completely arbitrary point.

The same prescription must be followed when the translation-twinning surface is of type II., with the additional rule that the interpolated layer must be crossed normally, taking an equal distance normal to the corresponding plane when repeating the circuit in the reference lattice.

If the lattice allows translation-twin surfaces of more than one kind ; *e. g.* two kinds, A and B, we may have an imperfect dislocation at the line where an A surface joins a B surface. In this case we make one Burgers circuit round the edge of the A surface, and a second one enclosing both this and the AB junction (fig. 3) : the difference of the residues of the associated paths is the Burgers vector of the AB junction.

The Burgers vector of an imperfect dislocation is not a lattice vector. The Burgers vectors of the various different dislocations which may bound a given translation-twin surface (or provide the junction between two) all differ by lattice vectors.

§ 13. Kinematics of Imperfect Dislocations.

Compared with perfect dislocations, imperfect dislocations are subject to an additional kinematic restraint. As the imperfect dislocation moves it extends or contracts the bounding surface between crystal regions in translation-twin relationship. This boundary has low energy only when it is parallel to a particular crystallographic plane—the conformity plane. In any other orientation the boundary will have high energy, like an ordinary intercrystalline boundary. Estimates for the metals indicate that the stress required to make the dislocation move into a non-conformity plane will always exceed the practical ultimate breakage stress of the work-hardened metal. This motion might therefore occur on the microscopic scale in regions where stress amplifications due to other dislocations raise the stress to values near to the theoretical yield stress of the perfect crystal. For ordinary stresses, however, we may consider such motions forbidden. Motion which extends or contracts the translation twin surface in the conformity plane is resisted or assisted by a force per unit length equal to the surface energy of the translation-twin surface. The estimates which can be made indicate that this is a force of the same order of magnitude as that exerted by the highest ordinarily applicable stress, higher in some metals and lower in others.

Briefly, under ordinary stresses an imperfect dislocation is confined to its conformity plane. If its Burgers vector does not lie in that plane, it cannot glide : if its Burgers vector does lie in that plane, it cannot climb. Frank (1949) proposed that imperfect dislocations for which glide is forbidden should be called " sessile ".

§ 14. Extended Dislocations.

Two imperfect dislocations forming the right and left boundaries of a strip of translation-twin surface may be the opposites of each other. In this case (except in a highly inhomogeneous stress field, or in a concentration of vacancies or interstitial atoms far from its equilibrium value) free energy will be released when they move together, annihilating the translation-twin surface and the dislocation pair. If they are not the opposites of each other they cannot annihilate, and if the scalar product of their Burgers vectors is positive (expressing the condition approximately) they repel each other with a force inversely proportional to their separation. This force is balanced against a constant force arising from the surface energy of the translation-twin surface. Hence they assume an equlibrium separation, forming an extended dislocation, as described for the face-centred cubic or close-packed hexagonal lattices by Heidenreich and Shockley (1947). The combination, being surrounded by good crystal, is necessarily a perfect dislocation. Conversely, a perfect dislocation, when brought into the conformity plane of a possible translation-twin, should spontaneously dissociate into a pair of imperfect dislocations with a ribbon of translation-twin surface between them, so lowering its energy.

If the Burgers vectors of both imperfect dislocations lie in the conformity plane, the combination is free to glide in that plane ; but in no other, even when it or one of its components becomes a screw dislocation

And it cannot climb. Both statements apply for ordinary stresses, not exceeding the practical ultimate strength.

We shall use the term extended dislocation, in general, for any stable set of imperfect dislocations, connected together by translation-twin surfaces. An extended dislocation is free to glide only if these surfaces, and the Burgers vectors of its components, are coplanar.

§ 15. DISLOCATIONS IN INTERCRYSTALLINE BOUNDARIES.

Intercrystalline boundaries in general constitute continuous " bad " regions separating the " good " regions on either side. It is then impossible to make a Burgers circuit, running continuously in good crystal, and encircling a portion of the boundary. When this is the case, we may prescribe that the boundary region should be crossed to the nearest ion in the good region on the other side, while in the associated path we make an equivalent displacement, and a further displacement to the nearest equivalent ion. This introduces an uncertainty of the order of magnitude of one lattice spacing into the resultant Burgers vector, at each crossing. These are generally negligible errors. However, to continue the path in the second good region we must re-establish the cardinal directions by choosing a further three ions, making a tetrahedron with the first, to associate with a tetrahedron of ions in the reference lattice. The number of ways in which this can be done depends on lattice symmetry—for example, in the cubic system it may be done in twenty-four different ways. For each of these choices we shall find a different value for the resultant Burgers vector of dislocations enclosed in the circuit. We can show (Frank 1950) that if $\mathbf{r}$ is the vector connecting the two points at which the circuit crosses the boundary, and the one crystal is brought parallel to the other by a rotation α about an axis $\mathbf{l}$ (a unit vector), this resultant Burgers vector is $\mathbf{r}\times\mathbf{l} \,.\, 2 \sin \frac{1}{2}\alpha$. We have the same multiplicity as before in the choice of $\mathbf{l}$ and α, and can adopt the convention that we choose the $\mathbf{l}$ which makes α least.

When α is small (say, less than 10° to 20°, according to the orientation of the boundary) the structure of the boundary which has lowest energy will probably be one consisting of discrete dislocation lines, a distance of the order of magnitude $|\mathbf{b}|/\alpha$ apart, separated by " good " regions (*cf.* Burgers (1939, 1940), van der Merwe (1950), Shockley and Read (1950)). A portion of the boundary can then be encircled by a Burgers circuit made entirely in good crystal, and its dislocation content can be unambiguously defined.

When α is large (it may take values up to $63\frac{1}{2}°$ for a cubic crystal), the analysis of a grain boundary into line dislocations is of formal value only.

§ 16. TWIN AND TWINNING DISLOCATIONS.

When the real crystal approximates to a perfect twin, the perfect twin may be taken as reference lattice ; the whole twinned real crystal, including the twin-boundary, being considered good. Ordinary perfect and imperfect dislocations may be present, but there are additional possibilities. For, since the twin boundary may be on any one of an infinite succession of parallel equivalent lattice planes called composition planes, the reference lattice is multivalued. The possible Burgers vectors include all the vectors joining a point of the lattice to the points of its twin lattice interpenetrating it. Such dislocations correspond to steps in the twinning boundary, and are therefore confined to the boundary. They may be called twin dislocations.

If the twinning law is one which can be represented by a shearing deformation, with all displacements parallel to the composition plane, the Burgers vector of the dislocation may be parallel to the composition plane (being then equal to the height of the step in the boundary, multiplied by the shear in twinning). If this is so the dislocation may glide under mechanical stress. This motion is the growth of a mechanical twin, and the dislocation involved will be called a twinning dislocation. Fig. (4) illustrates one (*cf*. Frank and van der Merwe, 1949).

Fig. 4.

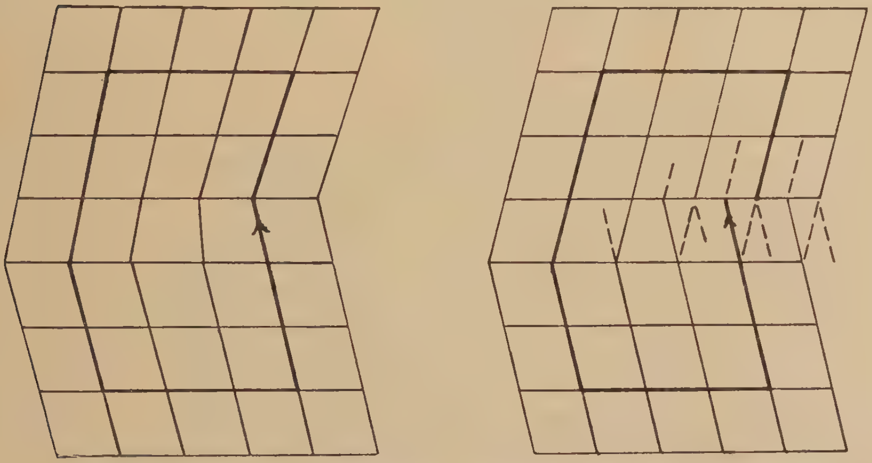

Burgers circuit and its associated path for a twinning dislocation.

References.

Burgers, J. M., 1939, *Proc. Kon. Ned. Akad. v. Wet.*, **42**, 293 ; *Proc. Phys. Soc.*, **52**, 23.

Frank, F. C., 1949, *Proc. Phys. Soc.* A, **62**, 202 ; 1950, *Report of the Pittsburgh Symposium on Plastic Deformation*, May 1950 (Pittsburgh : Carnegie Institute of Technology) (to be published).

Frank, F. C., and van der Merwe, J. H., 1949, *Proc. Roy. Soc.* A, **198**, 205.

Heidenreich, R. D., and Shockley, W., 1947, *Report of the Bristol Conference on the Strength of Solids* (London : The Physical Society), p. 71.

van der Merwe, J. H., 1950, *Proc. Phys. Soc.* A, **63**, 616.

Nabarro, F. R. N., 1951, *Phil. Mag.* [7], **42**, 213.

Peach, M., and Koehler, J. S., 1950, *Phys. Rev.* [2], **80**, 436.

Read, W. T., and Shockley, W., 1950, *Phys. Rev.*, **78**, 275.

LXXXIV. *The Axis of Distortion of a Twisted Elastic Prism*

By D. G. Ashwell,
Engineering Laboratory, Cambridge*.

[Received April 11, 1951.]

SUMMARY.

Duncan, Ellis and Scruton (1933) have shown that if an elastic cantilever is twisted, the displacement of its tip relative to its support consists of a rotation about the flexural centre of its cross-section. In this paper is considered the distortion of a twisted prism without reference to its support, and it is found that the axis of *distortion* of such a prism is in general quite different from the axis of *displacement* found by Duncan, Ellis and Scruton—an effect that has been previously noticed by Cullimore (1949). General expressions are derived for the determination of the axis of distortion, and its effect on practical cantilevers subjected to finite twisting is estimated. Experiments designed to test the analysis are described, and their results are found to confirm it satisfactorily.

§ 1. INTRODUCTION.

THE stresses and strains given by the St. Venant theory for the torsion of a prismatic elastic cantilever, held at one end and twisted at the other, are independent of the axis about which the prism is assumed to twist. Duncan, Ellis and Scruton (1933), discussing this fact, remark that it would appear as though the position of the axis of twist were actually indeterminate—" a conclusion quite at variance with physical intuition " —and go on to show that there can, in fact, be obtained from the St. Venant theory a position of the axis of twist for any specified relationship between the system of coordinate axes chosen and the root cross-section of the cantilever. This is because the root cross-section, like all other cross-sections, suffers warping out of its plane, and in order to specify the relationship between the cantilever and the frame of reference defined by the coordinate axes, three points in this cross-section must be regarded as fixed. The choice of these points determines the direction of the plane at the root of the cantilever relative to which its displacement is measured, and this determines the position of the axis of twist relative to the cantilever. In practical cases the direction of this plane will depend on the local stress distribution at the root—that is, on the system of local stresses which must be added to the St. Venant stresses in order to produce continuity between the cantilever root and its support.

Thus the axis of twist is essentially a means of specifying the *displacement* of the cantilever as opposed to its *distortion* ; for while the displacement may be expected to depend on the frame of reference chosen, the distortion

---

* Communicated by Professor J. F. Baker.

—that is, the displacements of various parts of the cantilever relative to each other—will be quite independent of the external frame of reference—local distortion at the root being, for the moment, ignored. Now physical intuition, while accepting the validity of the axis of twist as an axis of displacement, suggests that there must also be an axis of twist defining the distortion of the prism, and it is with the determination of this axis that the following four sections are concerned. The effect has been previously noticed by Cullimore (1949), who has given a tentative solution based on energy considerations. (See § 4, below.)

The distinction between the axes of twist and distortion is made clear in § 6, where is considered the effect of each of them on practical cantilevers.

Fig. 1.

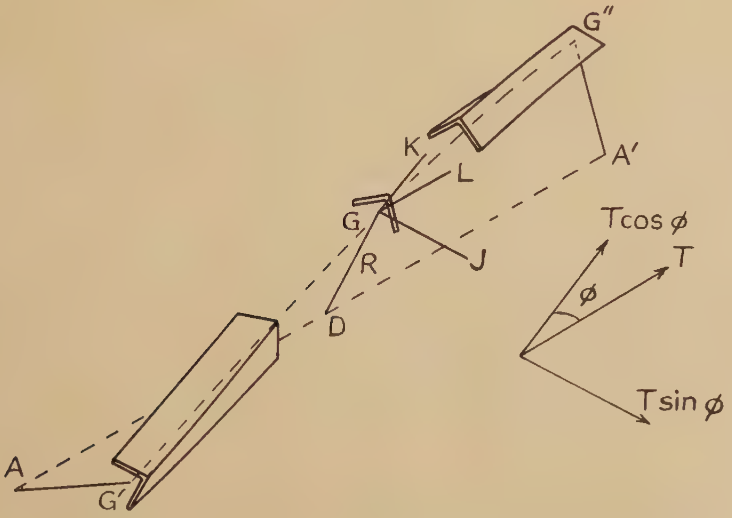

§ 2. DETERMINATION OF THE DISTORTION AXIS.

First will be considered an elastic prism twisted uniformly in such a way that its distortion is the same everywhere along its length, and that there is no constraint against warping of its cross-sections anywhere. In general, longitudinal filaments that were straight before the prism was strained will become distorted into helices, and since the twisting is uniform, these helices may be expected to have a common axis. The filament lying along this axis will be the only one to remain straight, and its position in any cross-section will be called the distortion centre of the cross-section, and the axis itself will be called the distortion axis of the prism.

Fig. 1 shows a prism being twisted. The centroidal axis has become distorted into the helix G′GG″, which has a radius R and makes an angle ϕ with the generators of the cylinder containing it. The torque necessary to maintain the twisting is T, and since its effect at all cross-sections is the same, it must act about an axis parallel to the axis AA′ of the cylinder containing G′GG″—that is, about the distortion axis of the prism. GL is the generator passing through G of the cylinder containing G′GG″, GD is a radius of the cylinder, and GJ is a line perpendicular to GD and to the tangent GK to G′GG″.

The torque T may be resolved into components $T\cos\phi$ twisting the prism about its centroidal axis, and $T\sin\phi$ bending the prism about GJ.

It can be shown from the geometry of the helix that the twist τ per unit length of the prism about its centroidal axis and its curvature $1/\rho$ about GJ are given by

$$\left.\begin{aligned}\tau&=\frac{1}{R}\sin\phi\cos\phi\\ \text{and}\qquad \frac{1}{\rho}&=\frac{1}{R}\sin^2\phi.\end{aligned}\right\}\qquad\ldots\ldots\ldots\quad(1)$$

Consider an elastic prism constrained to twist in such a way that its centroidal axis remains straight, and let its twist per unit length be constant and equal to τ. Let r be the distance of a longitudinal filament from the axis. Then the radius of the helix into which the filament distorts will be r, and its angle $\phi_r=\tan^{-1}(r\tau)$. Further, if e_0 is the strain of the filament lying along the axis, the filament distant r from the axis will suffer an additional strain of $1-\cos\phi_r$, due to its distortion into a helix, giving a total strain of $e_0+1-\cos\phi_r$. Here it must be mentioned that the warping of cross-sections of the prism out of their planes, due to the twisting, will cause axial displacements of points on the filament, but that since τ is constant and warping unrestricted, this displacement will also be constant along the length of any filament, and hence will produce no additional strain.

The strain of the filament considered, then, is $e_0+1-\cos\phi_r$, and if it may be assumed that lateral stresses acting upon it may be neglected (see § 3, below), the stress in it will be $E(e_0+1-\cos\phi_r)$, where E is Young's Modulus for the material of the prism. The component of this stress in the direction of the centrodial axis will be $E(e_0+1-\cos\phi_r)\cos\phi_r$, and since $\phi_r=\tan^{-1}(r\tau)$, this may be expanded in terms of $r\tau$ to give

$$E[e_0+\tfrac{1}{2}(r\tau)^2-\tfrac{1}{2}e_0(r\tau)^2-\tfrac{5}{8}(r\tau)^4\ \ldots\ldots].$$

If, now, e_0 and $(r\tau)^2$ may be limited to the usual small order of elastic strains, the axial stress at a distance r from the centroidal axis may be taken as $E[e_0+\frac{1}{2}(r\tau)^2]$, terms containing higher powers of e_0 and $(r\tau)^2$ being neglected. The implications of this limitation are discussed in the next section.

Since there is no resultant axial force in the prism, the value of e_0 may be found by integrating these stresses over the cross-section and equating their sum to zero. This gives

$$Ee_0=p_0=-\tfrac{1}{2}Ek^2\tau^2,\qquad\ldots\ldots\ldots\quad(2)$$

where p_0 is the stress corresponding to e_0 and k is the polar radius of gyration of the cross-section about its centroid.

Let Gx and Gy be the principal axes of the cross-section (see fig. 2). Then if (x, y) is the position of an element of area δA referred to these axes, and r is the distance of δA from G, the axial stresses will have resultant moments M_x and M_y about Gx and Gy given by

$$M_x = \tfrac{1}{2}E\tau^2 \int r^2 y \, dA$$

and

$$M_y = -\tfrac{1}{2}E\tau^2 \int r^2 x \, dA \,,$$

where the integrals are taken over the whole cross-section.

Fig. 2.

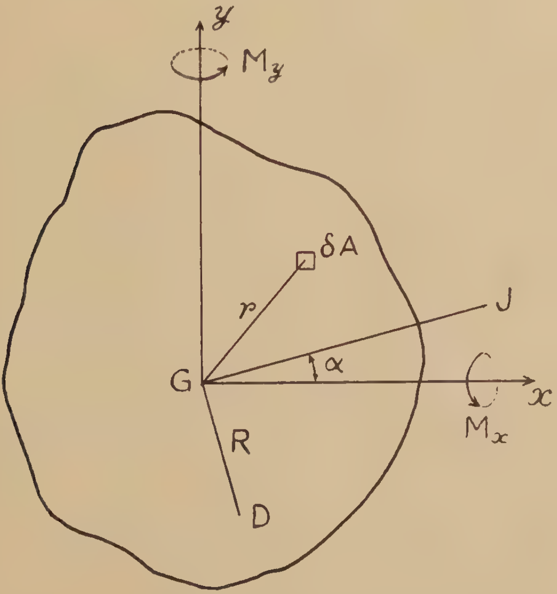

For convenience, let $\int f dA$ be written (f), so that, for example, $\int r^2 y \, dA = (r^2 y)$. Then

$$\left.\begin{aligned} M_x &= \tfrac{1}{2}E\tau^2(r^2 y) \\ \text{and} \quad M_y &= -\tfrac{1}{2}E\tau^2(r^2 x). \end{aligned}\right\} \quad \ldots\ldots\ldots \quad (3)$$

M_x and M_y have the sense shown in fig. 2.

Thus if the prism is to twist about its centroidal axis, in addition to the couple required to produce the twist, moments M_x and M_y must be applied. In the absence of such moments the prism will tend to take up curvatures $-M_x/EI_x$ and $-M_y/EI_y$, where I_x and I_y are the moments of inertia of the cross-section about Gx and Gy. These curvatures will combine to produce a curvature about some other axis through G, and this, together with the twist τ, will cause the centroidal axis of the prism to distort into a helix, Consider again the prism constrained to twist with its centroidal axis straight. The moments about Gx and Gy will be given by (3). Let it now be caused to distort so that its centroidal axis becomes a helix of radius R and angle ϕ. Let D be the position of the distortion centre in fig. 2 and GJ be parallel to the axis about which the resulting curvature $1/\rho$ of the centroidal axis takes place; $\widehat{DGJ}$ will be a right angle. Let $J\widehat{G}x$ be α. Then the curvatures of the centroidal axis about Gx and Gy will be $(1/\rho)\cos\alpha$ and $(1/\rho)\sin\alpha$ and these will require moments about these axes of $(\mathrm{EI}_x\cos\alpha)/\rho$ and $(\mathrm{EI}_y\sin\alpha)/\rho$. Thus the total moments to be provided about Gx and Gy are

$$\frac{\mathrm{EI}_x\cos\alpha}{\rho}+\mathrm{M}_x$$

and

$$\frac{\mathrm{EI}_y\sin\alpha}{\rho}+\mathrm{M}_y.$$

If this distortion is to be that actually suffered by the prism when subjected to a pure torque T applied about the distortion axis, the components of T about Gx and Gy must equal these required moments. Now it was shown above that the component of T tending to bend the prism is T sin ϕ acting about GJ, and so its components about Gx and Gy are T sin ϕ cos α and T sin ϕ sin α. Thus the equations of equilibrium for the bending of the prism about Gx and Gy are

$$\left.\begin{aligned}\mathrm{T}\sin\phi\cos\alpha&=(\mathrm{EI}_x/\rho)\cos\alpha+\mathrm{M}_x\\ \text{and}\qquad \mathrm{T}\sin\phi\sin\alpha&=(\mathrm{EI}_y/\rho)\sin\alpha+\mathrm{M}_y.\end{aligned}\right\}\quad .\ .\ .\ .\ .\ (4)$$

Furthermore, the component of T twisting the prism about its centroidal axis is T cos ϕ, and thus, if CJ is the torsional rigidity of the prism,

$$\mathrm{T}\cos\phi=\tau\mathrm{CJ}.\qquad .\ .\ .\ .\ .\ .\ .\ .\ (5)$$

Finally, τ and ρ are related to R and ϕ by (1) above, and M_x and M_y are given by (3). Eliminating T, τ, ρ, M_x and M_y from (1), (3), (4) and (5), it is found that

$$\left.\begin{aligned}\cos\alpha&=-\frac{\mathrm{E}(r^2y)\cos^2\phi}{2\mathrm{R}(\mathrm{EI}_x-\mathrm{CJ})}\\ \text{and}\qquad \sin\alpha&=\frac{\mathrm{E}(r^2x)\cos^2\phi}{2\mathrm{R}(\mathrm{EI}_y-\mathrm{CJ})},\end{aligned}\right\}\quad .\ .\ .\ .\ .\ .\ (6)$$

Squaring and adding these equations, the following equation relating R and ϕ is obtained:

$$\frac{4\mathrm{R}^2}{\mathrm{E}^2\cos^4\phi}=\frac{(r^2y)^2}{(\mathrm{EI}_x-\mathrm{CJ})^2}+\frac{(r^2x)^2}{(\mathrm{EI}_y-\mathrm{CJ})^2}\quad .\ .\ .\ .\ (7)$$

An alternative form of this equation relates R and the angle of twist of the prism per unit length measured along the distortion axis. If θ is this angle of twist, from the geometry of the helix

$$\cos\phi=(1+\mathrm{R}^2\theta^2)^{-\frac{1}{2}},\quad .\ .\ .\ .\ .\ .\ .\ .\ .\ .\ (8)$$

and thus

$$\frac{4R^2(1+R^2\theta^2)^2}{E^2}=\frac{(r^2y)^2}{(EI_x-CJ)^2}+\frac{(r^2x)^2}{(EI_y-CJ)^2}, \quad . \quad . \quad . \quad . \qquad (9)$$

where

$$\left.\begin{aligned}(r^2y)&=\int r^2y\,dA\\ (r^2x)&=\int r^2x\,dA,\end{aligned}\right\} \quad . \quad . \quad . \quad . \quad . \quad . \quad . \quad . \quad . \qquad (10)$$

and

the integrations being performed over the whole cross-section.

If Gx is an axis of symmetry of the cross-section, (r^2y) will be zero, and the equation relating R and θ becomes

$$2R(1+R^2\theta^2)(EI_y-CJ)=E(r^2x)\,. \quad . \quad . \quad . \quad . \qquad (11)$$

It is worth pointing out that although equations (9) and (11) are cubic in R, they each have only one real root. If θ is given, and $R^2\theta^2$ is not immoderately large, R can be found quickly to any desired degree of accuracy by the usual iterative method for such equations. The position of D can then be found using equations (6) and (8). If Gx is an axis of symmetry, D is the point (R, 0).

§ 3. ASSUMPTIONS INVOLVED.

In deriving these expressions two assumptions have been made.

The first is that the stresses in longitudinal filaments are E times their strains. Now since the sum of the axial stresses must be zero, and since $\frac{1}{2}(r\tau)^2$ is always positive, e_0, the strain of the filament lying along the centroidal axis, will be negative—see equation (2). Thus, in general, the assumption is not valid, for if the cross-section has a compact shape with no internal boundaries, the tension in filaments near the external boundary will cause lateral contractions tending to squeeze the centre of the prism, which experiences longitudinal compression ; and so the ratio between stress and strain will depend on Poisson's ratio as well as on Young's Modulus. However, prisms with such cross-sections may be expected to have distortion centres closely coinciding with their centroids, and their behaviour in this field is not of much interest. In other types of cross-sections, such as open and closed hollow sections, there will be little or no resistance to lateral contraction, and the ratio between stress and strain may safely be taken as Young's Modulus.

The second assumption is that e_0 and $(r\tau)^2$ may be restricted to the order of magnitude of small elastic strains. This also need not always be true, for if the material of the prism is at a fairly constant distance from the centroidal axis, and if $r\tau$ could be at all large, e_0 and $(r\tau)^2$ might have large numerical magnitudes of opposite sign without overstraining the material. But this could happen only in the case of a circular, or nearly circular, thin-walled hollow tube with a longitudinal slit—a special case in which, again, the distortion centre would very nearly coincide with the centroid.

In all cases which are likely to be of interest, therefore, these two assumptions may be taken as valid.

§ 4. TYPICAL POSITIONS OF THE DISTORTION CENTRE—AN APPROXIMATE EXPRESSION.

In the case of most thin-walled open sections CJ may be neglected in comparison with EI and Rθ will be small compared with unity. Equation (11) then becomes

$$R \simeq (r^2x)/2I_y \quad . \quad . \quad . \quad . \quad . \quad . \quad . \quad . \quad . \quad (12)$$

This approximation will be true enough for many practical cases, and typical results obtained from it for thin-walled symmetrical sections are given in the Table. It should be noticed that the Δ given in the Table is not equal to R since it is not measured to the centroids of the sections.

Equation (12) can be obtained very quickly if two modifications are made in the above analysis. Firstly, the bending component T sin ϕ must be ignored; this has the effect of omitting the term CJ from (9) and (11). Secondly, the expression for the longitudinal stresses obtained in § 2 must be referred directly to the distortion axis instead of to the centroidal axis; the effect of this is to invalidate the argument of the second part of § 3, and to cause the omission of the factor $(1+R^2\theta^2)$ from (9) and (11). These effects cannot be ignored in the case of flexible sections twisted considerably, or if it is desired to extend the analysis to include the effects of axial forces. A tentative solution due to Cullimore (1949) uses an energy method which yields results for channel and angle sections identical with those obtained from (12) above. The approximate nature of this solution seems to arise because an exact solution cannot be obtained by treating the problem as a small-deflection problem.

§ 5. GENERAL COMMENTS ON THE DISTORTION AXIS.

Previous writers on this subject have ignored the effect of the longitudinal stresses here considered, and the curvature they produce, on the ground that they are second-order effects (see Duncan, Ellis and Scruton 1933). But they seem to have overlooked the fact that from (1) and (8) it can be shown that the twist τ of the distorted centroidal axis is $\theta(1+R^2\theta^2)^{-1}$ and its curvature $1/\rho$ is $R\theta^2(1+R^2\theta^2)^{-1}$. Thus the distortion of the centroidal axis into a helix does in fact require that its curvature should be of the second order in τ even if R is large, and so in determining the position of the axis of distortion second-order effects cannot be ignored.

It must be emphasized that all the analysis in this paper so far is true only if all the cross-sections of the prism are allowed to warp out of their planes in the manner required by the St. Venant stress distribution. If one section is restrained against warping, the torque will be resisted near that section partly by the twisting of the prism and partly by the differential bending of its various parts. In this case the second-order longitudinal stresses due to twisting will certainly be negligible compared with the first-order stresses due to the differential bending near the constrained cross-section, and the usual methods for estimating the additional stiffness of the prism due to the constraint will be unaffected by the work contained in this paper.

§ 6. FINITE DISPLACEMENTS OF PRACTICAL CANTILEVERS.

It remains to distinguish between the axes of twist and distortion by considering their effects on the behaviour of practical cantilevers.

TABLE.

Section.	Δ (measured to mid-line) defines the position of the distortion centre.
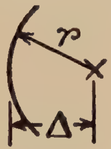	$\Delta = r$
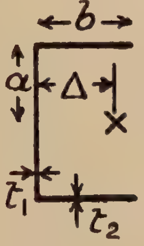	$\Delta = \dfrac{4a^3t_1+3ab^2t_1+b^3t_2}{8abt_1+2b^2t_2}$
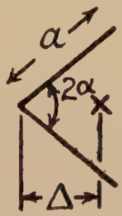	$\Delta = \dfrac{a}{2\cos\alpha}$
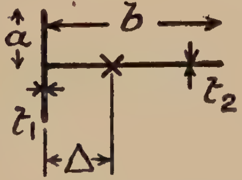	$\Delta = \dfrac{-4a^3t_1+6ab^2t_1+b^3t_2}{16abt_1+2b^2t_2}$

Consider a prismatic cantilever as shown in fig. 3. At the root its cross-section is everywhere attached to a rigid plane support. Its length is l, and

C is the flexural or shear centre at its tip, while D is the distortion centre there. The corresponding points at its root are C′ and D′. Let it be twisted by a torque about an axis perpendicular to the supporting plane. The stress distribution along the greater part of its length will be that predicted by St. Venant, and its cross-sections will tend to warp out of their original planes. This they will be able to do except near the root, where an additional stress-system must be applied to produce continuity between the prism and the plane support. These continuity stresses applied at the root will have no resultant force or moment, and their effect may be expected to die out fairly quickly along the prism, so that at no great distance from the root they will have become negligible. Nevertheless, although they are confined to a short length of the cantilever, they may affect its displacement significantly by producing a rotation of it about some axis in the fixed plane. Their precise nature is not known in general, and so it is not possible to determine exactly their effect except in special cases. Duncan, Ellis and Scruton, however, have shown that if the cantilever is twisted slightly, the tip ABC will rotate about C, the centre of flexure. In other words, the continuity stresses are such that the flexural axis of the cantilever remains perpendicular to the root plane.

Fig. 3.

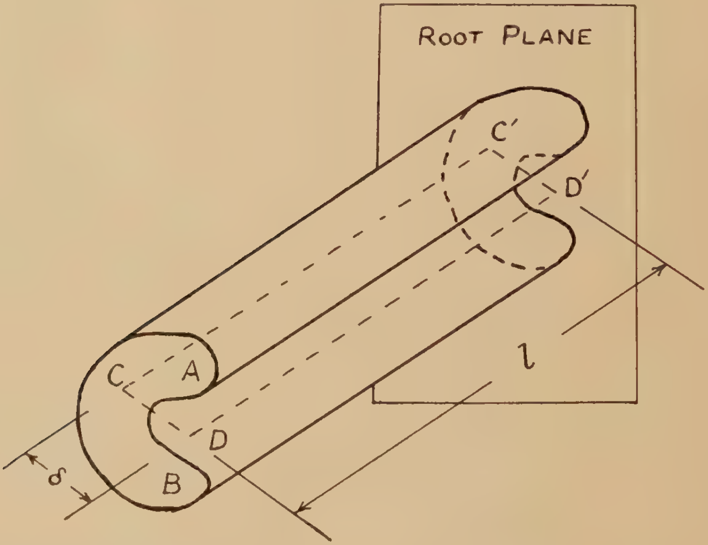

If the rotation of the tip becomes large, CC′ will not remain straight but, according to the analysis given earlier in this paper, will distort into a helix with DD′ as axis. This will be true for the greater length of the cantilever, except near the root, where the continuity stresses will determine the distortion. It will still be true, however, that near the root the filament lying along CC′ will be perpendicular to the root plane. Thus, since the length affected by the continuity stresses is small compared with l, it can be said that the distortion of the cantilever will be that discussed in previous sections, while its displacement will be such that the tangent to the flexural axis at the root will remain perpendicular to the root plane. This statement is not strictly accurate owing to the short length affected by the continuity stresses, but if l is sufficiently large for the rotation of the tip to be appreciable, the error involved may be expected to be small.

It is now possible to estimate the displacement of the tip for large deflections. If the twist of the cantilever per unit length is θ, and the distance C′D′ is δ, it can be shown from the geometry of the helix that the rotation of DD′ relative to the tangent to CC′ at C′ takes place about C′D′ and is of magnitude $\tan^{-1}(\theta\delta)$. In most cases likely to arise in practice this rotation will be small and may be safely approximated to $\theta\delta$. This means that since DD′ remains straight, D suffers a linear displacement at right angles to C′D′ of magnitude $\theta l\delta$. Now the rotation of ABC, ψ, say, will equal $l\theta$, and so the linear displacement of D will be $\psi\delta$.

If DD′ becomes inclined to the root plane, the applied torque, T, assumed above to be about an axis perpendicular to that plane, will have a component tending to bend the cantilever as a beam, but this component, $T\theta\delta$, will be small, and as prisms of types likely to be met with are stiff in bending, the distortion caused by this component will be ignored. It would not be a difficult matter to take account of it in any particular case.

Thus if the quantity $\theta\delta$ is small, and l is large compared with the length near the root affected by the continuity stresses, the displacement of the tip ABC consists of (i) a rotation ψ about D together with (ii) a linear displacement of D equal to $\psi\delta$ perpendicular to C′D′. The usually accepted centre of displacement, C, is now seen to be rather the instantaneous centre of rotation of the tip for the position $\psi=0$.

To determine the finite displacement of the tip of a twisted cantilever it is thus necessary first to determine the positions of the flexural and distortion centres for the value of θ concerned, and then to superimpose the linear and rotational displacements stated above.

§ 7. EXPERIMENTAL RESULTS.

A series of experiments was carried out to test the analysis given in this paper. They consisted of applying a pure torque to cantilevers with different cross-sections and determining the displacements of their tips for different angles of rotation.

Three specimens were used. Specimens I. and II. were made from beryllium–copper strip of thickness 0·0125 in. Specimen I was formed by bending this strip into a symmetrical angle of side 0·576 in. and length 10 in., the two legs of the angle being at right angles to each other. Specimen II. was a symmetrical channel of dimensions 0·633 in. web, 0·242 in. flanges and length 16·5 in. Specimen III. was a commercial steel pocket tape-measure of the type having a transverse curvature for stiffness. It was especially chosen from a number of such tapes for its initial straightness, and its dimensions were: thickness 0·0065 in., width 0·596 in., radius of transverse curvature 0·615 in., and length 17 in. Each specimen was provided with a specially made steel clamp which firmly held it at its root along the whole of its cross-section.

Fig. 4.

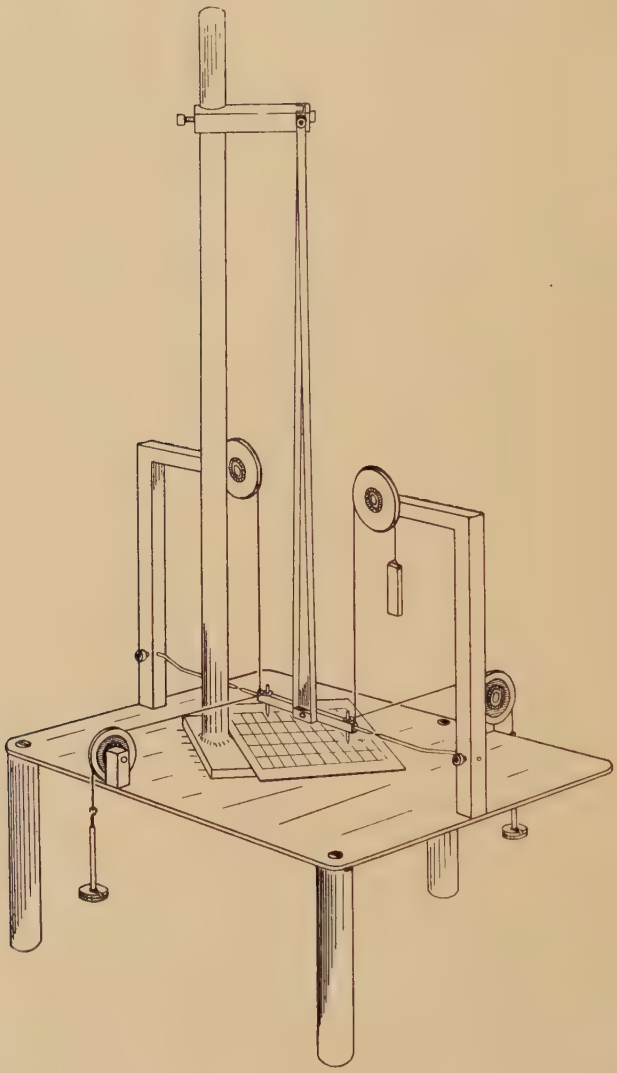

The testing apparatus is shown in fig. 4. The specimen was held vertically by its clamp, which was supported from the movable base-plate by means of the vertical rod. This base-plate could be moved about on the horizontal table, and carried on its upper surface a piece of graph paper. Attached to the bottom, free, end of the cantiliver was a horizontal cross-piece that had a vertical pointer at some distance on each side of its centre and a horizontal one projecting from each end. By sliding the base-plate about on the table the tips of these two horizontal pointers could be made to correspond with the tips of two other horizontal pointers that were fixed relative to the table. The apparatus was so arranged that when this was done the forces applied to the cross-piece—and hence to the specimen—by the pair of horizontal strings, resulted in a pure couple about a vertical axis, while the tensions in the vertical strings exactly balanced the weight of the cross-piece. In this way, by varying the equal weights on the two hangers, the displacements of the two vertical pointers relative to the graph paper, and hence to the support of the cantilever, could be measured for various angles of twist. It was hoped that these displacements could be read directly from the lower

Fig. 5.

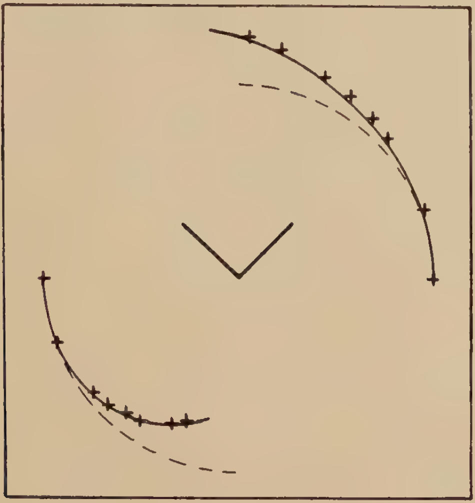

Fig. 6.

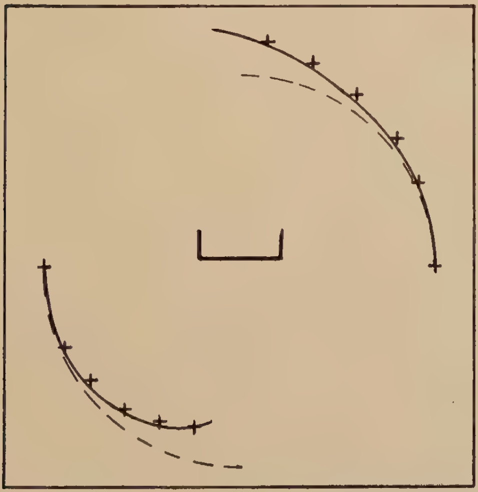

ends of the vertical pointers, but the cross-piece tilted slightly as the specimen distorted, and this introduced an appreciable error due to the length of the pointers. So, instead, a small set square was used, with which, by sighting along the lines on the graph paper the coordinates of the centres of the pointers at the level of the end of the specimen could be determined. This method was found to give consistent and satisfactory results.

In figs. 5, 6, and 7 are shown typical results for each specimen. As the tip of the cantilever rotated in an anti-clockwise direction the two vertical pointers traced out paths on the graph paper. In each case the cross-section is shown in its initial position. The full lines show the paths predicted by the analysis of this paper, while the broken lines show the paths that would be traced out if the tips of the cantilevers experienced only rotations about their centres of twist. The crosses are experimental points.

Fig. 7.

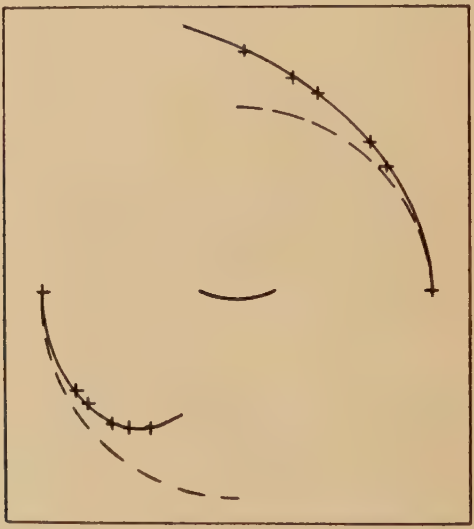

It is seen that in each case the agreement between experiment and the analysis given in this paper is satisfactory, while the distinction between this theory and the assumption that the sections rotate about their centres of displacement is most marked.

ACKNOWLEDGMENTS.

The author wishes to express his gratitude to Professor C. Gurney and Dr. E. N. Fox for many helpful discussions during the course of this work, and also to the members of the workshops staff at the Engineering Laboratory, Cambridge, who made the apparatus and specimens.

REFERENCES.

CULLIMORE, M. S. G., 1949, *Research, Engineering Structures Supplement*, 153.
DUNCAN, W. J., ELLIS, D. L., and SCRUTON, C., 1933, *Phil. Mag.* [7], **16**, 201.

LXXXV. *The Reflection of very Low Frequency Radio Waves at the Surface of a Sharply Bounded Ionosphere with Superimposed Magnetic field.*

By K. G. Budden,
Cavendish Laboratory, Cambridge*.

[Received April 10, 1951.]

Contents.

	Page
Summary	833
§ 1. Introduction	834
1.1. Previous work on the theory of the reflection of very low frequency waves	834
1.2. Scope of the present paper	835
§ 2. The formulæ of the magneto-ionic theory	836
§ 3. The reflection and transmission coefficients for the ionosphere	838
§ 4. Numerical results	839
4.1. The parameters p_r/p and τ	839
4.2. The reflection coefficients ${}_{\parallel}R_{\parallel}$ and ${}_{\parallel}R_{\perp}$	841
4.3. Comparison with experimental results	841
4.4. Comparison with Bremmer's results	845
4.5. The transmitted waves	845
4.6. The thickness of the ionosphere	846
§ 5. Validity of the approximations	847
5.1. The quasi-longitudinal approximation	847
5.2. Variation of parameters with angle of incidence	848
5.3. The longitudinal component of the electric field	849
Acknowledgments	850
References	850

Summary.

The paper discusses the theory of the reflection of very low frequency electromagnetic waves at the boundary of an ionized medium. The medium is assumed to be sharply bounded and homogeneous, and to have a steady magnetic field superimposed. The quasi-longitudinal approximation to the magneto-ionic theory is used (Booker 1935), and the reflection coefficients are then independent of the horizontal direction of the transmission path. The results of the theory are compared with the experimental observations of the propagation of very low

---

* Communicated by J. A. Ratcliffe, F.R.S.

frequency radio waves (Bracewell *et al.* 1951). It is concluded that the theory will account for the general form of some of the experimental results for frequencies of 16 kc./s. and above. It is likely to be most useful for extending the theory of the propagation of very low frequencies (10 kc./s. and lower) such as are used in the study of the propagation of radio-atmospherics (Gardner 1950, Bowe 1951, Budden 1951).

---

§ 1. INTRODUCTION.

1.1. *Previous Work on the Theory of the Reflection of Very Low Frequency Waves.*

A CONSIDERABLE amount of information now exists on the nature of the reflection of very low frequency radio waves from the ionosphere (Budden, Ratcliffe and Wilkes 1936, Bracewell *et al.* 1951). By " very low " we mean frequencies from about 10 kc./s. to 100 kc./s. It is of interest to consider what structure of the ionosphere would account for the observed phenomena. Several attempts at this have been made. A number of authors assumed that the ionosphere was a sharply bounded homogeneous medium containing electrons subject to collision damping, and neglected the effect of the earth's magnetic field. Thus Yokoyama and Namba (1932) showed that for such a medium there is an angle of incidence, the quasi-Brewster angle, for which the reflection coefficient is a minimum. They attempted to explain the minimum which is often observed near sunset in the signal from a distant long wave station, by a change in the quasi-Brewster angle during the passage from day to night conditions. Bremmer (1949) and Rydbeck (1949), using similar assumptions about the ionosphere, were able to account for many of the observed facts relating to the propagation of very low frequency waves to great distances. However, it is known that when a plane polarized wave is incident nearly vertically on the ionosphere, the polarization of the reflected wave is different from that of the incident wave. This cannot be accounted for if the reflecting medium is isotropic, that is—if the earth's magnetic field is neglected.

Another group of authors has treated the ionosphere as a horizontally stratified medium, in which the constants vary with height in a distance small compared with one wavelength. The differential equations for the case where the earth's magnetic field is not neglected were first given by Hartree (1929). Solutions for particular models of the ionosphere have been given by Wilkes (1940 and 1947) and Stanley (1950).

It is the purpose of the present paper to give some numerical solutions for the case where the ionosphere is a sharply bounded homogeneous medium with a superimposed magnetic field, and to discuss their applicability to the experimental results. A problem very similar to this was discussed by Lorentz (1909) and Voigt (1915), who were concerned with the theory of the magneto-optical Kerr effect. This effect concerns the change of polarization which occurs when light is reflected from the metal pole piece of a magnet. Lorentz and Voigt both derived a set of four reflection coefficients similar to equations (22) to (25) of this paper, but they discussed a reflecting medium with properties very different from those of the ionosphere. Bremmer (1949) has given expressions for the various reflection coefficients, but points out that their use in numerical computations is extremely complex. The few numerical results which he gives are discussed in § 4.4. They are based on values of the parameters which are probably different from those which would be expected to apply at the level of reflection of very low frequency waves.

1.2. *Scope of the Present Paper.*

The experimental results on the propagation of very low frequency waves refer mainly to frequencies of 16 kc./s. and higher. We shall show that for these frequencies some—but not all—of the experimental results can be explained by assuming the ionosphere to be homogeneous and sharply bounded. We conclude that at the level of reflection of these waves the variation of the characteristics of the ionosphere, in a vertical distance of one wavelength, is too small for the assumption of a sharp boundary to be valid. It would be necessary to adopt a full wave solution, of the type given by Wilkes (1940, 1947) and Stanley (1950), allowing for the finite rate of variation of the electron density and collision frequency with height. At still lower frequencies, however, such as those used in the study of radio atmospherics (Bureau 1930, 1932, Gardner 1950, Bowe 1951), the wavelength is very long (30 km. or more), and we may expect the theory of the sharply bounded ionosphere to be of some value.

In § 2 of this paper we discuss the application of the Appleton-Hartree magneto-ionic formula to the region of the upper atmosphere, at about 70 to 90 kms. where very low frequency waves are reflected. The quasi-longitudinal approximation (Booker 1935) is used. In § 3 we use the boundary conditions at the surface of the medium to deduce expressions for the various reflection and transmission coefficients. It is convenient to describe the incident and reflected waves in terms of their component electric fields parallel to, and perpendicular to, the plane of propagation, and to consider four coefficients denoted by ${}_{\parallel}R_{\parallel}$, ${}_{\parallel}R_{\perp}$, ${}_{\perp}R_{\parallel}$, ${}_{\perp}R_{\perp}$, to indicate the complex ratio of a specified electric field in the wave after reflection to a specified electric field in the wave before reflection. The first subscript denotes whether the electric field specified in the incident wave is parallel ($\parallel$) or perpendicular ($\perp$) to the plane of incidence and the second subscript refers in the same way to the electric field in the reflected wave. In § 4 the results of some numerical calculations are given and their relation to the experimental results are discussed. In § 5 we discuss the validity of the various approximations used.

§2. THE FORMULÆ OF THE MAGNETO-IONIC THEORY.

The complete Appleton-Hartree magneto-ionic formula may be written (Appleton 1932) :—

$$x/(\mu^2-1)=1-jz-\tfrac{1}{2}y_{\mathrm{T}}^2/(1-x-jz)\pm\tfrac{1}{2}\{y_{\mathrm{T}}^4+4y_{\mathrm{L}}^2(1-x-jz)^2\}^{\frac{1}{2}}/(1-x-jz) \quad . \quad . \quad . \quad (1)$$

where μ=complex refractive index of the medium.

$x=p_0^2/p^2$.

$y=p_{\mathrm{H}}/p$.

$z=\nu/p$.

$p=2\pi\times$frequency of the wave.

$p_0^2=4\pi\mathrm{N}e^2/\epsilon_0 m$.

$p_{\mathrm{H}}=\mu_0\mathbf{H}e/m$=gyro frequency of electrons in the earth's magnetic field.

y_{T}=component of y perpendicular to direction of wave propagation.

y_{L}=component of y in direction of wave propagation.

$p_{\mathrm{T}}=y_{\mathrm{T}}/p$.

$p_{\mathrm{L}}=y_{\mathrm{L}}/p$.

e, m=charge and mass of the electron.

N=number of electrons per c.c.

ν=collision frequency.

H=strength of earth's magnetic field.

ϵ_0, μ_0=electric and magnetic permittivities of free space. (This is the only place in this paper where μ_0 is used for the magnetic permittivity of free space. The same symbol is later used for the refractive index of the ordinary wave, but there should be no confusion.)

In this paper we consider the ionosphere to be a homogeneous medium governed by equation (1), with a sharp lower boundary. For this medium there are two characteristic waves, the ordinary and extraordinary waves, corresponding to the two values of μ given by (1). For each of these waves the value of μ and the state of polarization depend on the direction of propagation. This would make the calculation of reflection coefficients very involved for the most general case.

Equation (1) becomes much simpler if it is permissible to make the "Quasi-longitudinal" approximation (Booker 1935). This approximation is valid if

$$|y_{\mathrm{T}}^4/4y_{\mathrm{L}}^2|\ll|1-x-jz|^2. \quad . \quad . \quad . \quad . \quad . \quad . \quad . \quad . \quad (2)$$

Then (1) reduces to

$$\mu^2=1-x/(1-jz\pm y_{\mathrm{L}}) \quad . \quad . \quad . \quad . \quad . \quad . \quad . \quad . \quad (3)$$

and it can be shown that the ordinary and extraordinary waves are circularly polarized with opposite senses (Booker 1935). Both waves also have a component of the electric vector in the direction of propagation, but it will be shown in § 5.3 that this component is usually small. The quasi-longitudinal approximation is used in obtaining all the numerical results given in this paper. Its applicability is discussed in § 5.1.

The value of μ given by (3) still depends upon the direction of propagation, on account of the term y_L. We shall at first, however, assume that y_L is a constant, and the validity of this assumption will be discussed in § 5.2. Moreover, at the low frequencies considered here, $y_L \gg 1$ and we may write (3)

$$\mu^2 = 1 - jx/(z \pm jy_L) = 1 - j(p_r/p)\exp(\pm j\tau) \quad . \quad . \quad . \quad (4)$$

If y_L is purely real, then

$$p_r/p = x/\sqrt{(z^2+y_L^2)} = p_0^2/p\sqrt{(\nu^2+p_L^2)} \quad . \quad . \quad . \quad . \quad . \quad . \quad (5)$$

$$\tan\tau = y_L/z \qquad = p_L/\nu \quad . \quad . \quad . \quad . \quad . \quad . \quad . \quad . \quad . \quad (6)$$

Later, in § 5.2, we shall consider the possibility that y_L may be complex, and the expressions for p_r and τ are then more complicated.

We now take coordinate axes, x_1, x_2, x_3, where x_3 is measured vertically upwards. We consider a wave with its wave normal in the (x_1, x_3) plane, inclined at an angle, θ, to the x_3 axis and travelling in the direction of both x_1 and x_3 increasing. Let the variation with time, t, be given by a factor e^{jpt}. We denote by $E_{\parallel}$ the component of the electric vector of the wave in the (x_1, x_3) plane, and by $E_{\perp}$ the component in the direction of x_2. For such a wave in the northern hemisphere it can be shown that $E_{\perp}/E_{\parallel} = -j$, or $+j$, for the ordinary and extraordinary waves, respectively.

When a plane wave is incident on the ionosphere from below, the disturbance in the ionosphere consists of two waves, the ordinary and the extraordinary, for which the values of θ are different. We shall therefore write

For the ordinary wave :

$$\text{Complex refractive index} = \mu_0 = 1 - j(p_r/p)e^{j\tau} \quad . \quad . \quad . \quad . \quad . \quad . \quad (7)$$

$$\text{Direction of wave normal} = \theta_0$$

$$\text{Polarization } E_{\perp 0}/E_{\parallel 0} \quad = -j \quad . \quad . \quad . \quad . \quad . \quad . \quad . \quad . \quad . \quad . \quad . \quad (8)$$

For the extraordinary wave :

$$\text{Complex refractive index} = \mu_e = 1 - j(p_r/p)e^{-j\tau} \quad . \quad . \quad . \quad . \quad . \quad . \quad (9)$$

$$\text{Direction of wave normal} = \theta_e$$

$$\text{Polarization } E_{\perp e}/E_{\parallel e} \quad = +j \quad . \quad . \quad . \quad . \quad . \quad . \quad . \quad . \quad . \quad . \quad (10)$$

§ 3. THE REFLECTION AND TRANSMISSION COEFFICIENTS FOR THE IONOSPHERE.

Now consider a plane wave incident from below on the boundary of the ionosphere, with its wave normal at an angle i to the vertical, and with its electric field components given by :

$$\left.\begin{matrix} E_{\parallel i} \\ E_{\perp i} \end{matrix}\right\} \exp\,[jp\{t-(x_1 \sin i + x_3 \cos i)/c\}]. \quad . \quad . \quad . \quad . \quad (11)$$

The reflected wave may similarly be denoted by the expression

$$\left.\begin{matrix} E_{\parallel r} \\ E_{\perp r} \end{matrix}\right\} \exp\,[jp\{t-(x_1 \sin i - x_3 \cos i)/c\}]. \quad . \quad . \quad . \quad . \quad (12)$$

In the ionosphere, the two transmitted waves are described by the expressions

$$E_{\parallel 0} \exp\,[jp\{t-(x_1 \sin \theta_0 + x_3 \cos \theta_0)\mu_0/c\}] \quad . \quad . \quad . \quad (13)$$

and

$$E_{\parallel e} \exp\,[jp\{t-(x_1 \sin \theta_e + x_3 \cos \theta_e)\mu_e/c\}] \quad . \quad . \quad . \quad (14)$$

together with equations (8) and (10).

The variation of all these waves in the x_1 direction at the boundary must be the same, and hence we have Snell's law

$$\sin i = \mu_0 \sin \theta_0 = \mu_e \sin \theta_e \quad . \quad . \quad . \quad . \quad . \quad . \quad . \quad (15)$$

It should be noted that because μ_0 and μ_e are, in general, complex, the angles θ_0 and θ_e are complex. Consequently y_L is complex. We shall investigate the consequences of this in § 5.2, where we show that, for practical purposes, it is sufficient to ignore the imaginary part of y_L.

Let E_1, H_1 and E_2, H_2, be the components of the electric and magnetic fields E and H parallel to the x_1 and x_2 axes respectively, in either medium. Then the boundary conditions that must be satisfied are :—

$$E_1 \text{ and } E_2 \text{ continuous} \quad . \quad . \quad . \quad . \quad . \quad . \quad . \quad . \quad (16)$$

$$H_1 \text{ and } H_2 \text{ continuous} \quad . \quad . \quad . \quad . \quad . \quad . \quad . \quad . \quad (17)$$

Application of these to the wave expressions gives the following four equations :—

$$E_{\parallel i} \cos i - E_{\parallel r} \cos i = E_{\parallel 0} \cos \theta_0 + E_{\parallel e} \cos \theta_e \quad . \quad . \quad (18)$$

$$E_{\perp i} + E_{\perp r} = -j\,E_{\parallel 0} + jE_{\parallel e} \quad . \quad . \quad . \quad . \quad (19)$$

$$E_{\parallel i} + E_{\parallel r} = \mu_0 E_{\parallel 0} + \mu_e E_{\parallel e} \quad . \quad . \quad . \quad . \quad (20)$$

$$E_{\perp i} \cos i - E_{\perp r} \cos i = -j\mu_0 E_{\parallel 0} \cos \theta_0 + j\mu_e E_{\parallel e} \cos \theta_e \quad . \quad . \quad (21)$$

From these we can evaluate the reflection and transmission coefficients. For example, to find ${}_{\parallel}R_{\perp}$, we put $E_{\perp i}=0$, and eliminate $E_{\parallel r}$, $E_{\parallel 0}$ and

$E_{\parallel e}$ from the equations. The result is an equation for $E_{\perp r}/E_{\parallel i}$, which is ${}_{\parallel}R_{\perp}$. The results are as follows :—

$$ {}_{\parallel}R_{\parallel}=\{(\mu_0+\mu_e)(\cos^2 i-\cos\theta_0\cos\theta_e)+(\mu_0\mu_e-1)(\cos\theta_0+\cos\theta_e)\cos i\}/D \quad . \; . \; . \; . \; . \quad (22) $$

$$ {}_{\perp}R_{\parallel}=2j\cos i(\mu_0\cos\theta_0-\mu_e\cos\theta_e)/D \quad . \; . \; . \; . \; . \; . \; . \; . \; . \; . \; . \quad (23) $$

$$ {}_{\perp}R_{\parallel}=2j\cos i(\mu_0\cos\theta_e-\mu_e\cos\theta_0)/D \quad . \; . \; . \; . \; . \; . \; . \; . \; . \; . \; . \quad (24) $$

$$ {}_{\perp}R_{\perp}=\{(\mu_0+\mu_e)(\cos^2 i-\cos\theta_0\cos\theta_e)-(\mu_0\mu_e-1)(\cos\theta_0+\cos\theta_e)\cos i\}/D \quad . \; . \; . \; . \; . \quad (25) $$

where

$$ D=(\mu_0+\mu_e)(\cos^2 i+\cos\theta_0\cos\theta_e)+(\mu_0\mu_e+1)(\cos\theta_0+\cos\theta_e)\cos i. \quad . \quad (26) $$

We may similarly evaluate transmission coefficients at the surface of the ionosphere. These will be denoted by ${}_{\parallel}T_0$, ${}_{\parallel}T_e$, ${}_{\perp}T_0$, ${}_{\perp}T_e$. Here the first subscript indicates whether the incident wave has its electric vector parallel ($\parallel$) or perpendicular ($\perp$) to the plane of incidence, and the second subscript indicates whether the transmitted wave is the ordinary (0) or extraordinary (e) component. The transmitted wave is assumed always to be described by that component of its electric vector which is parallel to the plane of incidence, so that

$$ {}_{\parallel}T_0=E_{\parallel 0}/E_{\parallel i}=\;\;jE_{\perp 0}/E_{\parallel i} \qquad {}_{\perp}T_0=E_{\parallel 0}/E_{\perp i}=\;\;jE_{\perp 0}/E_{\perp i} $$

$$ {}_{\parallel}T_e=E_{\parallel e}/E_{\parallel i}=-jE_{\perp e}/E_{\parallel i} \qquad {}_{\perp}T_e=E_{\parallel e}/E_{\perp i}=-jE_{\perp e}/E_{\perp i} $$

The values of the transmission coefficients are given below :—

$$ {}_{\parallel}T_0=\;\;2\,\mu_0\cos i(\;\;\cos i+\mu_e\cos\theta_e)/D \quad . \; . \; . \; . \; . \quad (27) $$

$$ {}_{\parallel}T_e=\;\;2\,\mu_e\cos i(\;\;\cos i+\mu_0\cos\theta_0)/D \quad . \; . \; . \; . \; . \quad (28) $$

$$ {}_{\perp}T_0=-2j\mu_0\cos i(\mu_e\cos i+\;\;\cos\theta_e)/D \quad . \; . \; . \; . \; . \quad (29) $$

$$ {}_{\perp}T_e=-2j\mu_e\cos i(\mu_0\cos i+\;\;\cos\theta_0)/D \quad . \; . \; . \; . \; . \quad (30) $$

where D is given by (26).

As a partial check of the formulæ (22) to (30), it is readily verified that they reduce to the Fresnel formulæ for a homogeneous medium, when we put $\mu_0=\mu_e$, and $\theta_0=\theta_e$.

§ 4. NUMERICAL RESULTS.

4.1. *The parameters p_r/p and τ.*

The preceding formulæ have been used to calculate values of ${}_{\parallel}R_{\parallel}$ and ${}_{\parallel}R_{\perp}$ as functions of the angle of incidence, for various values of the parameters p_r/p and τ. The values of these parameters are given approximately by equations (5) and (6), although, as we have already mentioned, some slight modification may be necessary when account is taken of the fact that y_L may be complex. This modification will be discussed in § 5.2, and will be shown to be small. Equation (6) shows that $\tan \tau$ is proportional to the magnetic gyro frequency for electrons, and inversely proportional to the collision frequency, ν. Equation (5) shows that p_r is equal to $p_0^2/\sqrt{(\nu^2+p_L^2)}$ where p_0 is the critical frequency that the medium would have in the absence of collisions and magnetic field p_r is therefore directly proportional to the electron density N.

If the earth's magnetic field is zero, τ is zero. Some results for this case are shown in figs. (1) and (9).

If the collision frequency ν is zero, then $\tau=90°$, and $p_r=p_0^2/p_L$. Some curves for this case, for two different values of p_r/p are shown in figs. 7, 8, 15 and 16.

Table I.

Figure No.	p_r/p	τ	Frequency $p/2\pi$ kc./s.	Collision frequency ν sec.$^{-1}$	Electron Density N cm.$^{-3}$
1, 9	1	0°	16	($\nu/\text{N}=3{\cdot}17\times10^4$)	
1, 9	1	0°	100	($\nu/\text{N}=5{\cdot}08\times10^3$)	
2, 10	$\frac{1}{2}$	15°	16	$2{\cdot}7\times10^7$	$0{\cdot}44\times10^3$
2, 10	$\frac{1}{2}$	15°	100	$2{\cdot}7\times10^7$	$2{\cdot}75\times10^3$
3, 11	2	15°	16	$2{\cdot}7\times10^7$	$1{\cdot}76\times10^3$
3, 11	2	15°	100	$2{\cdot}7\times10^7$	$11{\cdot}00\times10^3$
4, 12	2	60°	16	$4{\cdot}2\times10^6$	$0{\cdot}53\times10^3$
4, 12	2	60°	100	$4{\cdot}2\times10^6$	$3{\cdot}30\times10^3$
5, 13	4	60°	16	$4{\cdot}2\times10^6$	$1{\cdot}06\times10^3$
5, 13	4	60°	100	$4{\cdot}2\times10^6$	$6{\cdot}62\times10^3$
6, 14	8	75°	16	$1{\cdot}9\times10^6$	$1{\cdot}85\times10^3$
6, 14	8	75°	100	$1{\cdot}9\times10^6$	$11{\cdot}60\times10^3$
7, 15	2	90°	16	0	$0{\cdot}46\times10^3$
7, 15	2	90°	100	0	$2{\cdot}88\times10^3$
8, 16	8	90°	16	0	$1{\cdot}83\times10^3$
8, 16	8	90°	100	0	$11{\cdot}40\times10^3$

We should expect the ionosphere to have characteristics somewhere between the extreme cases just mentioned. To consider the behaviour of a particular medium, we first decide what values to assume for ν and p_L, and derive the corresponding value of τ from equation (6). We can then fix p_r if we know the critical frequency of the medium p_0. Any pair of values of p_r and τ therefore refers to fixed values of ν and N. The complex refractive indices can then be found from equations (7) and (9), using the known values of p_r, τ, and the wave frequency $p/2\pi$. p_r and p enter these expressions only as a ratio. Since it is convenient to discuss the results in terms of particular wave frequencies, the values of N and ν appropriate to the curves of figs. 1 to 16 for selected wave frequencies are listed in Table I. The frequency 16 kc./s. has been included because many of the experimental results apply to it. The values of ν and N in Table I refer to vertical incidence when the angle of magnetic dip is 60°. It will be shown in § 5.2 that only small modifications are needed at other angles of incidence, and that the form of the results is independent of the relative directions of the transmission path and the magnetic meridian.

4.2. *The Reflection Coefficients* $_{\|}R_{\|}$ *and* $_{\|}R_{\perp}$.

Figs. 1 to 8 show some typical numerical values for the amplitudes of $_{\|}R_{\|}$ and $_{\|}R_{\perp}$, plotted as functions of the angle of incidence i. Figs. 9 to 16 show the corresponding curves for the phases of $_{\|}R_{\|}$ and $_{\|}R_{\perp}/_{\|}R_{\|}$. This last quantity gives the relative phases of the normal and abnormal components of the reflected wave, and thus determines its state of polarization.

Figs. 1 to 8 show clearly that there is an angle of incidence for which $|_{\|}R_{\|}|$ is a minimum. This is the quasi-Brewster angle, which exists also when the superimposed magnetic field is zero. Figs. 9 to 16 show that there is a change in the phase of $_{\|}R_{\|}$ as the angle of incidence varies. The change is most rapid near the quasi-Brewster angle.

4.3. *Comparison with Experimental Results.*

The experimental results for a frequency of 16 kc./s. may be summarized as follows :—(Bracewell *et al.* 1951). For an angle of incidence of about 30° the wave reflected from the ionosphere is roughly circularly polarized with a left-handed sense. The reflection coefficient $|_{\|}R_{\|}|$ at night is 0·4 to 0·5. In the daytime it is about 0·25 for winter and 0·1 for summer, and increases as the angle of incidence is increased.

The theoretical curves of figs. 10 to 16 show that the polarization of the reflected waves would be elliptical with a left-handed sense. The theoretical curves for which the polarization, at $i=30°$, would be most nearly circular are those of figs. 4 and 12. Here the phase difference between $_{\|}R_{\|}$ and $_{\|}R_{\perp}$ is about 240°, whereas for circular polarization it should be 270°. The corresponding value of $|_{\|}R_{\|}|$ is about 0·34, so that for this particular angle of incidence the curves of figs. 4 and 12 represent the experimental results fairly well for a winter day. The appropriate values of the parameters are : $p_r/p=2$, and $\tau=60°$. Table I. shows that these correspond to the values : $\nu=4{\cdot}2\times10^6$ sec.$^{-1}$ and $N=530$ cm.$^{-3}$. There are no values of the parameters which will fit the experimental results much better than these.

The curves of figs. 10 to 16 show that as the angle of incidence increases, the polarization of the reflected wave changes, and for very oblique incidence becomes nearly linear. An effect of this sort has been reported by Weekes (1950), whose experiments show that for very oblique incidence the reflected wave is roughly linearly polarized with its plane of polarization at about 45° to the vertical. Weekes' experiments do not give any information about the direction of tilt of the plane of polarization, but it would appear from the results of some experiments made by Mr. Bain in Aberdeen, that the observed direction of tilt is opposite to that given by figs. 10 to 16.

Figs. 1 to 16.

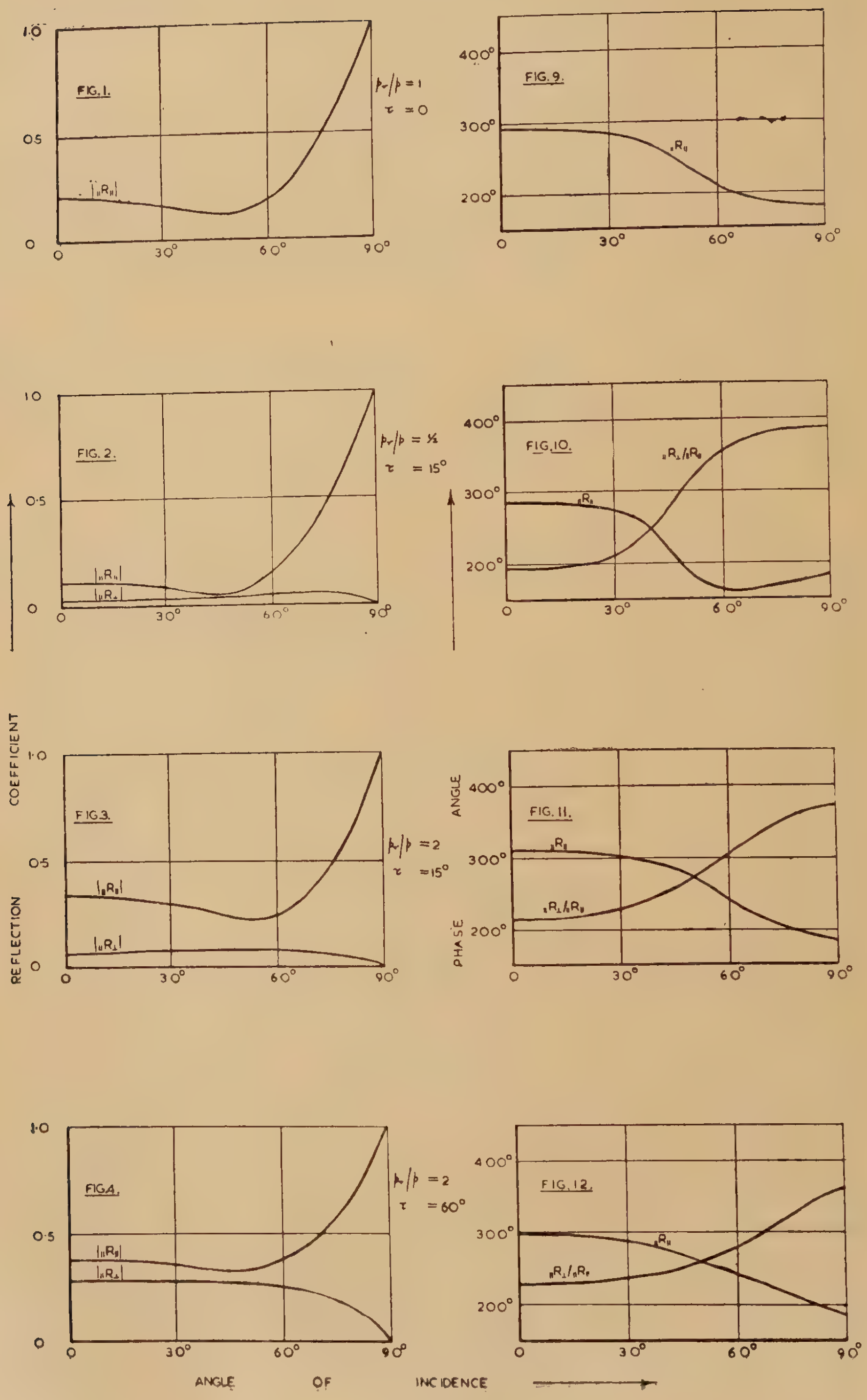
1.0
0.5
0
FIG. 1.
|∥R∥|
p_r/p = 1
τ = 0
0
30°
60°
90°
400°
300°
200°
FIG. 9.
∥R∥
0
30°
60°
90°
1.0
0.5
0
FIG. 2.
|∥R∥|
|∥R⊥|
p_r/p = ½
τ = 15°
0
30°
60°
90°
400°
300°
200°
FIG. 10.
∥R⊥/∥R∥
∥R∥
0
30°
60°
90°
REFLECTION COEFFICIENT
1.0
0.5
0
FIG. 3.
|∥R∥|
|∥R⊥|
p_r/p = 2
τ = 15°
0
30°
60°
90°
PHASE ANGLE
400°
300°
200°
FIG. 11.
∥R∥
∥R⊥/∥R∥
0
30°
60°
90°
1.0
0.5
0
FIG. 4.
|∥R∥|
|∥R⊥|
p_r/p = 2
τ = 60°
0
30°
60°
90°
400°
300°
200°
FIG. 12.
∥R∥
∥R⊥/∥R∥
0
30°
60°
90°
ANGLE OF INCIDENCE

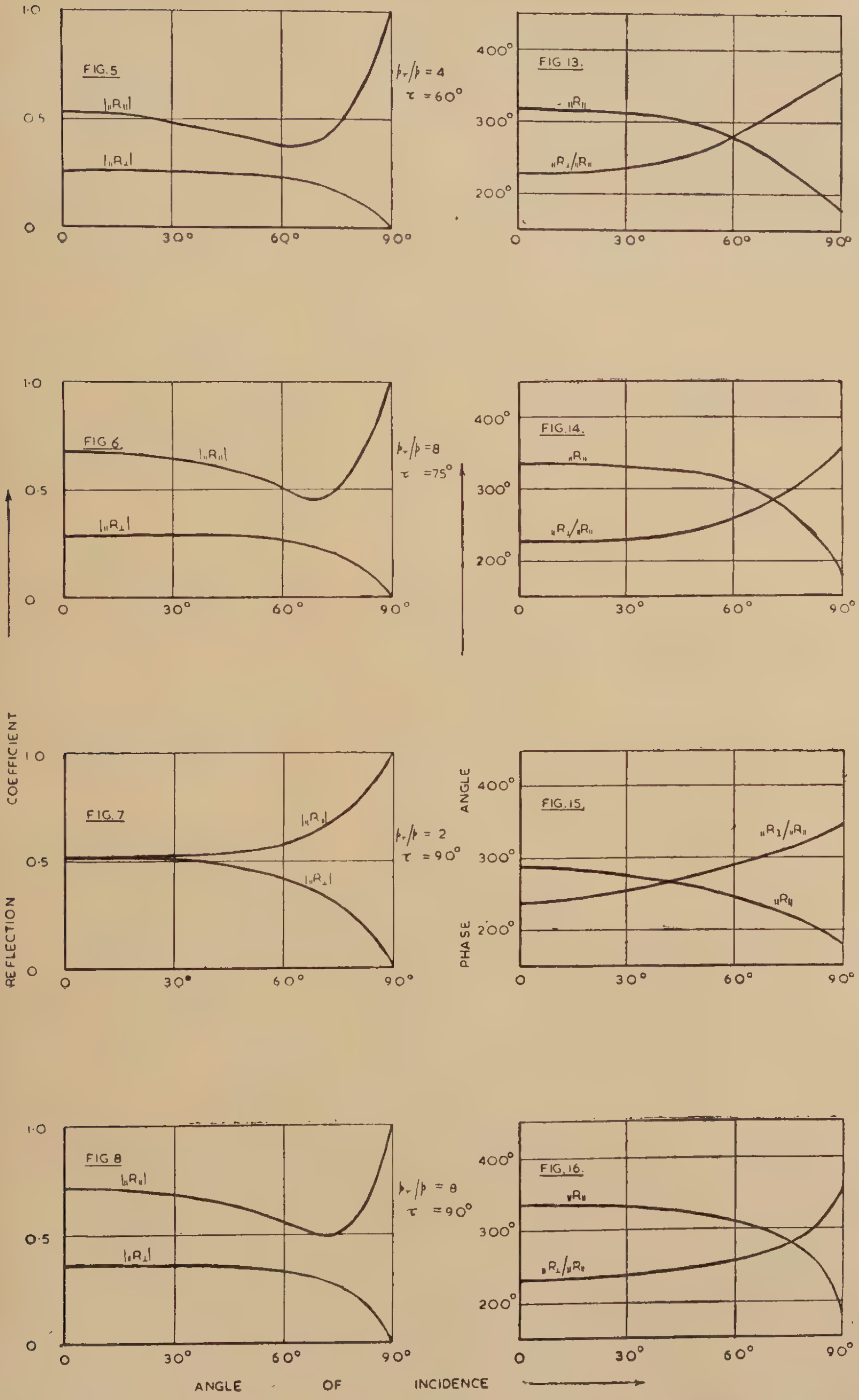

Curves showing reflection coefficients $|_{\parallel}R_{\parallel}|$ and $|_{\parallel}R_{\perp}|$ and phases of $R_{\parallel}$ and $_{\parallel}R_{\perp}/_{\parallel}R_{\parallel}$ as functions of angle of incidence. Quasi-longitudinal approximation used. Results are independent of horizontal direction of transmission path.

In fig. 17 we show the values of the reflection coefficients $|{}_{\parallel}R_{\parallel}|$ and $|{}_{\parallel}R_{\perp}|$ plotted as functions of frequency for an angle of incidence 30°. It is seen that $|{}_{\parallel}R_{\parallel}|$ decreases as the frequency increases, and this is in qualitative agreement with the observations. The theoretical decrease of $|{}_{\parallel}R_{\perp}|$ with frequency is very slight, and the observed decrease is much more rapid.

We conclude that, if we assume the ionosphere to be a sharply bounded homogeneous medium to which the quasi-longitudinal approximation

Fig. 17.

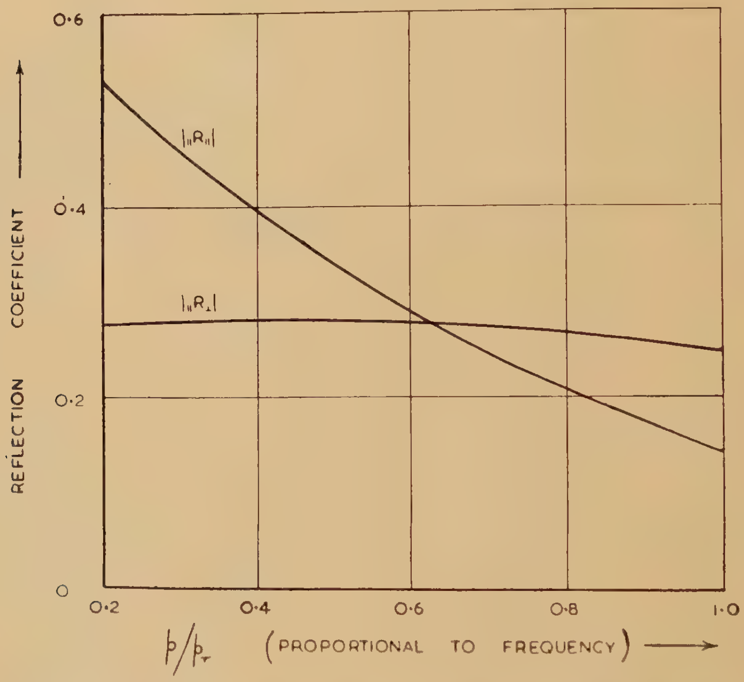

Variation of reflection coefficients $|{}_{\parallel}R_{\parallel}|$ and $|{}_{\parallel}R_{\perp}|$ with frequency. Angle of incidence $i=30°$. $\tau=60°$.

is applicable, we cannot account for the observed phase difference of 90° between the normal and abnormal components of the reflected wave. For an exact theory a more complete treatment is necessary. For example, we might investigate the properties of an ionosphere with values of N and ν for which the quasi-longitudinal approximation is not valid, but Bremmer (1949) has shown that the analysis of this case is extremely complex. Alternative treatments taking account of the finite rate of variation of N and ν with height have been made (Wilkes 1940 and 1947, Stanley 1950), and, for reasons given in § 4.6, these are probably preferable to any extension of the theory of the sharply bounded ionosphere, However, the sharply bounded model discussed in this paper gives a good rough approximation to the behaviour of the ionosphere for very low frequency waves*.

4.4. *Comparison with Bremmer's Results.*

Bremmer (1949: Terrestrial Radio Waves, pp. 286 to 301) has discussed the reflection of waves at a sharply bounded, homogeneous non-isotropic ionosphere using the full magneto-ionic formula, without making the quasi-longitudinal approximation. He gives numerical results for two cases only. He assumes the earth's magnetic field to be vertical, with $p_H = 9{\cdot}4 \times 10^6$ sec.$^{-1}$. His results are given in Table II., together with the corresponding values of τ, p_r/p and N. (Bremmer assumes the waves to have a time factor e^{-jpt}. The signs of arg $({}_{\parallel}R_{\parallel})$ and arg $({}_{\parallel}R_{\perp}/{}_{\parallel}R_{\parallel})$ have been adjusted to agree with the time factor e^{jpt} and the system of axes used in the present paper.)

TABLE II.

Angle of Incidence	76°	76°
Frequency (kc./s.)	300	30
τ	84°	84°
ν (sec.$^{-1}$)	10^6	10^6
p_r/p	13	29
N (cm.$^{-3}$)	$7{\cdot}2 \times 10^4$	$1{\cdot}6 \times 10^4$
$\lvert {}_{\parallel}R_{\parallel} \rvert$	0·231	0·427
arg $({}_{\parallel}R_{\parallel})$	−138°	−55°
$\lvert {}_{\parallel}R_{\perp} \rvert$	0·214	0·166
arg $({}_{\parallel}R_{\perp}/{}_{\parallel}R_{\parallel})$	312°	256°

It should be noted that the values assumed for the electron density N are very large, and correspond to critical frequencies of 2·4 Mc./s. and 1·1 Mc./s. respectively. These might apply somewhere near the maximum of the E-region, but are much too large for the levels, usually between 65 and 95 km., where very low frequency waves are reflected. The values of $|y^2/(1-x-jz)^2|$ are of the order of ·0004 and ·007 respectively for the two cases discussed, so that the quasi-longitudinal approximation might have been applied with fair accuracy.

4.5. *The Transmitted Waves.*

It may be of interest to know the ratio of the amplitudes of the ordinary and extraordinary waves transmitted into the ionosphere. The values of this ratio for various values of the parameters have been calculated from (27) and (28) and are shown in the following Table III.

---

* It is hoped to use this model to discuss the effects of the earth's magnetic field on the propagation of a radio atmospheric, and it was originally developed for this purpose. For a discussion of the propagation of atmospherics which neglects the earth's magnetic field, see Budden 1951.

It is found that the ratio is always fairly close to unity. It is also of interest to know the direction of propagation of the two waves in the ionosphere. Let ϕ_0 and ϕ_e be the inclination to the vertical of the normals to the planes of constant phase for the ordinary and extraordinary wave, respectively. Then

$$\tan\phi_0 = \mathscr{R}(\sin\theta_0)/\mathscr{R}(\cos\theta_0)\ ;\ \tan\phi_e = \mathscr{R}(\sin\theta_e)/\mathscr{R}(\cos\theta_e)$$

The values of ϕ_0 and ϕ_e are also shown in Table III.

TABLE III.

Angle of incidence		10°	80°	10°	80°	10°	80°
p_r/p		$\frac{1}{2}$	$\frac{1}{2}$	2	2	8	8
τ		15°	15°	60°	60°	75°	75°
Ratio of amplitudes, ordinary wave to extraordinary wave		1·04	1·05	1·09	1·40	0·84	1·06
Inclination of wave normal	ordinary	8° 20′	56° 12′	4° 50′	39° 20′	4° 4′	19° 10′
	extraordinary	9° 46′	59° 18′	3° 40′	17° 52′	1° 22′	3° 4′

4.6. *The Thickness of the Ionosphere.*

It is of interest to ask how thick the ionosphere must be for the assumption of homogeneity to be justified. The two transmitted waves are both attenuated as the height increases in the ionosphere, and it is found that the ordinary wave is the least attenuated component. The height at which the amplitude of the ordinary wave is reduced to one-half of its value at the boundary has been calculated for some selected values of the parameters. The results are shown in Table IV.

TABLE IV.

Angle of incidence	0°	80°	0°	80°	0°	80°
p_r/p	8	8	4	4	1	1
τ	75°	75°	60°	60°	15°	15°
Thickness of medium in wavelengths for reduction to half amplitude	0·32	0·30	0·24	0·22	0·27	0·19

The above results perhaps provide the strongest reason for rejecting the sharply bounded ionosphere when an accurate theory of the reflection of very long waves is required. Thus, for a frequency of 16 kc./s. (wavelength 18·75 km.), the last row of Table IV. shows thicknesses of the order of 6 km., and there is little doubt that there are large variations of N and ν in distances of this order at the level of reflection of very low frequency waves.

§ 5. VALIDITY OF THE APPROXIMATIONS.

5.1. *The Quasi-longitudinal Approximation.*

We see from equation (2) that the quasi-longitudinal approximation is valid if

$$|y_T^4/\{4y_L^2(1-x-jz)^2\}| \ll 1. \quad . \quad . \quad . \quad . \quad . \quad . \quad . \quad . \quad (31)$$

The values of this quantity for some selected values of p_r/p, τ and i, are shown in Table V.

TABLE V.

p_r/p	τ	Angle of incidence i	$\lvert y_T^4/\{4y_L^2(1-x-jz)^2\}\rvert$
$\frac{1}{2}$	15°	90°	0·21
2	60°	0°	0·0044
2	60°	30°	0·031
2	60°	60°	0·12
2	60°	90°	0·19
4	60°	30°	0·0055
1	75°	30°	0·79
8	75°	90°	0·0039
2	90°	90°	0·24
8	90°	90°	0·0031

These values all refer to propagation from south to north in the magnetic meridian, since it is for this case that the quasi-longitudinal approximation would be least accurate. It is found that the quantity (31) is greatest for large angles of incidence, for large values of τ, and for small values of p_r/p. It is clear that the quasi-longitudinal approximation may be treated as valid for most of the range covered by the curves of figs. 1 to 16. It begins to be inaccurate at high angles of incidence in figs. 2, 10, 4, 12, 7 and 15.

It might be suggested that further curves of the type of figs. 1 to 16 could be calculated using the quasi-transverse approximation, which is valid if

$$|y_T^4/\{4y_L^2(1-x-jz)^2\}| \gg 1.$$

However, this condition requires values of ν rather lower than 2×10^6 sec.$^{-1}$, and this is less than would be expected to apply at the level of reflection of very low frequency waves. Moreover, for propagation in the direction of the magnetic meridian the quasi-transverse approximation would show that the reflected wave should always be linearly polarized in the plane of incidence, whereas the experiments (Bracewell *et al.* 1951) show that it is roughly circularly polarized for small or moderate angles of incidence.

We conclude that as long as p_r/p is large enough, the quasi-longitudinal approximation represents fairly well the behaviour of a sharply bounded ionosphere. It would therefore be the best approximation to use in discussing the propagation of waves of very low frequency (10 kc./s. or less) such as are used in the study of the propagation of atmospherics (Gardner 1950, Bowe 1951).

5.2. *Variation of Parameters with Angle of Incidence.*

If d is the angle of magnetic dip, and we consider transmission in a horizontal direction ϕ, measured east from magnetic north, then y_L is given by

$$y_L = y(\sin\theta \cos d \cos\phi + \cos\theta \sin d), \quad . \quad . \quad . \quad . \quad (32)$$

where θ may be either θ_0 or θ_e. We shall assume in what follows that $d=60°$.

TABLE VI.

	Ordinary wave			Extraordinary wave		
Angle of incidence	0°	30°	90°	0°	30°	90°
τ	61° 4′	60°	56° 23′	58° 18′	60°	64° 40′
p_r/p	3·95	4	4·18	4·05	4	3·89

It was mentioned in § 3 that when Snell's Law (equation (15)) was used to derive the directions θ_0 and θ_e of the two waves in the medium, these angles proved to be complex, because the refractive indices μ_0 and μ_e are complex. As a result y_L is complex. We now investigate the consequences of this.

If y_L is a complex number, the denominator of equation (4) must be written

$$z \mp \mathscr{I}(y_L) \pm j\mathscr{R}(y_L) \quad . \quad . \quad . \quad . \quad . \quad . \quad . \quad (33)$$

($\mathscr{R}$ means " real part of " and $\mathscr{I}$ means " imaginary part of "). Both $\mathscr{R}(y_L)$ and $\mathscr{I}(y_L)$ vary with angle of incidence and the result is a change in the values of p_r/p and τ. The modification is most serious at very oblique incidence, but even then the associated changes in the parameters p_r/p and τ are small. If we assume that $\tau=60°$ and $p_r/p=4$ are correct for an angle of incidence 30°, then for west to east transmission in the northern hemisphere, and for a frequency of 16 kc./s. the correct values of τ and p_r/p for other angles of incidence are as shown in Table VI.

The above variations of τ and p_r/p with angle of incidence are not sufficient to affect the general form of the results. It is sufficiently accurate to regard fixed values of p_r/p and τ as referring to fixed values of N and ν for all angles of incidence. This is equivalent to treating y_L as a constant. An important consequence of this is that the reflection coefficients are independent of the horizontal direction of the transmission path.

5.3. *The Longitudinal Component of the Electric Field.*

The whole of the preceding theory has been worked out on the assumption that the waves in the ionosphere had only transverse electric fields. It is known, however, that the electric fields also have components in the direction of the wave normal. We shall call these the longitudinal fields and denote them by E_{L0} and E_{Le}, respectively, for the ordinary and extraordinary waves, or simply by E_L when the formulæ apply to either wave. It can be shown that if the quasi-longitudinal approximation is valid, then for either ordinary or extraordinary wave

$$|E_L/E_{\parallel}|=|\mu^2-1|\,.\,|y_T/(1-x-jz)|. \quad . \quad . \quad . \quad . \qquad (34)$$

TABLE VII.

p_r/p	τ	Angle of incidence	$\lvert E_L/E_{\parallel}\rvert$	$\lvert E_L/E_{\parallel}\rvert\,.\,\lvert\tan\theta\rvert$	Component
$\frac{1}{2}$	15°	90°	0·15	0·21	ext.
2	60°	0°	0·48	0	ext.
2	60°	30°	0·74	0·14	ext.
2	60°	60°	0·99	0·50	ext.
2	60°	90°	1·08	0·66	ext.
4	60°	30°	0·67	0·036	ord.
1	75°	30°	1·32	1·11	ext.
8	75°	90°	4·2	0·53	ext.
2	90°	90°	2·2	2·7	ord.
8	90°	90°	1·2	0·18	ord.

The longitudinal electric fields will in general have components parallel to the boundary of the ionosphere. This would mean that additional terms should appear in the boundary condition equation (18). The ratio of the magnitude of the additional terms to those already on the right hand side of (18) is proportional to the expression (34) and to $\tan\theta$, where θ is either θ_0 or θ_e.

The ratio is therefore small for nearly vertical incidence, for then θ is small and the longitudinal electric field is nearly perpendicular to the boundary. The values of $|E_L/E_{\parallel}|$ and of $|E_L|E_{\parallel}|\,.\,|\tan\theta|$ for some other cases are shown in Table VII. These all refer to propagation from south to north in the magnetic meridian, and the figures apply to that wave, ordinary or extraordinary, for which the value is the larger.

A comparison of Tables V. and VII. shows that the errors which arise by neglecting the longitudinal electric field become serious for about the same values of the parameters as those for which the quasi-longitudinal approximation becomes inaccurate. It is found that for very large values of p_r/p the errors are small, which provides further encouragement for using the theory in discussing the behaviour of the lowest frequencies (10 kc./s. and lower).

ACKNOWLEDGMENTS.

This work was carried out at the Cavendish Laboratory as part of a programme of Radio Research supported by the Department of Scientific and Industrial Research.

REFERENCES.

APPLETON, E. V., 1932, *Journ. Inst. Elec. Eng.*, **71,** 642.
BOOKER, H. G., 1935, *Proc. Roy. Soc.* A, **150,** 267.
BOWE, P. W. A., 1951, *Phil. Mag.*, **42,** 121.
BRACEWELL, R. N., BUDDEN, K. G., RATCLIFFE, J. A., STRAKER, T. W., and WEEKES, K., 1951, *Proc. Inst. Elec. Eng.*, **98,** III, 221.
BREMMER, H., 1949, *Terrestrial Radio Waves* (Elsevier Pbl. Co.).
BUDDEN, K. G., 1951, *Phil. Mag.*, **42,** 1.
BUDDEN, K. G., RATCLIFFE, J. A., and WILKES, M. V., 1939, *Proc. Roy. Soc. A*, **171,** 188.
BUREAU, R., 1930, *Comptes rendus, Acad. Sci.* Paris, **191,** 64; 1932, *Ibid.*, **195,** 69.
GARDNER, F. F., 1950, *Phil. Mag.*, **41,** 1259.
HARTREE, D. R., 1929, *Proc. Camb. Phil. Soc.*, **25,** 97.
LORENTZ, H. A., 1909, *Encyk. der Math. Wiss.*, **3,** 199.
RYDBECK, O. E. H., 1944, *On the Propagation of Radio Waves.* Trans. Chalmers Univ., Gothenburg, Sweden, 34.
STANLEY, J. P., 1950, *Journ. Atm. & Terr. Phys.*, **4,** 65.
VOIGT, P., 1915, *Graetz ,, Handbuch d. Elecktr. und des Magn.*" IV. 2, 667 and 710.
WEEKES, K., 1950, *Proc. Inst. Elec. Eng.*, **97,** III, 100.
WILKES, M. V., 1940, *Proc. Roy. Soc.* A, **175,** 143; 1947, *Ibid.*, **189,** 130.
YOKOYAMA, E., and NAMBA, S., 1932, *Reports, Radio Research in Japan*, **2,** 131.

LXXXVI. *Note on the Analytic Continuation of the S-matrix.*

By N. G. van Kampen,
Institute for Theoretical Physics, Copenhagen, Denmark*.

[Received April 23, 1951.]

Summary.

It is shown that methods which try to avoid the redundant poles are not likely to be successful. On the other hand, the analytic continuation of the S-matrix is an ill-defined procedure, which cannot be applied until more properties of the S-matrix are known. The redundant poles are caused by the use of the asymptotic expression of the wave function instead of its actual value and have no physical meaning.

§ 1. Preliminaries.

The scattering of a non-relativistic particle by a fixed central field of force may be described by the equation

$$u''(r)+\{E-V(r)\}u(r)=0 \quad . \quad . \quad . \quad . \quad . \quad . \quad (1)$$

with the boundary condition $u(0)=0$. Let $u(E, r)$ be the solution, the arbitrary constant factor being determined by $u'(E, 0)=1$. For each r the function $u(E, r)$ is an integral function in the complex E-plane. For real positive E we shall write $E=k^2$ with $k>0$. Then the asymptotic expression of $u(E, r)$ for $r\rightarrow\infty$ is

$$u(E, r)\sim C(k) \sin \{kr-\eta(k)\} \quad \text{for} \quad E=k^2>0. \quad . \quad . \quad . \quad (2)$$

The problem at issue is to find the discrete eigenvalues E_n of (1) from the phase function $\eta(k)$ only.

Let Γ denote the complex E-plane with the exception of the positive real axis. For each value of E in Γ there is (apart from a constant factor) one solution of the equation (1) which goes to zero for $r\rightarrow\infty$. It can be defined uniquely as the solution $f(E, r)$ of (1) which is asymptotically $\exp [i(\sqrt{E})r]$, where $\sqrt{E}$ is made unique in Γ by the condition $\text{Img} \sqrt{E}>0$. For each r, $f(E, r)$ is a one-valued function of E in Γ. When E approaches the cut along the positive real axis from above, $f(E, r)$ tends to that solution for $E=k^2>0$ which is asymptotically $f(E+, r)\sim\exp [ikr]$; when E approaches from below $f(E, r)$ becomes $f(E-, r)\sim\exp [-ikr]$.

As shown below (see also Jost 1947), the function $f(E, 0)=f(E)$ is analytic in Γ without singularities. Its zeros are the energies of the bound states; they are necessarily on the negative real axis:

$$f(E_n)=0, \quad E_n<0. \quad . \quad . \quad . \quad . \quad . \quad . \quad . \quad . \quad (3)$$

---

* Communicated by Prof. C. Møller.

The discontinuity of $f(\mathrm{E})$ on the cut is connected with the S-matrix by the relation (Jost 1947)

$$\mathrm{S}(\mathrm{E}) \equiv \exp\,[-2i\eta(k)] = f(\mathrm{E}-)/f(\mathrm{E}+). \quad . \quad . \quad . \quad . \quad (4)$$

It should be noted that as yet no appeal has been made to analytic continuation, with the consequence that S(E) has a meaning only for real positive E. Now consider a second sheet Γ_1 of the complex E-plane, connected with Γ along the positive real axis in such a way that one enters Γ_1 on crossing this axis upwards. If $f(\mathrm{E})$ can be continued analytically in Γ_1, taking the values $f_1(\mathrm{E})$ say, then $\mathrm{S}(\mathrm{E}) = f_1(\mathrm{E})/f(\mathrm{E})$ is an analytic continuation of (4) in Γ. From (3) it follows that S(E) has poles (in general) for $\mathrm{E}=\mathrm{E}_n$, which suggests that the discrete spectrum can be found from the analytic continuation of the S-matrix (4).

It is clear, however, that S(E) may have " redundant poles " (Ma 1946), namely, if $f_1(\mathrm{E})$ has poles. Also, if $f_1(\mathrm{E}_n)=0$ for any E_n, then this eigenvalue is not exhibited as a pole of S(E). Because of these difficulties it is tempting to seek a method of determining the discrete spectrum from (4) without an analytic continuation of $f(\mathrm{E})$. This was tried by Wildermuth (1950) without conclusive result. We shall now show why it is not possible.

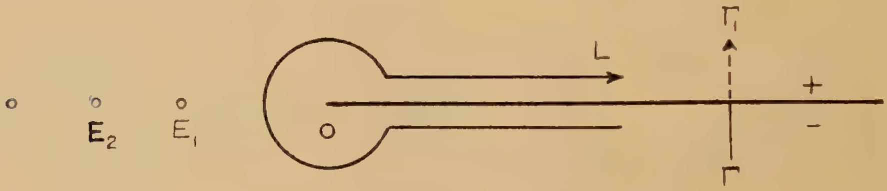

The complex E-plane.

§ 2. No Analytic Continuation of S(E).

Levinson (1949) in a different connection introduced the function

$$\mathrm{F}(\mathrm{E}) \equiv 1 + \int_0^\infty \exp\,[i(\sqrt{\mathrm{E}})r]\mathrm{V}(r)u(\mathrm{E}, r)\,dr, \quad . \quad . \quad . \quad . \quad (5)$$

and proved the following properties. (i) F(E) is analytic in Γ and tends to 1 at infinity. (ii) F(E) tends to a limit when E tends to a point $\mathrm{E}=k^2$ on the positive real axis, namely

$$\mathrm{F}(\mathrm{E}+) = k\mathrm{C}(k)\exp\,[i\eta(k)], \qquad \mathrm{F}(\mathrm{E}-) = k\mathrm{C}(k)\exp\,[-i\eta(k)]$$

(k chosen positive). (iii) The zeros of F(E) are simple and lie on the negative real axis; they determine the discrete spectrum. This last property suggests that F(E) is identical with $f(\mathrm{E})$, which can be shown as follows.

From the constancy of the Wronskian determinant follows

$$u'(\mathrm{E}, r)f(\mathrm{E}, r) - u(\mathrm{E}, r)f'(\mathrm{E}, r) = f(\mathrm{E}, 0) \equiv f(\mathrm{E}). \quad . \quad . \quad . \quad (6)$$

For large r the left-hand side becomes (if E is in Γ)

$$\{u'(\mathrm{E}, r)-i(\sqrt{\mathrm{E}})u(\mathrm{E}, r)\} \exp [i(\sqrt{\mathrm{E}})r].$$

On the other hand, it can be seen that the latter expression is equal to

$$1+\int_0^r \exp [i(\sqrt{\mathrm{E}})r]\mathrm{V}(r)u(\mathrm{E}, r)\, dr, \quad . \quad . \quad . \quad . \quad . \quad (7)$$

because it has the same value for $r=0$ and the same derivative for $r>0$. Hence, by taking $r=\infty$, one finds that (6) is equal to the limit of (7), which is (5). Thus it is proved that $\mathrm{F(E)}=f(\mathrm{E})$ and, consequently, $f(\mathrm{E})$ is analytic in Γ and tends to 1 at infinity.

Now Levinson showed that F(E) can be expressed in terms of the function $\eta(k)$, when F(E) has no zeros, *i. e.* when there are no bound states. We shall now derive a similar relation for the case that there is a finite number of bound states. In that case, the function

$$g(\mathrm{E}) \equiv \log \frac{f(\mathrm{E})}{\Pi(1-\mathrm{E}_n/\mathrm{E})} = \log f(\mathrm{E}) - \Sigma \log\left(1-\frac{\mathrm{E}_n}{\mathrm{E}}\right) \quad . \quad . \quad (8)$$

is one-valued analytic in Γ (because the zeros of $f(\mathrm{E})$ are simple) and vanishes at infinity (when the appropriate branch of the logarithm is chosen). It has a discontinuity along the cut :

$$g(\mathrm{E}+)-g(\mathrm{E}-)=\log f(\mathrm{E}+)-\log f(\mathrm{E}-)=\log \mathrm{S(E)}. \quad . \quad . \quad (9)$$

By means of the Cauchy integral $g(\mathrm{E})$ can be expressed as an integral along the path L in the figure, with the result (for E in Γ)

$$g(\mathrm{E})=\frac{1}{2\pi i}\int_{\mathrm{L}} \frac{g(\mathrm{E}')}{\mathrm{E}'-\mathrm{E}}\, d\mathrm{E}' = \frac{1}{2\pi i}\int_0^{\infty} \frac{g(\mathrm{E}'+)-g(\mathrm{E}'-)}{\mathrm{E}'-\mathrm{E}}\, d\mathrm{E}'.$$

Inserting (8) and (9) one obtains

$$\log f(\mathrm{E}) = \frac{1}{2\pi i}\int_0^{\infty} \frac{\log \mathrm{S(E')}}{\mathrm{E}'-\mathrm{E}}\, d\mathrm{E}' + \Sigma \log\left(1-\frac{\mathrm{E}_n}{\mathrm{E}}\right), \quad . \quad . \quad (10)$$

where all logarithms are chosen in such a way that they vanish when E (or E′) tends to infinity.

From (10) it is clear that the values of S on the positive real axis together with those of E_n, determine the function $f(\mathrm{E})$.* On the other hand, when only S is given, the values of E_n may still be chosen arbitrarily, because for each choice an $f(\mathrm{E})$ results from (10), which has the zeros E_n and the required discontinuity (4) along the cut. Hence it appears that the discrete spectrum cannot be determined by using the function $f(\mathrm{E})$ inside Γ only, so that the analytic continuation of $f(\mathrm{E})$ beyond the cut becomes inevitable.

---

* The same conclusion was reached by Jost (1947).

It may be that $f(E)$ must satisfy some further requirements, which reduce the arbitrariness of the choice of the E_n in (10). For instance, it follows from (10) that for small E

$$\log f(E) = -\left\{\frac{1}{2\pi i}\log S(0) + N\right\}\log E + \text{finite function},$$

where N is the number of zeros E_n. Now, according to its definition, $f(0)$ is finite when $rV(r)$ is finite for $r=0$. In that case, therefore, the choice of E_n is restricted by the condition

$$N \leqslant -(1/2\pi i)\log S(0) = \eta(0)/\pi.$$

(If $N < \eta(0)/\pi$, then $f(0)=0$ and there is a bound state with energy 0 (Bargmann 1949).) However, it is unlikely that the choice of the E_n can be made unique by such general conditions. Consequently, our conclusion can still be maintained.

Wildermuth's method (1950) consists of defining an auxiliary function with a parameter $\alpha > 0$

$$S(E, \alpha) = f(E - i\alpha)/f(E + i\alpha).$$

This function is analytic in the E-plane with the two cuts $i\alpha + \lambda$ and $-i\alpha + \lambda$ $(0 < \lambda < \infty)$. Hence it is determined by its values on the positive real axis. For E on the negative real axis one has

$$\lim S(E, \alpha) = 1 \quad \text{for} \quad \alpha \to 0,$$

except if $f(E)=0$. In that case one finds, by taking the derivatives of numerator and denominator, $\lim S(E_n, \alpha) = -1$ (since $f'(E_n) \neq 0$). Consequently, the discrete spectrum can be determined if $S(E, \alpha)$ is known for all $E > 0$ and for α in a certain interval $0 < \alpha < \alpha_0$. All the same this is not a solution of the problem, for $S(E, \alpha)$ itself is not determined by the phase function $\eta(k)$. It seems, however, premature to conclude from this (Wildermuth 1950, Heisenberg 1950) that the knowledge of $\eta(k)$ alone is insufficient for the determination of the E_n, because there is still the alternative possibility of analytic continuation of S(E) (as in Kramers' original idea).

§ 3. The Use of Analytic Continuation.

The problem of finding the analytic continuation of a function given on the real axis is equivalent to the problem of solving the potential equation in two dimensions, with given values of the potential and the charge density on an open boundary. It is the initial-value problem for a partial differential equation of elliptic type, and can be solved only if the boundary function is given by means of some analytic expression (see for example Courant-Hilbert 1937). That is indeed the case when the function S(E) is obtained by solving equation (1) rigorously. However, in case the S-matrix is found experimentally, or from some approximate calculation, it is known only with a certain error. Then the analytic continuation is undetermined and the poles E_n cannot be found.

In order that the concept of analytic continuation be applicable to that case, it is necessary that S(E) is known on the whole boundary of the domain Γ. Now it appears from Ning Hu's work (1948) that the behaviour of S(E) at infinity can indeed be found from general considerations. However, the values on the lower side of the positive real axis (*i. e.* $S(E-)=f_1(E-)/f(E-)$ for $E>0$) do not seem to follow from *a priori* arguments. Usually it is postulated (Heisenberg 1946, Ning Hu 1948) that $S(E-)=S(E)^*$, but there is no guarantee that this is the value which follows from analytic continuation through Γ. Until this difficulty has been cleared it is impossible to find the bound states from the S-matrix in practical calculations.

In the same way, when S(E) is given for $E>0$ with a finite precision, it is impossible to find the poles that do not correspond to bound states. Indeed, we know that they can always be introduced or suppressed by an arbitrarily small alteration of S(E) obtained by changing the potential at some large distance (Jost 1947). This change in the potential has no physical meaning, since any actual measurement is performed at a finite distance. Hence it is seen that the redundant poles are caused by using the asymptotic expression of the wave function instead of the actual value at the point of observation. One might ask whether this means that the S-matrix theory is based on an unjustified separation of physical systems or only that the equation (1) is too much simplified. At any rate, an uncertainty is involved of the same order as the error made in cutting off the potential (ter Haar 1946) at a distance comparable to the distance of the measuring instruments. Therefore it is legitimate to discard the redundant poles by this device.

I am indebted to Prof. C. Møller for his interest and advice, to Prof. Niels Bohr for the opportunity to work at the Copenhagen Institute, and to the Rask-Ørsted Foundation for a grant which enabled me to stay in Denmark.

Note added in proof.—Recently P. Jauho (Ann. Acad. Scient. Fennicae, A1, nr. 80, 1950) has extended Levinson's work so as to include a Coulomb potential. In the present article that case has been excluded because of eq. (2), but it can be checked that our conclusions remain valid. In particular, it is not possible to build an S-matrix theory on Jauho's function χ (the counterpart of Levinson's F), as he suggested (p. 29).

REFERENCES

Bargmann, V., 1949, *Rev. Mod. Phys.*, **21**, 488.
Courant-Hilbert, 1937, *Meth. Math. Phys.*, **2**, 177 (Berlin).
ter Haar, D., 1946, *Physica*, **12**, 501.
Heisenberg, W., 1946, *Zs. f. Naturf.*, **1**, 608; 1950, *Ibid.*, **5a**, 368.
Jost, R., 1947, *Helv. Phys. Acta*, **20**, 256.
Levinson, N., 1949, *Kgl. Danske Vid. Selsk.*, **25**, nr. 9.
Ma, S. T., 1946, *Phys. Rev.*, **69**, 668.
Ning Hu, 1948, *Phys. Rev.*, **74**, 131.
Wildermuth, K., 1950, *Zs. f. Phys.*, **127**, 85.

LXXXVII. *The Attenuation of Nucleon Cascades in Lead.*

By W. G. V. Rosser and M. W. Swift,
The University, Manchester*.

[Received May 1, 1951.]

Abstract.

The frequency variation of nuclear interactions under lead has been studied by comparing the rates of stars in Ilford G5 emulsions exposed above and below 30 cms. of lead. The size frequency distribution is the same for stars in both sets of plates.

The attenuation lengths in lead are :--

(305 ± 7) gm./cm.^{2} for all stars,
(380 ± 65) gm./cm.^{2} for penetrating showers ($n_s\geqslant 2$),
(405 ± 31) gm./cm.^{2} for events with charged relativistic primaries,
(260 ± 34) gm./cm.^{2} for events with uncharged primaries (excluding simple evaporation stars).

The ratio of the attenuation length to the interaction meanfree path for penetrating showers is $(1{\cdot}8\pm 0{\cdot}3)$.

The percentage of all stars produced by charged relativistic primaries increases from $(13{\cdot}1\pm{\cdot}9)$ per cent for the unshielded plates to $(17{\cdot}0\pm 1{\cdot}0)$ per cent for the plates under lead due to the formation of stars by π mesons generated in lead. The ratio of charged to uncharged penetrating-shower primaries increases from $(0{\cdot}86\pm 0{\cdot}21)$ for the air plates to $(1{\cdot}94\pm 0{\cdot}32)$ for the plates exposed under 30 cms. of lead. It is suggested tentatively that the increase is due to the production of penetrating showers by fast π mesons created in the lead.

§1. Introduction.

The main properties of cosmic rays in the atmosphere can be accounted for in terms of nucleon cascades initiated by the primary cosmic rays in the upper atmosphere. The primary protons, α-particles and heavier nuclei collide with air nuclei and fast nucleons and mesons are emitted. Following Rossi (1948) the interacting particles will be called N-rays.

It is important to define the interaction mean-free-path λ_I and the attenuation length λ_A of the interacting particles. The interaction mean-free-path is defined as the average distance an N-ray goes before giving rise to a nuclear interaction. The attenuation length is defined as the thickness of absorber in which the intensity of N-rays is reduced by a factor 1 : *e*. It is found experimentally that in the lower atmosphere the variation of N-rays with altitude is roughly exponential so that

$$I=I_0\,(\exp -x/\lambda_A)$$

---

* Communicated by Professor P. M. S. Blackett, F.R.S.

where x is the thickness of the absorber. In each nuclear interaction the primary particle loses energy so that in general the next nuclear interaction will be a less energetic event. The attenuation length is defined for the frequency variation of a particular type of event. It is not confined to the absorption of particles in a given energy range which produce these events, because after the first collision these particles will have left the energy range. The attenuation length therefore represents the decrease in intensity of a spectrum of particles which undergo collisions with energy loss, the attenuation being due mainly to the fact that there are fewer high energy particles to take the place of lower energy particles as the N-rays traverse matter.

Following Fujimito and Hayakawa (1949), we shall call the primaries of penetrating showers the A-rays and the primaries of evaporation stars the B-rays. The division is not complete but is useful in discussing the nature of nucleon cascades. The average energy of B-rays is about 1 BeV. and these rays are, in the main, secondary to the A-rays.

The present experiment had the following main objectives :—

1. To investigate the effect of lead on the A and B components separately.
2. To compare the value of λ_A obtained for penetrating shower primaries under lead with the value of λ_I determined by counter experiments.
3. To ascertain what fraction of stars under lead can be ascribed to fast π mesons whose mean-free-path for star production in lead is shorter than the mean-free-path for decay into μ mesons.

§2. EXPERIMENTAL PROCEDURE.

Ilford G5 plates with emulsion 300μ in thickness were exposed for 21 days at the Pic du Midi, altitude 2860 m., one group of the plates (the " lead " plates) being placed under 30 cm. of lead built in the form of a hemisphere, and the other plates (the " air " plates) 1·5 m. from the lead. Both groups of plates stood on the concrete floor of a hut with a thin aluminium roof, which was covered with about 1 inch of snow during the exposure, making a total thickness of less than 2 gm./cm.^{2}. It is estimated that this reduced the star rates by about 0·1 stars/c.c./day and, since both sets of plates were equally affected, no correction was applied. The plates were collected as soon as dry at Messrs. Ilfords, taken at sea level to Bagnères-de-Bigorre and then transported as quickly as possible to the summit of the Pic du Midi. The plates were brought back to sea level immediately after exposure. Since the times at various altitudes were known accurately, the background rate could be calculated. It amounted to 3·3 per cent of the total number of stars observed on the air plates.

The plates were developed in acidified Amidol, using the temperature-cycle method of Dilworth, Occhialini and Payne (1948). They were shown to be sensitive to minimum ionization by observation of $\mu \rightarrow e$ decays

TABLE I.

Types of Stars in Air Plates at 2860 m.

$N_H \longrightarrow$

	3	4	5	6	7	8	9	10	11	12	13	14	15	16	17	18	19	20	21	22	23	24	25	Total
0*n*	572	380	193	91	56	51	28	11	8	4	2	1	5	1	1		1							1402
0*p*	31	28	26	18	8	11	6	3	3	1	1	1		1	1	1		1			1			142
1*n*	37	19	21	15	8	7	6	3	2	1	2		1		1	1								124
1*p*	18	13	16	5	3	4	2	2			1							1						65
2*n*	1	2	5	3	4		3	1	2	1	2	1					1	1						27
2*p*	3	5	1		1	3	2			1		1		1										18
3*n*				1		1	1		1	1														5
3*p*	2			1	1	1			1												1			7
4*n*											1		1											2
4*p*	1				1																			2
5*n*			1	1																				2
5*p*				1																				1
>5*n*																					1(11*n*)			1
>5*p*		1(6*p*)												1(7*p*)										2

To get the rate/c.c./day after correcting for the background multiply by $\sim 5{\cdot}0 \times 10^{-3}$.

TABLE II.

Types of Stars under 30 cms. of Lead at 2860 m.

$N_H \longrightarrow$

	3	4	5	6	7	8	9	10	11	12	13	14	15	16	17	18	19	20	21	22	23	24	25	Total
0*n*	554	356	202	88	45	25	20	5	4	6	2	1		1	2			1						1312
0*p*	35	31	32	21	18	8	10	4	2	4	2	1		2			1							171
1*n*	24	22	14	10	4	8	7	3	1	1		2	1			1				1				99
1*p*	17	16	9	13	8	2	1	1	4	2		2				2								77
2*n*		2	2	2		1	2			1						1		1				1		13
2*p*	5	7	1	2	1	1	1		2	1		2		2	1						1			27
3*n*	1	1			2			1				1			1									7
3*p*	1	3	1		1				1		1			1		1					1	1		12
4*n*				1	1				1						1									4
4*p*													1										1	2
5*n*																1								1
5*p*				1						1														2
>5*n*														1(6*n*)						1(14*n*)				2
>5*p*														1(9*p*)		1(6*p*)								2

To get the rate/c.c./day after correcting for the background rate multiply by $\sim 1{\cdot}74 \times 10^{-3}$.

in the emulsion. The efficiency of detection of minimum ionization tracks was probably only about 90 per cent (Cosyns *et al.* 1949) because of the loss of tracks dipping steeply into the emulsion. Since, however, the main conclusions deduced from the present experiment depend on the relative rates of events above and below lead, if the same percentage loss of minimum ionization tracks occurs in both sets of plates the effect is not important. There is also a possibility of non-associated tracks passing so close to a star that they are accepted as being associated with the star. A strict criterion was adopted, namely, two minimum ionization tracks were not accepted as belonging to a star unless there was an observable deflection between the tracks at the star. In this way spurious events were cut to a minimum.

The choice of thickness of emulsion was dictated by the need for fast and accurate scanning. The rate of accumulation of data increases with increasing thickness of emulsion, but the percentage of events missed also increases. After some test scanning on plates of different thickness it was decided that a thickness of about 300 μ was the optimum value for our experiment.

The results obtained, when the same area of plate was scanned using first a 10× objective, then a 20× objective, then a 45× objective, were compared. It was found that with the 10× objective 20–30 per cent of all stars were lost, but with the 20× objective less than 2 per cent of all stars were missed. This was less than the statistical accuracy aimed at and, furthermore, the losses affected both sets of plates equally. The scanning was therefore carried out using 20× Cooke objectives and 10× eyepieces. The stars were examined in detail with 45× oil immersion objectives and grain counts were made on the tracks. To be accepted in the analysis a star had to have at least three prongs or two prongs and a short nuclear fragment. No two-pronged stars were accepted, as it was difficult in a large number of cases to distinguish between a two-prong star and a scattering of a heavy particle. Stars which had all tracks less than 65 μ long were excluded on the grounds that they were probably of radioactive origin. No separation of σ meson stars was made, and thus stars of two or more prongs produced by π mesons at rest were included in the analysis.

The stars were classified in the same way as was used by Brown *et al.* (1949), and the results are shown in Tables I. and II. The number of tracks with a grain density less than 1·5 times minimum is denoted by n_s, and the number with grain density greater than 1·5 times minimum by N_H.

§ 3. EXPERIMENTAL RESULTS.

The results obtained with the air and lead plates are shown in Tables I. and II. respectively. The total rate of stars observed in the air plates was 9·0±0·3 stars/c.c./day, after correcting for the background rate. This rate can be compared with rates obtained by Brown *et al.* (1949) and Bernardini *et al.* (1950) at 3500 m. Assuming the attenuation length for all stars in the atmosphere to be 135 gm./cm.^{2}, the rate observed at the Pic du Midi is equivalent to a rate of 14·1±0·4 stars/c.c./day at 3500 m. The rate obtained by Brown *et al.* was 10·8 stars/c.c./day. This value is significantly lower than the present result, but the difference is confined to 3- and 4-prong stars. The present result is, however, consistent with the rate of 14·2±0·5 stars/c.c./day observed by Bernardini *et al.*

The rate observed under 30 cms. of lead was 2·96±0·09 stars/c.c./day after correcting for the background rate.

Assuming that the absorption is exponential, the attenuation length of all stars in lead is 305±7 gm./cm.^{2}. This value compares favourably with the values of 310±20 gm./cm.^{2} and 300±20 gm./cm.^{2} obtained by George and Jason (1949) and Bernardini *et al.* (1949 a) respectively.

The attenuation lengths for the various types of events are shown in Table III.

TABLE III.

Attenuation Lengths in Lead.

Type of event	Attenuation length gm./cm.^{2}
All stars	305±7
$0p+1p+2p+\ldots$	405±31
$1n+2n+3n+\ldots$	260±34
$2n+2p+3n+3p+\ldots$ (Penetrating showers)	380±65

The significance of these results will be discussed in the next section.

§4. DISCUSSION OF EXPERIMENTAL RESULTS.

4.1 *Constancy of the Size Frequency Distribution.*

The experiments of Bernardini, Cortini and Manfredini (1949 a) showed that the size frequency distribution of the stars observed in Ilford C2 emulsions varied little between sea level and 20,000 m., which suggests that the energy spectrum of N-rays has the same shape at all depths in the lower atmosphere. To compare these results with those from the present experiment, the numbers of stars with different numbers of heavy tracks are collected in Table IV. for both sets of plates. The numbers are normalized to 100 for $N_H=5$.

Comparing row (i.) with row (ii.), it will be seen that the frequency distribution for different values of N_H is the same above and below 30 cms. of lead. The results of Bernardini *et al.* (1950) show, however, that there is a much larger proportion of 3- and 4-prong stars under 2 cms. of lead; under 30 cms. of lead this transition effect vanishes.

The results of Malaspina *et al.* (1950) showed a higher rate of stars in plates placed on top of a lead absorber than in plates not placed on lead, suggesting that there is a larger backward emission of secondary neutrons capable of producing 3- and 4-prong stars than in an equivalent thickness of air. The difference is probably connected with the larger size of stars in lead than in air. Under large thicknesses of lead the excess backward flux of star primaries will combine with the secondary N-rays emitted in the forward direction in the lead above the plates, giving the same form for the spectrum of N-rays as in air. In the present experiment the plates were placed on concrete, so that there is a deficiency of star primaries incident on the plates from the concrete. Comparison with the results of Bernardini *et al.* (1950) under 2 cms. of lead shows that the decrease should be equivalent to about 6 per cent of all stars. There is, however, a compensating effect which increases the proportion of 3- and 4-prong stars, namely, an increase in σ meson stars due to the fact that in lead π mesons have a greater probability of stopping before decaying into μ mesons than in air. Two-prong stars produced by σ mesons are included in the present analysis. The number of such stars in the air plates depends on the proximity of dense absorbers. Various estimates place the proportion of σ meson stars with two or more evaporation prongs to be about 3 per cent of all stars. According to Bernardini *et al.* (1949 b), the proportion of such stars increases by a factor (2·6±0·7), under large thicknesses of lead, making an overall increase of about 5 per cent in all stars. The increase occurs mainly in stars of 3 and 4 prongs. This effect tends to compensate the transition effect and accounts for the constancy of the size frequency distribution.

TABLE IV.

Size Frequency Distribution of Stars.

	Numbers of stars (normalized to 100 for $N_H=5$)								
N_H / Absorber	3	4	5	6	7	8	9	≥10	≥6
(i.) light roof	251±10	163±8	100±6	52±4	31±4	30±4	18±5	32±3	162±9
(ii.) 30 cm. lead	245±10	168±7	100±6	53±5	31±4	17±3	16±3	35±3	152±8
(iii.) 2 cm. lead. (After Bernardini *et al.* 1950)	360±20	244±20	100±6						150±5

4.2 *The Attenuation Length for all Stars.*

The attenuation length in lead for all stars is :

$$\lambda_A = 305 \pm 7 \text{ gm./cm.}^2.$$

It is interesting to compare this value with that obtained under other absorbers by various workers.

It has been suggested that the values are proportional to $A^{1/3}$, suggesting that the cross-section for star production is proportional to the geometrical cross-section. As pointed out by Ritson (1950), however, the values given in Table V. are not very consistent with an $A^{1/3}$ law.

The picture of nucleon cascades allows us to interpret the results in a different way. Since the B-component is to a large extent secondary to the A-component the attenuation length of the primaries of evaporation stars depends on the attenuation length of the parent penetrating-shower primaries. This dependence is not complete under 30 cm. of lead since a large number of the N-rays present are due to the B-component incident from the atmosphere. Moreover, since the nuclear interactions of the A-component are included in the analysis, λ_A for all stars depends to a large extent on λ_A for penetrating showers ($n_s \geqslant 2$). The interaction mean-free-paths of the primaries of penetrating showers have been determined for lead and carbon by Cocconi (1949 a, b) and by Walker *et al.* (1950) using counter arrangements. The value for lead is 160 gm./cm.^{2} and is consistent with a cross-section equal to the geometrical cross-section. For carbon Walker *et al.* find (81±5) gm./cm.^{2} which is longer than the interaction mean-free-path corresponding to the geometrical cross-section, suggesting that there is some transparency of the carbon nucleus.

TABLE V.

Attenuation Length in Different Materials (in gm./cm.^{2}).

Authors	Material				
	Carbon	Ice	Aluminium	Lead	Air
Barton, George and Jason (1951)	166±7				
George and Jason (1949)				310±20	150
Bernardini *et al.* (1949 a)			220	300±20	135
Harding, Lattimore, Li and Perkins (1949)		200±10			

We see that

$$\frac{\lambda_{I(C)}}{\lambda_{I(Pb)}} \simeq \frac{81}{160} \sim \frac{1}{2}$$

$$\sim \frac{\lambda_{A(C)}}{\lambda_{A(Pb)}}$$

for penetrating showers. This is the same ratio as the attenuation length for all stars. Thus the ratio of the values of λ_A for all stars under lead and carbon can be understood in terms of the absorption of penetrating-shower primaries, with the B-rays keeping in equilibrium with the A-rays.

This is not completely true since some B-rays are incident from the atmosphere but due to the transparency for penetrating showers λ_I need not necessarily be proportional to $A^{1/3}$. Furthermore, approximately one-quarter of all stars are due to B-rays emitted in the backward direction. The number of these depends on the nature of the absorber beneath the plate so that the value for the attenuation length of all stars varies with experimental conditions.

Another interesting fact, pointed out by Barton, George and Jason (1951) is that for all stars λ_A (carbon) is greater than λ_A (air) even though the atomic weight of carbon is less than the atomic weight of air. Barton *et al.* suggested that the difference was due to the production of stars by π mesons since for carbon the mean-free-path for star production is smaller than the mean-free-path for $\pi \rightarrow \mu$ decay whereas in air the mean-free-path for $\pi \rightarrow \mu$ decay is shorter. Therefore the attenuation length for all stars in dense absorbers depends on the local production of π mesons.

4.3. *Comparison of λ_A and λ_I for the Primaries of Penetrating Showers.*

The interaction mean-free-paths of the primaries of penetrating showers in lead has been determined by Cocconi (1949 a, b), Walker (1950) and Sitte (1950) from experiments with counters. These workers found $\lambda_I \sim 160$ gm./cm.^{2}, which is consistent with a cross-section equal to the geometrical cross-section of the lead nucleus. Walker (1950) found that λ_I increased with decreasing number of relativistic secondaries required to trigger his penetrating shower set, for example, λ_I was (150 ± 8) gm./cm.^{2} for $n_s > 5$ and 208 gm./cm.^{2} for $n_s = 3$.

Penetrating showers in the photographic emulsion will be defined as events with $n_s \geqslant 2$, that is events of the types $2n + 2p + 3n + 3p + \ldots$. The attenuation length is determined by observations made with the photographic emulsion and the value obtained is $\lambda_A = (380 \pm 65)$ gm./cm.^{2}. The comparable value from Walker's experiment for λ_I is probably ~ 208 gm./cm.^{2}. It is seen that the attenuation length is longer than the interaction mean-free-path. The probability that λ_A is less than or equal to 208 gm./cm.^{2} is less than 0·5 per cent so that the increase can be taken as significant, which means that on the average penetrating-shower primaries give rise to more than one penetrating shower in lead. The experimental value of λ_A/λ_I is $(1{\cdot}85 \pm 0{\cdot}3)$ for events with $n_s \geqslant 2$.

The value of the interaction mean-free-path in carbon is rather uncertain, because of the inconsistency in the experimental results, so that λ_I for carbon cannot be compared with the attenuation length for penetrating-shower primaries in air. It must be borne in mind that the value of λ_A/λ_I for lead may be larger than the corresponding ratio for air because of the contribution from π mesons produced locally in the lead. On the other hand the ratio may be reduced because of the larger probability for successive nucleon collisions within the same nucleus, with a consequent larger energy loss per interaction.

4.4. *Stars Produced by Fast π Mesons under Lead.*

In the present experiment it is possible to observe stars produced directly by fast π mesons as they should lead to an increase under lead in the proportion of stars with charged relativistic primaries. The attenuation length in lead for events of the type $0p+1p+2p+\ldots$ is (405 ± 31) gm./cm.^{2}, and for events of the type $1n+2n+3n+\ldots$ is (260 ± 34) gm./cm.^{2}. In the lower atmosphere these lengths should be approximately equal. The value of λ_A for events of the type $0p+1p+2p$ is larger than the value for events of the type $1n+2n+\ldots$ by almost exactly three times the standard deviation of their difference so that it is safe to conclude that some stars under lead are due to fast π mesons generated locally in lead. From Tables I. and II. it can be seen that the ratio of $0p+1p+2p+\ldots$ events to all stars increases from $(13{\cdot}1\pm0{\cdot}9)$ per cent for the air plates to $(17{\cdot}0\pm1{\cdot}0)$ per cent for the plates under 30 cm. of lead, giving an increase equivalent to $(3{\cdot}9\pm1{\cdot}3)$ per cent of all stars.

Twenty-six of the fast charged primaries in the lead plates were suitable for identification from measurements of their multiple Coulomb scattering and grain density (*cf.* Fowler 1950), and of these eight were shown to be less massive than protons. This result is consistent with the estimated proportion of such events which are due to fast π mesons.

The number of stars due to fast π mesons under 30 cm. lead is approximately equal to the number of σ meson stars produced by π mesons at rest. The two are comparable because the probability of a π meson stopping in the emulsion is of the same order as the probability of a fast π meson passing through the emulsion giving rise to a nuclear interaction (*cf.* Bernardini, Cortini and Manfredini (1949 b).

It is possible that some of the events of the type $1p$, $2p$, $3p$, etc., in the lead plates are the same as the events observed by George and Evans (1950) at 60 m. water equivalent underground. According to these authors the rate of such events at the altitude of the Pic du Midi should be about 0·03 stars/c.c./day, that is, about 1 per cent of all stars in the lead plates or 12 per cent of $1p+2p+3p+\ldots$ events. It is not possible to confirm the presence of such events due to μ mesons because of poor statistics and because such events may be produced by π mesons generated locally.

Since the observed proportion of stars due to π mesons in the lead plates is $(3{\cdot}9\pm1{\cdot}3)$ per cent of all stars probably less than 6 per cent of all stars are produced directly by π mesons generated locally. This proportion in itself is not sufficient to account for the difference between λ_A (air) and λ_A (carbon) observed by Barton *et al.* (1951). However, the π mesons generated locally may give rise to energetic secondary nucleons in nuclear interactions in the absorber above the plates thus increasing the proportion of stars associated with the π mesons generated locally.

From Tables I. and II. the ratio of charged to uncharged primaries of penetrating showers (*i. e.* events of the types $n_s\geqslant2$) is $(0{\cdot}86\pm0{\cdot}21)$ for the air plates and $(1{\cdot}67\pm0{\cdot}37)$ for the plates exposed under 30 cm. of lead.

For nucleon cascades in air the ratio should remain constant and close to unity at all depths in the lower atmosphere. However, under lead the ratio increases to $1{\cdot}67 \pm 0{\cdot}37$). Our statistics alone are not good enough to establish the increase with certainty, but a similar experiment carried out at Bristol leads to a similar result. During a preliminary analysis the Bristol workers observed 84 penetrating showers under 30 cm. of lead and of these showers 58 appeared to have charged primaries and 26 neutral. Combining the two sets of results the ratio of charged to uncharged penetrating shower primaries under 30 cm. of lead is $(1{\cdot}94 \pm 0{\cdot}32)$. This figure is greater than one with a probability of more than 99 per cent.

It is possible that part of the increase may be due to events of the type observed by George and Evans (1950) who found that four of the ten stars produced at 60 m. water equivalent underground by relativistic primaries had more than one relativistic secondary. This would correspond to an increase of about 15 per cent in the ratio of charged to uncharged penetrating showers but is not sufficient to double the ratio.

A more likely explanation is the production of events of the type $2p+3p+\ldots$ by π mesons generated locally in the lead. One possible scheme for the production of events of the type $2p$ is the elastic collision of a π meson with a proton in a nucleus, both the π meson and proton emerging from the nucleus with relativistic velocities. Such a process is energetically possible for a primary π meson of energy about 2×10^9 eV. The probability for the process depends on the cross-section for the elastic collision of π mesons with protons, and since this cross-section is not yet known the contribution cannot be estimated. Two further possible theoretical schemes for the production of penetrating showers by π mesons have been suggested by Heitler and Janossy (1950). In the first scheme it is suggested that a π meson might give a large fraction of its energy to a nucleon inside a nucleus and the nucleon then give rise to a penetrating shower. According to Camerini *et al.* (1950 b) a nucleon needs on the average an energy of 4×10^9 eV. to give rise to an event of the type $n_s \geqslant 2$, so that the π meson would need more than this energy. Now it has already been shown that approximately 4 per cent of the stars under 30 cm. of lead are due to fast π mesons. Less than 10 per cent of these π mesons would, however, have energies greater than 4×10^9 eV. These π mesons could contribute to a small increase in the ratio of the charged to uncharged penetrating-shower primaries; the maximum increase due to this effect is estimated to be 20 per cent, which is hardly sufficient to account for the observed ratio of $(1{\cdot}94 \pm 0{\cdot}32)$. In the second scheme suggested by Heitler and Janossy π mesons may give rise to penetrating showers by a multiple process in which the primary π meson splits up into several mesons. These authors suggest that if the energy of a π meson is about 10^9 eV. it might split into two or three secondary mesons which would be observed as events of the type $2p$ and $3p$ in electron sensitive emulsions. Approximately 30 per cent of the π mesons under 30 cm. of lead have energies greater than 10^9 eV. so that if the probability for such a process were high it could lead to an appreciable increase in the ratio of charged to uncharged penetrating-shower primaries.

At present no definite conclusions can be drawn about the nature of these events, but it is suggested tentatively that they are mainly produced by fast π mesons generated locally in the lead.

ACKNOWLEDGMENTS.

This experiment was started with the co-operation of Miss C. Dilworth of Brussels University and Dr. Bonetti of Genoa, and we wish to record our thanks for their assistance in the initial stages of the work.

We are greatly indebted to Professor P. M. S. Blackett, F.R.S. for facilities to carry out this work and to Dr. G. D. Rochester who has given us continual help both during the experiment and in the discussion of the results.

We also wish to thank Professor Powell, F.R.S. and Dr. Camerini for sending us the preliminary results obtained at Bristol on the ratio of charged to uncharged primaries of penetrating showers, Professor J. Rösch for facilities to expose the plates on the Pic du Midi, Mr. C. Waller of Ilford Ltd. for supplying the plates, Mr. S. J. Goldsack for exposing them, and Mrs. E. Birchall and Mrs. V. Bouch for carrying out the tedious work of scanning them.

REFERENCES.

BARTON, J. C., GEORGE, E. P., and JASON, A. C., 1951, *Proc. Phys. Soc.* A, **64,** 175.

BERNARDINI, G., CORTINI, G., and MANFREDINI, A., 1949 a, *Phys. Rev.*, **76,** 1792 ; 1949 b, *Nuovo Cimento*, **6,** *Supplemento*, **3,** 431 ; 1950, *Phys. Rev.*, **79,** 952.

BROWN, R. H., CAMERINI, U., FOWLER, P. H., HEITLER, H., KING, D. T., and POWELL, C. F., 1949, *Phil. Mag.*, **40,** 812.

CAMERINI, U., FOWLER, P. H., LOCK, W. O., MUIRHEAD, H., 1950 a, *Phil. Mag.*, **41,** 413.

CAMERINI, U., FOWLER, P. H., LOCK, W. O., MUIRHEAD, H., and YEKUTELI, 1950 b, private communication.

COCCONI, G., 1949 a, *Phys. Rev.*, **75,** 1074 ; 1949 b, *Ibid.*, **76,** 948.

COSYNS, M. G. E., DILWORTH, C. C., OCCHIALINI, G., SCHOENBERG, M., and PAGE, N., 1949, *Proc. Phys. Soc.* A, **62,** 801.

DILWORTH, C., OCCHIALINI, G., and PAYNE, R. N., 1948, *Nature, Lond.*, **162,** 102.

FOWLER, P. H., 1950, *Phil. Mag.*, **40,** 169.

FUJIMOTO, Y., and HAYAKAWA, S., 1949, *Prog. Theor. Phys.*, **4,** 502.

GEORGE, E. P., and EVANS, J., 1950, *Proc. Phys. Soc.* A, **63,** 1248.

GEORGE, E. P., and JASON, A. C., 1949, *Proc. Phys. Soc.*, **62,** 243.

HARDING, J. B., LATTIMORE, S., LI, T. T., and PERKINS, D. H., 1949, *Nature, Lond.*, **163,** 320.

HEITLER, W., and JANOSSY, L., 1950, *Helv. Phys. Acta*, **23,** 417.

MALASPINA, L., MERLIN, M., PROVACCI, D., and ROSTAGNI, A., 1950, *Nuovo Cimento*, **7,** 145.

RITSON, D. M., 1950, private communication.

ROSSI, B., 1948, *Rev. Mod. Phys.*, **20,** 537.

SITTE, K., 1950, *Phys. Rev.*, **78,** 714.

WALKER, W. D., 1950, *Phys. Rev.*, **77,** 686.

WALKER, W. D., WALKER, S. P., and GREISEN, K., 1950, *Phys. Rev.*, **80,** 546.

LXXXVIII. *On the State of Stress in a Plastic-Rigid Body at the Yield Point.*

By R. Hill,
H. H. Wills Physical Laboratory, University of Bristol†.

[Received May 9, 1951.]

Summary

The yield point of a plastic-rigid body is defined as the moment when deformation first becomes possible as the load is increased. The practical significance of the yield-point load for an actual plastic-elastic body is discussed. It is then shown that part of the plastic zone at the yield point, namely the part where deformation occurs, depends only on the current surface tractions and not on the previous loading programme. By means of the principle of maximum plastic work and its complimentary minimum principle (Hill 1950) approximations from above and below to the yield-point load can be obtained ; some examples are given. Recent American work on the plastic limit design of structures is critically reviewed and shown, when properly regarded, to be a particular application of the principle of maximum plastic work.

§ 1. The Definition and Significance of the Yield Point.

The following considerations relate to an ideal work-hardening plastic-rigid material in which Young's modulus is indefinitely large. Consider a mass of such material subjected to some loading sequence. The moment when it first becomes locally plastic is usually known as the *elastic limit*, while the moment when it begins to deform will here be called the *yield point* (the term *collapse*, which has also been suggested, is suitable only when the subsequent deformation would render the body useless). When the elastic limit and the yield point are not coincident, the body remains entirely rigid in the corresponding loading interval, even though partly plastic. The calculation of the stress state and development of the plastic zone while the whole body is rigid have already been discussed by the writer (1950 a, pp. 237–245). Here, it is proposed to examine certain properties of the stress state at the yield point itself which depend only on the current surface tractions and not on the previous loading history.

In the absence of passive constraints the rate at which the loads need to be increased to enforce further distortion following the yield point is governed mainly by the rate of strain-hardening—though also by the changes of shape (so that even if the hardening is zero the load does not

---

† Communicated by the Author.

generally remain constant during a finite distortion†). When the rate of hardening is of the order of the yield stress, only a slight increase in load is sufficient to produce strains of a magnitude which would, in an actual structure, be regarded as amounting to callapse.

Correspondingly, in a slowly hardening *plastic-elastic* body such strains generally occur under loads differing little from the plastic-rigid yield-point loads. The previous permanent deformation, occurring since the elastic limit, is of an elastic order of magnitude, due to the constraint of the non-plastic material ; an overall load-displacement curve has therefore a pronounced bend in a small loading interval in the neighbourhood of the plastic-rigid collapse load. (An obvious exception is when the plastic zone is entirely contained within an elastic zone which accommodates the severe local distortions, as when pressure is applied to a small cavity). In this sense, the plastic-rigid yield-point loads have a significance for an actual (plastic-elastic) body in which the definition of a precise moment of collapse, or yielding, must be somewhat arbitrary. More exactly, if a non-hardening plastic-elastic body is monotonically strained, the requisite loads approach asymptotically (though not necessarily steadily) to the plastic-rigid yield-point loads when changes of shape are ignored in the analysis. The asymptotic values are generally not reached in any finite strain (the contrary is often wrongly stated), but the actual loads differ from them only by an insignificant amount after a permanent strain which is still of an elastic order of magnitude.

The main purpose of the present paper is to examine the factors governing the distribution of stress in a plastic-rigid body at the yield point, and to draw attention to some rather surprising properties which have not been observed before.

These properties are intimately related to certain extremum theorems for a plastic-rigid body, namely the principle of maximum plastic work and its complementary minimum principle established by the writer (1948 and 1950 b). These principles refer to the rate of working of forces on the surface of a plastic zone, at all points of which deformation is occurring (the zone does not necessarily extend over the whole body). Since any equilibrium system of forces acting on a rigid zone does no work, the extremum principles apply also to the work of the forces on a body which is only partly plastic. These theorems supply a means of obtaining approximations, from above and below, to the actual rate of work, and also, in certain situations, to the yield-point loads themselves. However, by contrast to the analogous methods for a perfectly elastic body, they do not furnish approximations to the whole *internal* state of stress in a partly plastic body at the yield point since this depends, *in part*, on the previous loading programme. It is only for particular surface tractions, such that deformation can occur under them at all points, that the whole internal state of stress is unique (this was first shown by the writer in discussing the problem of a uniformly bent and twisted beam ; 1948).

---

† For this reason the term "flow limit", suggested in a recent paper by Pell and Prager, is unsatisfactory, as "flow" signifies deformation under constant stress.

Recently, approximation methods, identical in principle, have been applied by American writers on limit design of structures (*e. g.* Greenberg and Prager 1951). Owing, presumably, to the simplifications involved in the conventional idealization of a structure, it has escaped notice that the relevant theorems are special cases of the maximum work principle and its complement. This is even unremarked by Pell and Prager (1951) who treat the continuum problem of the yield point of a completely plastic plate under uniform loading, and also by Drucker, Greenberg, and Prager (1951)†. To the latter is due the first illustration of the usefulness of the methods when the body is *partly* plastic, viz. that of the collapse of a pressure vessel. A further illustration has been given by the writer in the problem of the indentation of a thin strip by a pair of opposed dies (described by A. P. Green, 1951, who has obtained the exact solution). Other applications are outlined below.

§ 2. The Plastic Stress-state at the Yield Point.

Let the criterion of yielding of an element be

$$f(\sigma_{ij})=0 \quad . \quad . \quad . \quad . \quad . \quad . \quad . \quad . \quad . \quad (1)$$

in some given state of hardening. The rate of strain under continued loading is taken as

$$\dot{\epsilon}_{ij}=\lambda \frac{\partial f}{\partial \sigma_{ij}} \quad . \quad . \quad . \quad . \quad . \quad . \quad . \quad . \quad . \quad (2)$$

where λ is a positive scalar factor of proportionality. This relation between the ratios of the components of the stress and strain-rate tensors is suggested by experiment, and has also been derived theoretically for an aggregate of crystals which deform by slip according to the Schmid law (Bishop and Hill 1951).

If the criterion (1) be regarded as a surface in stress hyperspace, equation (2) states that the vector representation of $\dot{\epsilon}_{ij}$ is parallel to the outward normal at the stress point σ_{ij}. If the yield surface is everywhere concave to the origin (so that the relation between the directions of the stress and strain-rate vectors is one-one), it is evident that

$$(\sigma_{ij}-\sigma^*_{ij})\dot{\epsilon}_{ij}\geqslant 0 \quad . \quad . \quad . \quad . \quad . \quad . \quad . \quad . \quad . \quad (3)$$

where σ^*_{ij} is any stress within or on the surface (the summation convention being adopted.) This is the maximum work principle for an element ; it states that the actual stress does work at a rate not less than any other stress compatible with the yield condition.

---

† The work of all these writers is marred by erroneous statements that the theorems apply to a plastic-elastic material ; furthermore, collapse is *defined* as deformation under constant load—a situation which generally does not occur, as mentioned previously.

Consider, now, the yield point of a body under given forces F_i per unit area over a part S_F of the surface S, and given velocities u_i over the remainder S_U (more generally, certain components of F_i and the complementary components of u_i may be given over the same part of the surface). Consider the set of equilibrium states of stress, and associated velocity distributions, corresponding to the same distribution of hardening and the same given surface conditions. The stress must satisfy (1) and (2) wherever the respective strain-rates do not vanish, and must not violate the yield condition elsewhere. Included among this set are, of course, actual yield-point stress states and their associated distortion modes; such actual states may be considered to be reached from different initial states of residual stress or by different loading programmes. Let (σ_{ij}, u_i) and (σ^*_{ij}, u^*_i) be any two members of the set. Across certain internal surfaces some of the components of stress may be discontinuous; for equilibrium, only the stress resultants need be continuous. Across other internal surfaces the velocity may be tangentially discontinuous; such a surface of discontinuity has to be regarded as the limit of a narrow layer through which the velocity component parallel to the surface changes rapidly. The state of stress at each point of a discontinuity is therefore that corresponding to a simple shear strain-rate in the direction of the relative velocity vector. The material being assumed isotropic, the stress is thus a pure shear, k say, along the discontinuity, together with some hydrostatic component; since f is concave to the origin and is assumed not to involve the hydrostatic component of stress, no shearing stress component can exceed k in a given state of hardening. Let τ^* be the shear component of σ^*_{ij} along a discontinuity of u_i, and τ be the shear component of σ_{ij} along a discontinuity of u^*_i. Then, by virtual work,

$$\int(\mathrm{F}_i-\mathrm{F}^*_i)(u_i-u^*_i)\,d\mathrm{S}=\int(\sigma_{ij}-\sigma^*_{ij})(\dot{\epsilon}_{ij}-\dot{\epsilon}^*_{ij})\,d\mathrm{V}+\int(k-\tau^*)[u]\,d\mathrm{S}_\mathrm{D} \\ +\int(k-\tau)[u^*]\,d\mathrm{S}^*_\mathrm{D}, \quad . \quad . \quad . \quad (4)$$

where the square brackets denote the absolute amount of the discontinuities across the respective surfaces S_D and S^*_D. The left-hand side vanishes identically since one or other of the factors is zero at each point of the surface of the body. According to (3) and the fact that τ and τ^* cannot exceed k numerically, all terms on the right-hand side are non-negative. Hence they must each be zero. This requires that the deviatoric parts of σ_{ij} and σ^*_{ij} are equal on S_D and S^*_D and wherever $\dot{\epsilon}_{ij}$ or $\dot{\epsilon}^*_{ij}$ is not zero.

In other words, stress states of the set considered, and in particular actual yield-point states, are identical wherever deformation is occurring and can differ only in the common rigid zone. In particular, in plane strain, the slip-line field in the plastically-deforming zone is uniquely determined by the given surface conditions and internal hardening at the yield point. On the other hand, the present analysis says nothing about the possible modes of distortion (except in so far as they must be compatible with the stress). This theorem justifies the procedure adopted in the past for calculating yield-point loads : namely, to ignore the development of the plastic zone and to find some stress and velocity distribution satisfying boundary conditions at the yield point only. It is necessary also to show that there is an associated stress distribution in the rigid zone, not violating the yield condition ; in so far as this is left unexamined, previous solutions are not completely rigorous, as the writer has frequently emphasized. If the yield condition is in fact locally exceeded in the rigid zone by a certain amount, such a solution is valid for a material which is at least that much harder there than the one under consideration. It is intuitively obvious, and an immediate consequence of the maximum work principle (5) below, that the yield-point load will then tend to be overestimated.

An example of the use of this theorem may be instanced. Consider the slip-line field and associated velocity solution proposed by Prandtl to satisfy the surface conditions at the yield point of a semi-infinite block indented by a flat die. If it could be proved (as seems probable) that there exists an associated stress distribution in the rigid zone, not violating the yield condition, then it would follow that the actual plastic zone certainly extends at least as far as Prandtl's slip-line field. Similar conclusions hold for the notched bar problem (Hill 1950 a, pp. 249–251). It would not necessarily follow, however, that the mode of distortion suggested by Prandtl is the actual one for an initially stress-free and uniformly hardened block. To prove that an assumed mode is correct, it is essential, as remarked by the writer (1950 c), to examine the stress increment occurring during an increment of distortion and to show that all elements assumed to deform have in fact remained plastically stressed. (There is no possibility of overlooking this point when dealing with a plastic-*elastic* material since the stress increment in any case enters the relations between the ratios of the components of stress and total strain-rate). This applies equally to the alternative mode suggested by the writer for this problem (*op. cit.*). To what extent a yield-point mode is independent of loading history is a matter for future research.

§ 3. EXTREMUM PRINCIPLES.

Let σ^*_{ij} now refer to any equilibrium state that does not violate the yield condition at any point where $\dot{\epsilon}_{ij}\neq 0$ (σ^*_{ij} is not necessarily any actual yield-point state). Then, as in (4),

$$\int(\mathrm{F}_i-\mathrm{F}^*_i)u_i\,d\mathrm{S}_{\mathrm{U}}=\int(\sigma_{ij}-\sigma^*_{ij})\dot{\epsilon}_{ij}\,d\mathrm{V}+\int(k-\tau^*)\,[u]\,d\mathrm{S}_{\mathrm{D}}\geqslant 0 \quad . \quad . \quad . \quad (5)$$

if $\mathrm{F}^*_i=\mathrm{F}_i$ on S_{F}. This is the maximum work principle for a finite body (Hill 1948).

In particular, if $\mathrm{F}^*_i=\mathrm{F}_i$ all over the surface the left-hand side of (5) vanishes. Since each term on the right-hand side is non-negative, both must be zero and σ^*_{ij} must equal σ_{ij} wherever deformation is occurring (including, of course, velocity discontinuities.) Thus, if given forces act on the surface of a body in a given state of hardening and if it is possible to find some corresponding internal equilibrium distribution of stress σ_{ij} and velocity u_i, satisfying (1) and (2) where $\dot{\epsilon}_{ij} \neq 0$ (with positive λ), then, wherever $\dot{\epsilon}_{ij} \neq 0$, the body must certainly be plastic and this σ_{ij} must be the actual stress.

For the complementary minimum principle consider any velocity distribution u_i^* having zero divergence and such that $u_i^* = u_i$ on S_U. Then, by virtual work,

$$\int F_i u_i^* \, dS = \int \sigma_{ij} \dot{\epsilon}_{ij}^* \, dV + \int \tau [u^*] \, dS_D^* .$$

Let σ_{ij}^* be the stress that would be needed to produce a strain-rate $\dot{\epsilon}_{ij}^*$ in the given state of hardening; the distribution σ_{ij}^* is not necessarily in equilibrium and is undefined where $\dot{\epsilon}_{ij}^* = 0$. Then, by the maximum work inequality (3) and the fact that $|\tau| \leqslant k$,

$$\int F_i u_i \, dS_U \leqslant \int \sigma_{ij}^* \dot{\epsilon}_{ij}^* \, dV + \int k [u^*] \, dS_D^* - \int F_i u_i^* \, dS_F , \quad . \quad . \quad . \quad (6)$$

which is complementary to (5). This result is more general than one obtained previously by the writer (1950 b), which was valid only for the yield criterion of von Mises. For the latter, $|\sigma'_{ij}| = \sqrt{(\sigma'_{ij}\sigma'_{ij})} = \text{const.}$, where σ'_{ij} is the stress deviator, and $\sigma_{ij}^* \dot{\epsilon}_{ij}^* = |\sigma'_{ij}| |\dot{\epsilon}_{ij}^*|$. In plane strain, $\sigma_{ij}^* \dot{\epsilon}_{ij}^* = k \dot{\gamma}^*$ whatever the function f, where $\dot{\gamma}^*$ is the maximum shear strain-rate (twice the tensor component).

§ 4. APPROXIMATE ESTIMATION OF YIELD POINT LOADS.

According to (5) a lower bound to the rate of work by the forces over S_U is to be obtained by selecting any equilibrium distribution of stress not violating the yield condition. An upper bound, on the other hand, is to be obtained from (6) by means of any distribution of velocity. With a well-judged choice these bounds can be brought close enough to give a useful approximation to the actual rate of work on S_U.

When the prescribed velocity on S_U is uniform in magnitude and direction, a knowledge of the rate of work is equivalent to a knowledge of the load on S_U in that direction (and similarly when a component of velocity and the complementary component of force are given). This situation arises, for example, when a single load is applied to the body through a rigid plane die (as in indentation) or through a rigid part of the body itself (as in a notched-bar test). Similarly, when the velocity distribution on S_U amounts to a rigid-body rotation or twist, the bending or twisting couple is immediately calculable from the rate of work.

A slightly different problem presents itself when several loads are applied, their ratios at the yield point being given; this includes proportional loading, to which writers on limit design have restricted their attention. The single parameter specifying the absolute magnitudes of the loads is derivable from the extremum principles. To see this, let S_R now denote the part of the surface where the load-ratios r_i are given, S_F standing as before for the part where absolute values of certain loads are prescribed. In addition there may be fixed frictionless constraints, but specified non-zero velocities can no longer be admitted since the corresponding forces would appear as further unknowns. If $F_i = Fr_i$ on S_R at the yield point, then, as in (5),

$$F \geqslant F^*, \qquad (7)$$

on cancelling the factor $\int r_i u_i \, dS_R$, where σ^*_{ij} is such that $F^*_i = F^* r_i$ on S_R and $F^*_i = F_i$ on S_F. It follows from (7), as remarked by Greenberg and Prager (1951), that the value of F is unique. When the deformation zone develops from a single point a limiting argument appears sufficent to establish the same result. Also, as in (6),

$$F \int r_i u^*_i \, dS_R \leqslant \int \sigma^*_{ij} \dot{\epsilon}^*_{ij} \, dV + \int k[u^*] \, dS^*_D - \int F_i u^*_i \, dS_F. \qquad (8)$$

§ 5. Some Applications.

It is to be noted that the entire discussion and the approximation methods are equally relevant for those problems of steady motion where there is no hardening and where the external contour of the body is known *a priori*. Steady motion can, in fact, be regarded as the integrated result of incremental distortions due to a succession of yield points. So, for that matter, can any plastic problem, but since the external configuration is continually changing, or is not known beforehand, the present methods cannot be applied directly.

As an example of the estimation of a steady-state load, consider the drawing of a sheet in plane strain through a smooth wedge-shaped die (without bulging). An intuitively obvious lower bound is provided by the stress distribution corresponding to radial flow towards the virtual apex of the die : r being the fractional reduction, (5) gives $2k \ln\{1/(1-r)\}$ for a lower bound to the drawing stress, as in elementary theories of drawing. An upper bound is provided by a velocity distribution in which the reduction is effected by block-sliding over a criss-cross of lines, of which the extreme pairs pass respectively through the points of entry and exit. If the lines make equal angles θ with the axis, there is a constant velocity discontinuity across each pair. This is $\sin\alpha/\sin(\theta-\alpha)$ at the first, where 2α is the die angle, and is multiplied at each successive pair by a factor $\sin(\theta+\alpha)/\sin(\theta-\alpha)$. Since the dimensions of successive pairs are multiplied by the inverse factor the work of shearing for each line is the same. If there are n pairs (6) gives an upper bound of

$$\frac{2kn \sin\alpha \cos\alpha}{\sin(\theta-\alpha)\sin(\theta+\alpha)}$$

where

$$(1-r)^{1/n} = \frac{\sin(\theta-\alpha)}{\sin(\theta+\alpha)}.$$

The best approximation, with the corresponding value of θ, is to be obtained from the integral value of n making this upper bound least. In the practical range of reductions only the values $n=1$ and 2 need be considered. For those reductions not so far covered by an exact theory (see Hill 1950 a,

p. 167), the greatest difference between these upper and lower bounds is of order 5 per cent. In this range, then, the elementary theory (which assumes homogeneous distortion) is a fairly good approximation. However, contrary to general belief, there are reasons for thinking that the relative amount of redundant work does not tend to zero *steadily* as the reduction increases, but *oscillates* with a steadily decreasing amplitude.

Consider, finally, the yield point of a symmetrically-notched bar extended in plane strain. Let the width of the bar be w times the smallest section. An upper bound is obtained from a deformation consisting of block-sliding across a pair of lines from the notch roots, intersecting the longitudinal axis in an angle θ, say, and a pair passing from this point to the sides of the bar and making $\frac{1}{2}\pi-\theta$ with the axis. For the stress at the ends of the bar equation (6) gives an upper bound $k(\cot\theta+w\tan\theta)$. The smallest value of this is $2k\sqrt{w}$, when $\cot\theta=\sqrt{w}$. This is valid for any shape of notch geometrically compatible with this fictitious mode of yielding, but is obviously likely to be best for a parallel-sided notch with zero root radius (since this should have the highest constraint factor). An exact solution (Hill 1950, unpublished) gives a yield-point stress of $2{\cdot}05\times 2k$ for $w=4{\cdot}7$, compared with the upper bound of $2{\cdot}17\times 2k$. For $w\geqslant 8{\cdot}6$ exact calculation gives $2{\cdot}57\times 2k$ (Hill 1950 c), while the upper bound exceeds this value when $w\geqslant 6{\cdot}6$. We may infer that the constraint factor is not more than a few per cent less than $\sqrt{w}$ when w is less than about 3.

REFERENCES.

BISHOP, J. F. W., and HILL, R., 1951, *Phil. Mag.*, (April), **42,** 414.

DRUCKER, D. C., GREENBERG, H. J., and PRAGER, W., 1951, *J. App. Mech.* (in press). Paper No. 51–A3.

GREEN, A. P., 1951, B.I.S.R.A. Report MW/B/10/51. *Phil. Mag.* **42,** 900.

GREENBERG, H. J., and PRAGER, W., 1951, *Proc. Am. Soc. Civ. Eng.*, **77**.

HILL, R., 1948, *Quart. J. Mech. App. Math.*, **1,** 18 ; 1949, *idem*, **2,** 40 ; 1950 a, " The Mathematical Theory of Plasticity " (Clarendon Press) ; 1950 b, *J. App. Mech.*, **17,** 64 ; 1950 c, *Phil. Mag.*, **41,** 745.

PELL, W. H., and PRAGER, W., 1951, *Brown University Technical Report* 57.

LXXXIX. *A Theory of the α, α' Phases in the Al–Zn System.*

By R. S. Leigh,
Mathematics Department, Imperial College, London*.

[Received April 26, 1951.]

Summary.

In the binary alloys of Al–Zn there exists, above a certain temperature, a mixed crystal region in which the two phases α and α' both have the same face-centred cubic structure but with different compositions and lattice spacings. It is shown that an explanation for the formation of these phase boundaries is provided by the electronic theory of the elastic properties of single crystals of aluminium. A maximum in one of the shear constants at an electron concentration corresponding to the $\alpha+\alpha'$ region gives rise to a subsidiary maximum in the temperature-dependent part of the free energy, which leads, according to the usual construction, to a mixed phase region.

§ 1. Introduction.

In a recent paper (Leigh 1951) it has been shown that in aluminium solid solutions a maximum is to be expected in the shear constant $\frac{1}{2}(C_{11}-C_{12})$ at an electron concentration in the neighbourhood of 2·67 per atom. The elastic constants $\frac{1}{2}(C_{11}-C_{12})$ and C_{44} are shown in fig. 1 as functions of the concentration of a divalent solute. In the theory of the elastic properties of pure aluminium it was found necessary, in order to explain the observed values of the shear constants, to assume that there are a small number of electrons overlapping the square faces of the Brillouin zone. The sharp peak in $\frac{1}{2}(C_{11}-C_{12})$ occurs at the point at which this overlap disappears.

It is now shown that the maximum in $\frac{1}{2}(C_{11}-C_{12})$ provides an explanation for the existence of a mixed crystal region which, below 355° C., interrupts the range of stability of the primary solid solution of zinc in aluminium. The aluminium-rich end of the phase diagram of the Al–Zn system (Raynor 1944) is shown in fig. 2, with zinc concentration given in atomic per cent. The mixed crystal region in question is shown as $\alpha+\alpha'$. The phases α and α' both have the face-centred cubic structure, and only differ in composition and lattice spacing, the gap in the solubility disappearing above 355° C. The β phase is the primary solid solution of aluminium in zinc, and has the hexagonal close-packed structure.

---

* Communicated by Professor H. Jones.

Fig. 1.

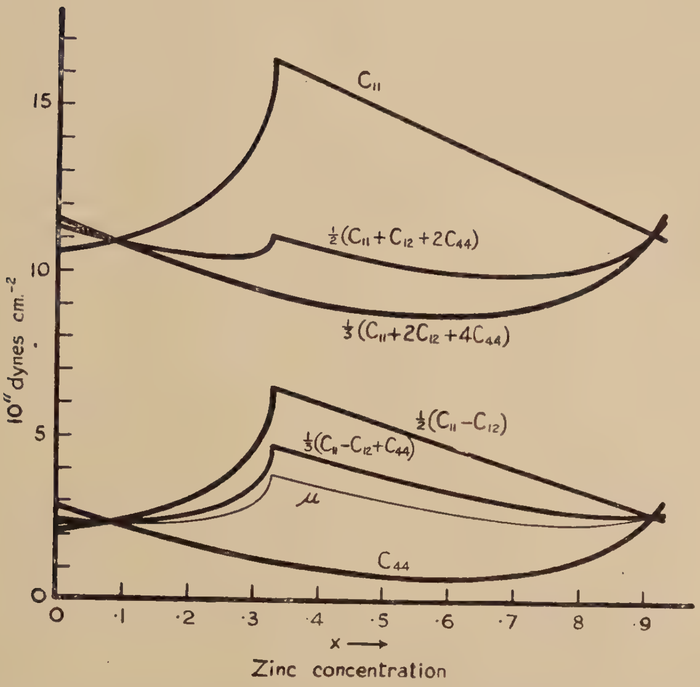

The elastic constants which give the wave velocities in certain special directions, shown as functions of zinc concentration. Also shown is μ, the mean of $\frac{1}{2}(C_{11}-C_{12})$ and C_{44}.

Fig. 2.

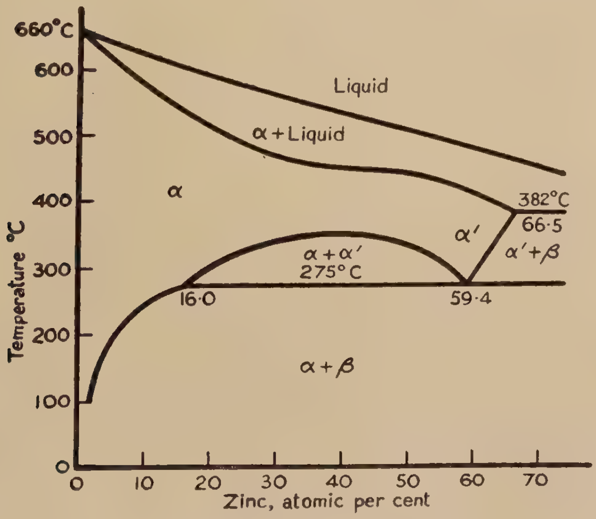

The aluminium–zinc phase diagram.

The existence of the solubility gap must be due to a subsidiary maximum in the free energy of the solution regarded as a function of zinc concentration. The positions of the phase boundaries are then given by the points of contact of the common tangent to the parts of the free energy curve on either side of the maximum. The present theory shows that the calculated maximum in $\frac{1}{2}(C_{11}-C_{12})$ leads to a subsidiary maximum of the required form in the contribution to the free energy from the thermal vibrations of the lattice. This provides some confirmation of the hypothesis of overlap over the square faces in pure aluminium.

§ 2. THE FREE ENERGY.

The free energy of a solid solution can be expressed as a sum of contributions from the electronic energy, the mixing entropy and the thermal vibrations.

The elastic constants of the solution, as shown in fig. 1, have been obtained by neglecting changes in the density of states curve as zinc is taken into solution. To this approximation the first derivative of the Fermi energy with respect to electron concentration cannot have a discontinuity anywhere; and the second derivative, given by $1/N(\zeta)$, where $N(\zeta)$ is the density of states at the Fermi surface, cannot be anywhere negative. In the present theory, therefore, no subsidiary maximum in the free energy can arise directly from the Fermi energy. (Compare the discussion by Hume-Rothery (1944), who also postulated overlap over the square faces in aluminium.) It will be assumed that the whole electronic energy varies smoothly and approximately linearly with zinc concentration. It can then be neglected, as it will not affect the positions of the phase boundaries.

The contribution to the free energy per atom from the mixing entropy is given, assuming complete disordering, by the expression

$$kT[x \log x+(1-x) \log (1-x)],$$

where T is the absolute temperature and x is the solute concentration.

The contribution to the free energy per atom from the thermal vibrations is given by the expression

$$\int_0^\infty \{\tfrac{1}{2}h\nu+kT \log [1-\exp(-h\nu/kT)]\}f(\nu)\,d\nu,$$

where $f(\nu)\,d\nu$ is the number per atom of normal modes of vibration of the lattice having frequencies lying in the interval ν to $\nu+d\nu$. We are here concerned primarily with the effect on the frequency spectrum $f(\nu)$ of changes in the elastic constants, rather than with the actual form of the spectrum. It is therefore reasonable to neglect the effect on the spectrum of the dependence of the wave-velocities on wavelength, since this effect may be assumed to remain constant or change smoothly with zinc concentration. As a first approximation we use the Debye spectrum for an isotropic crystal, taking for the value of the rigidity modulus the mean of $\frac{1}{2}(C_{11}-C_{12})$ and C_{44}. The contribution to the free energy per atom is then given by the expression

$$\frac{9}{8}k\Theta_D+9kT\left(\frac{T}{\Theta_D}\right)^3\int_0^{\Theta_D/T}\log\left(1-e^{-\xi}\right)\xi^2d\xi, \quad . \quad . \quad . \quad . \quad (1)$$

where Θ_D is the Debye characteristic temperature, given by the relation

$$\Theta_D=\frac{h}{k}\left(\frac{3}{4\pi\Omega}\right)^{\frac{1}{3}}c.$$

Ω is the atomic volume, and c is a mean wave velocity given in terms of the density ρ, the bulk modulus K, and the rigidity modulus μ, by the equation

$$\frac{3}{c^3}=\left(\frac{\rho}{K+\frac{4}{3}\mu}\right)^{3/2}+2\left(\frac{\rho}{\mu}\right)^{3/2}.$$

Fig. 3.

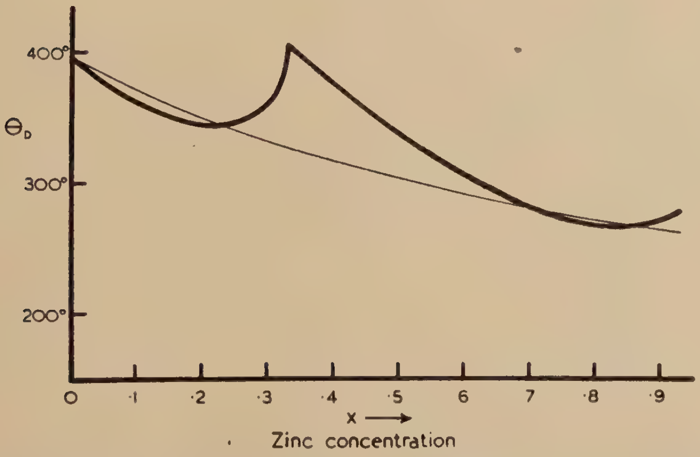

The Debye characteristic temperature as a function of zinc concentration. The thin curve shows how Θ_D would vary if the elastic constants remained constant.

In calculating Θ_D as a function of zinc concentration from the above formulæ, we can neglect the variation of Ω and K. The change in Ω is small, and it is easy to see that the effect on c of any change in K is small. Moreover, there is no reason to suppose that they do not vary smoothly with zinc concentration, and the effect on the positions of the phase boundaries would therefore be very small. In calculating c, K has been taken constant and equal to its value for pure aluminium, which is $7{\cdot}78\times10^{11}$ dynes cm.$^{-2}$ (Lazarus 1949). The large variation of ρ with zinc concentration, arising from the differing atomic weights of zinc and aluminium, has been taken into account.

Figs. 3 and 4 show the variation with zinc concentration of the Debye temperature Θ_D and the sum of the mixing entropy and Debye contributions to the free energy. The zero of F has been fixed arbitrarily at the value for pure aluminium. In each case the thin curves show the variation due to ρ alone, with μ constant at its value for pure aluminium. In calculating the free energy, T has been taken equal to 548° K., the lowest temperature at which the $\alpha+\alpha'$ region exists, though, in fact, the choice of the value of T has practically no effect on the calculated phase boundaries. The common tangent to the two parts of the curve is shown, the points of contact being at approximately 20 and 70 atomic per cent of zinc. The observed phase boundaries at 275° C. are at 16·0 and 59·4 atomic per cent. The positions of the calculated phase boundaries obviously depend almost entirely on the position of the peak in $\frac{1}{2}(C_{11}-C_{12})$, and, in view of the approximations involved in the calculation of the elastic constants, the agreement is surprisingly good.

Fig. 4.

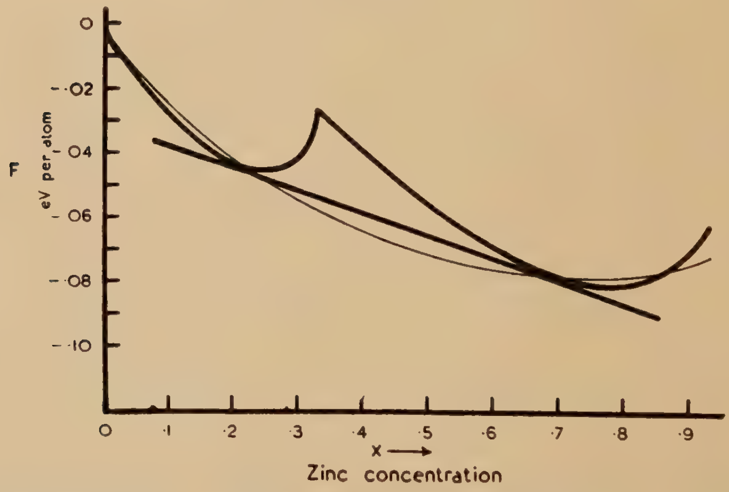

The free energy (Debye and mixing entropy contributions) as a function of zinc concentration. The thin curve shows how the free energy would vary if the elastic constants remained constant.

It is perhaps worth noticing that the qualitative result of this calculation, namely that the maximum in $\frac{1}{2}(C_{11}-C_{12})$ leads to a subsidiary maximum in the free energy, does not depend on the use of the Debye approximation to the frequency spectrum. Apart from neglecting the dependence of the wave velocities on wavelength, this approximation involves (i.) neglecting the dependence of the velocities on direction, and (ii.) allowing for the fact that the number of degrees of freedom of the crystal is limited, by the simple device of cutting off the total spectrum of the continuum (*i. e.* the sum of the contributions from the three frequency branches) at a single maximum frequency. A more general form for the contribution to the free energy per atom, in which only the dependence of the wave velocities on wavelength is neglected, is given by the expression

$$\frac{1}{3}\left(\frac{4\pi\Omega}{3}\right)\sum_{i=1}^{3}\int(\sigma^*)^3\left[\frac{9}{8}k\Theta_i^*+9k\mathrm{T}\left(\frac{\mathrm{T}}{\Theta_i^*}\right)^3\int_0^{\Theta_i^*/\mathrm{T}}\log\left(1-e^{-\xi}\right)\xi^2\,d\xi\right]\frac{d\omega}{4\pi}, \qquad (2)$$

in which the free energy is expressed as a sum of contributions from the three frequency branches, each contribution involving an integration over direction. $d\omega$ is an element of solid angle, and σ^* is the magnitude of the maximum wave vector in the direction of $d\omega$. In general the wave vector is restricted to lie within a polyhedron. (If the polyhedron is replaced by a sphere of equal volume, σ^* is constant and equal to $(3/4\pi\Omega)^{1/3}$). Θ_i^* is a temperature corresponding to the maximum frequency in the direction of $d\omega$ in the ith branch, and is given by the relation

$$\Theta_i^*=\frac{h}{k}\sigma^* c_i,$$

where c_i is the corresponding continuum wave velocity in that direction. The dependence of the c_i on direction is very complicated, but the extreme values of the velocity in each branch are simple functions of the elastic constants. The following table gives the values of the c_i in the principal sets of crystallographic directions (see, for example, Blackman 1938).

	(100)	(110)	(111)
ρc_1^2	C_{44}	C_{44}	$\frac{1}{3}(C_{11}-C_{12}+C_{44})$
ρc_2^2	C_{44}	$\frac{1}{2}(C_{11}-C_{12})$	$\frac{1}{3}(C_{11}-C_{12}+C_{44})$
ρc_3^2	C_{11}	$\frac{1}{2}(C_{11}+C_{12}+2C_{44})$	$\frac{1}{3}(C_{11}+2C_{12}+4C_{44})$

These values include the extreme values in each branch. In fig. 1 these values of ρc_i^2 are shown as functions of zinc concentration. The bulk modulus K, which is equal to $\frac{1}{3}(C_{11}+2C_{12})$, has been taken constant at its value for pure aluminium as before. The effect of an increase in $\frac{1}{2}(C_1-C_{12})$ on a value of c_i corresponding to a given direction is to increase it or leave it unchanged, but never to decrease it. The peak in $\frac{1}{2}(C_{11}-C_{12})$, regarded as a function of zinc concentration, therefore gives rise to similar peaks in the c_i in every direction, the size of the peak being very large in the neighbourhood of some directions, *e. g.* the (100) directions in the third branch, and vanishing in the neighbourhood of some others, *e. g.* the (100) directions in the second branch. The same is therefore true of the Θ_i^*, and, since the expression in square brackets in (2) is an increasing function of Θ_i^*, it follows that there must be a subsidiary maximum in the free energy.

The present theory does not account for the disappearance of the solubility gap at higher temperatures. This is not surprising, as the theory of the elastic constants only refers to absolute zero. It might be thought that the explanation lies simply in the direct effect on the Fermi energy contributions to the elastic constants of the finite temperature form of the Fermi distribution, this leading to a smoothing off of the sharp peak in $\frac{1}{2}(C_{11}-C_{12})$. Calculation shows, however, that this is not so, the effect on $\frac{1}{2}(C_{11}-C_{12})$ being only to shift the peak a little in the direction of lower electron concentration.

ACKNOWLEDGMENTS.

The author is indebted to Professor H. Jones for several helpful discussions, and to the Senate of the University of London for a Postgraduate Studentship.

REFERENCES.

BLACKMAN, M., 1938, *Proc. Roy. Soc.* A, **164**, 62.
HUME-ROTHERY, W., 1944, *Jour. Inst. Metals*, **70**, 229.
LAZARUS, D., 1949, *Phys. Rev.* [2], **76**, 544.
LEIGH, R. S., 1951, *Phil. Mag.* [7], **42**, 139.
RAYNOR, G. V., 1944, *Institute of Metals*, Annotated Equilibrium Diagram Series, No. 1.

XC. *Time and Frequency Uncertainty in Waveform Analysis**.

By P. M. Woodward, B.A.,
T.R.E., Ministry of Supply†.

[Received May 21, 1951.]

Summary.

The concept of a structural time-constant is introduced by considering the time auto-correlation function of any waveform, and a structural frequency-constant is similarly defined in terms of the spectral auto-correlation function. By setting up a combined time and frequency auto-correlation function χ, an absolute time-frequency constant is obtained. Its value is always unity, and it is suggested that this expresses time and frequency uncertainty more precisely than the relation $\delta t\,.\,\delta f \geqslant 1/4\pi$. To illustrate the function χ, two special waveforms are considered, namely, the complex Gaussian pulse and the real Gaussian pulse-train.

§1. Introduction.

No waveform $\psi(t)$ can be confined within a very short time interval and yet have a frequency spectrum $s(f)$ which occupies only a very narrow band of frequencies. A limit is set by the well-known relation

$$\delta t\,.\,\delta f \geqslant \frac{1}{4\pi}, \qquad \ldots\ldots\ldots \quad (1)$$

which in its wave mechanical form is of course the Heisenberg inequality. This is a property of any pair of Fourier transforms $\psi(t)$ and $s(f)$; the quantities δt and δf are the standard deviations of t and f in $|\psi|^2$ and $|s|^2$ respectively. Unfortunately, the relation (1) is an equality only when ψ and s are Gaussian in form. It is therefore tempting to seek some stronger expression which, while reducing to the equality (1) for Gaussian waveforms, would yet remain as an equality for waveforms in general. It might be, for instance, that the weakness of inequality arises from using the standard deviation as a measure of spread. This line of attack, however, is quickly ruled out by considering frequency modulated waveforms.

It is suggested in this paper that the elusive feature in terms of which the uncertainty principle can be exactly formulated, is contained in the idea of joint time and frequency auto-correlation. The statement of uncertainty which results from this approach becomes a statement, not about spreads, but about the lack of orthogonality between the waveform itself and the same waveform displaced both in time and frequency. Such a time and frequency domain was first discussed by Gabor (1946) and has also been treated by Ville (1948), though not perhaps in precisely the same way as is done here.

---

* Original version received April 12, 1951.

† Communicated by the Author.

§ 2. GENERALIZED TIME AND FREQUENCY CONSTANTS.

The notion of a "time constant" is familiar to every physicist and engineer, but it is not usually defined precisely except for a simple exponential transient. One of the simplest linear electric circuits, for example, is the one whose impulsive response is given by

$$\psi(t)=\left\{\begin{array}{ll} 0, & t<0, \\ A\exp(-t/t_0) & t>0, \end{array}\right\} \quad . \quad . \quad . \quad . \quad . \quad . \quad (2)$$

and t_0 is known as the time constant of the circuit, or of the waveform ψ. When the input is not a simple impulse the output can be deduced from the impulsive response by the principle of superposition: the output is simply the convolution or resultant of the input and the impulsive response. Rather loosely, it is a degraded form of the input in the sense that any time-structure which is fine compared with t_0 is smoothed out. To formulate *without explicit recourse to a frequency description* what is meant by the "time-structure" of any waveform is a problem which has received considerable attention in the field of random noise fluctuations. Here time-structure may for many purposes be adequately described in terms of a temporal auto-correlation function, though the formalism of auto-correlation is by no means restricted to the study of random functions. For a non-random (and in general complex) waveform $\psi(t)$, the temporal auto-correlation function is given by

$$g(\tau)=\int_{-\infty}^{\infty}\psi(t)\psi^*(t+\tau)\,dt. \quad . \quad . \quad . \quad . \quad . \quad . \quad . \quad (3)$$

If $\psi(t)$ be normalized as in wave mechanics, the function g has the value unity at the origin, and it can be shown that $|g|$ never exceeds unity. It therefore seems reasonable to define the *amount* of temporal auto-correlation, whether it be positive, negative or complex, by the integral

$$T=\int_{-\infty}^{\infty}|g(\tau)|^2\,d\tau, \quad . \quad . \quad . \quad . \quad . \quad . \quad . \quad . \quad (4)$$

since the vanishing of g implies no correlation, or more simply, the orthogonality of $\psi(t)$ and $\psi(t+\tau)$. The constant T may be called the *structural time-constant* of the waveform ψ without conflicting with established use of the unqualified term, since it is readily shown that when ψ is given by equation (2), T is equal to t_0. Using the proposed definition, the structural time-constant of a Gaussian waveform is given by

$$T=\delta t\sqrt{(4\pi)}, \quad . \quad . \quad . \quad . \quad . \quad . \quad . \quad . \quad . \quad (5)$$

where δt is the measure of spread which occurs in the Heisenberg inequality.

In a similar manner, we may define a *structural frequency-constant* for any spectrum $s(f)$ by the equation

$$F=\int|G(\phi)|^2\,d\phi, \qquad (6)$$

where $G(\phi)$ is a frequency auto-correlation function given by

$$G(\phi)=\int_{-\infty}^{\infty}s^*(f)s(f+\phi)\,df. \qquad (7)$$

The relation between $\psi(t)$ and $s(f)$ being the Fourier transformation

$$\psi(t)=\int_{-\infty}^{\infty}s(f)\exp(2\pi ift)\,df, \qquad (8)$$

$$s(f)=\int_{-\infty}^{\infty}\psi(t)\exp(-2\pi ift)\,dt, \qquad (9)$$

it is easy to show that $g(\tau)$ and $G(\phi)$ may be expressed in forms alternative to (3) and (7), thus

$$g(\tau)=\int_{-\infty}^{\infty}|s(f)|^2\exp(-2\pi if\tau)\,df, \qquad (10)$$

$$G(\phi)=\int_{-\infty}^{\infty}|\psi(t)|^2\exp(-2\pi i\phi t)\,dt. \qquad (11)$$

By applying Parseval's theorem to equations (10) and (11), we may now express the structural constants in the forms

$$T=\int_{-\infty}^{\infty}|s(f)|^4\,df, \qquad (12)$$

$$F=\int_{-\infty}^{\infty}|\psi(t)|^4\,dt. \qquad (13)$$

By comparing equation (5) with the Heisenberg *equality*, we see that for real Gaussian waveforms TF is equal to unity, but this product is certainly not invariant for all waveforms, nor should we expect it to be. Since $|s|^2$ encloses unit area—its normalization resulting from that of $|\psi|^2$—it can be seen from equation (12) that $1/T$ measures, in a peculiar way, the frequency spread of $|s|^2$. Similarly, $1/F$ is a measure of the extent to which $|\psi|^2$ is spread out in time. We might therefore expect that when we have $\delta t\,.\,\delta f\gg 1/4\pi$, we could also have $TF\ll 1$, and it will be shown in §4 that certain very simple frequency modulated waveforms do satisfy both these conditions.

§3. JOINT TIME-FREQUENCY AUTO-CORRELATION.

So far, we have considered auto-correlation independently in time and frequency, but although there may be no correlation between $\psi(t)$ and $\psi(t+\tau)$, nor between $s(f)$ and $s(f+\phi)$ for particular values of τ and ϕ, it can happen that a *combined* time and frequency displacement (τ, ϕ) will restore correlation. Let us therefore investigate the joint time-frequency auto-correlation function

$$\chi(\tau, \phi)=\int_{-\infty}^{\infty} \psi(t)\psi^*(t+\tau) \exp(-2\pi i\phi t)\, dt, \quad . \quad . \quad . \quad (14)$$

suggested by comparison of equations (3) and (11). A little manipulation reveals the alternative form

$$\chi(\tau, \phi)=\int_{-\infty}^{\infty} s^*(f)s(f+\phi) \exp(-2\pi i f\tau)\, df, \quad . \quad . \quad . \quad (15)$$

which is suggested by comparing equations (7) and (10). This function is not entirely a new one. Ville (1948) has considered it in a very similar form, and Gabor (1946) has considered it in discrete form, except that in his theory, the two ψ functions within the integral are different: one of them is a Gaussian analysis function, the other is the waveform under consideration. His treatment corresponds to cross-correlation rather than auto-correlation.

The main purpose of the present paper is to point out that the amount of auto-correlation in time and frequency combined, may be measured by the value of

$$C=\int_{-\infty}^{\infty}\int_{-\infty}^{\infty} |\chi|^2\, d\tau\, d\phi. \quad . \quad . \quad . \quad . \quad . \quad . \quad . \quad (16)$$

This is merely a generalization into two dimensions of the one-dimensional structural constants T and F. It is an *absolute structural constant*, because it turns out to be invariant for all waveforms. Thus, applying Parseval's theorem to equation (14), we have

$$\int_{-\infty}^{\infty} |\chi|^2\, d\phi=\int_{-\infty}^{\infty} |\psi(t)|^2\, |\psi^*(t+\tau)|^2\, dt, \quad . \quad . \quad . \quad . \quad (17)$$

and integration with respect to τ gives

$$C=\int_{-\infty}^{\infty}\int_{-\infty}^{\infty} |\chi|^2\, d\phi\, d\tau=\int_{-\infty}^{\infty} |\psi(t)|^2\, dt=1, \quad . \quad . \quad . \quad (18)$$

since $|\psi|^2$ is assumed normalized. This expresses the "uncertainty principle" of waveform analysis in an exact form. One may verify that in wave mechanics, C would equal Planck's constant. Whether or not it proves to be an interesting or useful expression of the uncertainty principle depends solely on whether the concept of time-frequency auto-correlation is found to have any genuine physical significance. It has already arisen in the theory of radar; upon its relevance, if any, to wave mechanics, the writer is not qualified to judge.

It seems worth remarking that, while the functions

$$g(\tau)=\chi(\tau, 0), \quad . \quad . \quad . \quad . \quad . \quad . \quad . \quad . \quad . \quad (19)$$

$$G(\phi)=\chi(0, \phi), \quad . \quad . \quad . \quad . \quad . \quad . \quad . \quad . \quad . \quad (20)$$

do not provide a complete description of the waveform ψ which generates them, there is no loss of information in passing from ψ to χ, a fact which may be proved by considering the two-dimensional Fourier transform of $\chi(\tau, \phi)$.

§4. THE COMPLEX GAUSSIAN WAVEFORM.

It has been remarked that certain "frequency modulated" waveforms are such that $TF \ll 1$. Thus, apparently, there is a lack of auto-correlation in time and frequency when considered separately, but not in a joint time-frequency domain, in view of equation (18). The simplest waveform which illustrates this is given by

$$\psi(t)=A \exp(-\alpha t^2), \qquad \ldots \ldots \ldots \quad (21)$$

where α is complex with positive real part. This waveform has a Gaussian modulus, and its instantaneous frequency, or rate of change of phase, is a linear function of time. If a large constant frequency shift were included, the real part would repressent a high-frequency pulse enveloping a frequency modulated carrier. Since, however, neither a frequency shift nor a time shift affects the function χ, it will be sufficient to consider the simplest form of ψ—as given by equation (21)—in which the instantaneous frequency is zero at $t=0$, where the modulus is a maximum.

When α is purely real, there is of course no frequency modulation, and figs. 1 and 2 illustrate typical forms of $|\psi|^2$, $|s|^2$, and $|\chi|^2$. In representing $|\chi|^2$, a shaded area has been given, its boundary representing a single contour. Since all the functions considered here have a Gaussian modulus, this representation by means of an ellipse should be adequate. In these two examples, it will be understood that

$$\delta t \,.\, \delta f=1/4\pi, \qquad \ldots \ldots \ldots \quad (22)$$

$$TF=1, \qquad \ldots \ldots \ldots \quad (23)$$

and as always $|\chi|^2$ is unity at the origin and encloses unit volume.

Suppose now, that α is complex. It is then possible to obtain both a wide $|\psi|^2$ and also a wide $|s|^2$ as in fig. 3, such that

$$\delta t \,.\, \delta f \gg 1/4\pi. \qquad \ldots \ldots \ldots \quad (24)$$

The "bandwidth" δf is large because of the spread in frequency occurring in $\psi(t)$, which does not show up in $|\psi|^2$, and therefore does not influence δt. The structural time and frequency constants, however, are each small, such that

$$TF \ll 1, \qquad \ldots \ldots \ldots \quad (25)$$

because of the phase-structure which is masked both in $|\psi|^2$ and in $|s|^2$. The form of $|\chi|^2$ shows that auto-correlation is distributed in a manner which makes mere time and frequency cross-sections quite deceptive.

It can be shown that if we write

$$\alpha=a+ib, \qquad \ldots \ldots \ldots \quad (26)$$

Fig. 1.

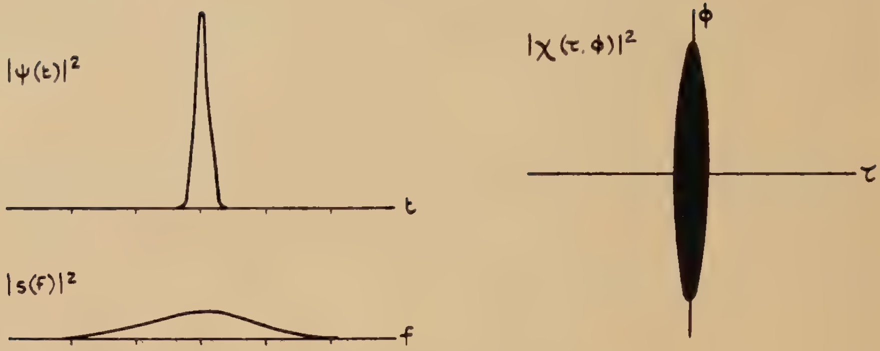

Short Gaussian pulse.

Fig. 2.

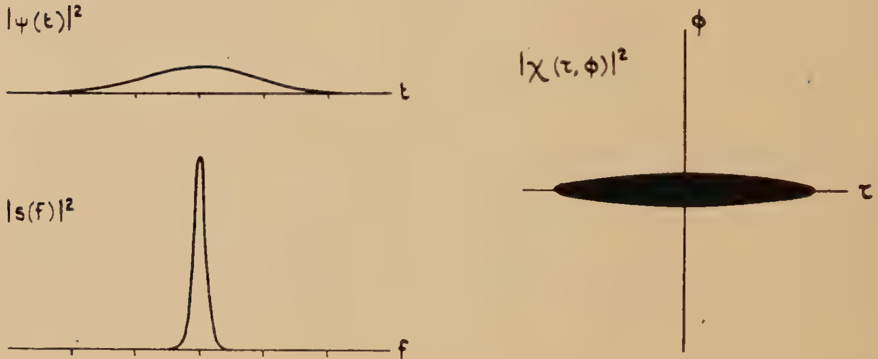

Long Gaussian pulse.

Fig. 3.

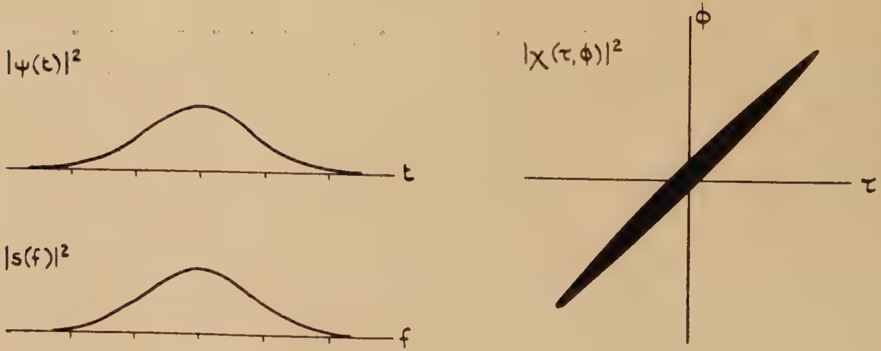

Complex Gaussian pulse.

the inclination θ of the major axis of $|\chi|^2$ to the τ-axis is given by

$$\tan 2\theta = \frac{2\pi b}{\pi^2 - |\alpha|^2}. \qquad (27)$$

The major axis is thus at 45° when $|\alpha| = \pi$. Pure frequency modulation is obtained by allowing the real part of α to tend to zero. The $|\chi|^2$ function then becomes drawn out into a "knife-edge" of unit amplitude and infinite length along a line through the origin which has a slope given by

$$\tan \theta = b/\pi. \qquad (28)$$

Apart from sign, this slope is simply the rate of change of the instantaneous frequency, given by

$$2\pi f_i = \frac{d}{dt}(-bt^2). \qquad (29)$$

The reason for the difference of sign is that $|\chi(\tau, \phi)|^2$ is unity when a time-advance of τ_0 combined with a frequency advance of ϕ_0 leaves ψ unchanged. If τ_0 and ϕ_0 have the same sign, then the instantaneous frequency must decrease with time.

Knife-edge distributions of $|\chi|^2$ can be obtained mathematically only as the result of a limiting process. A knife-edge along the ϕ-axis arises from a waveform consisting of a single impulse occurring at any time, a knife-edge along the τ-axis arises from a purely sinusoidal waveform or monochromatic spectrum. Pure linear frequency modulation gives a knife-edge at some other angle and is associated with infinite values of both the δf and the δt in the Heisenberg relation.

§5. THE REAL GAUSSIAN PULSE-TRAIN.

As a final illustration, we may consider a train of real positive Gaussian pulses, varying in amplitude according to a wider Gaussian envelope, as indicated in fig. 4. It is assumed that the pulses do not overlap appreciably and that there are a large number having comparable amplitudes. All the following results apply to this approximation.

The forms of $|\psi|^2$ and $|s|^2$ are the same: they differ only in their parameters. Denoting as previously the standard deviations of t and f in $|\psi|^2$ and $|s|^2$ by δt and δf respectively, it is easily shown that

$$\delta t \,.\, \delta f \geqslant 1/4\pi. \qquad (30)$$

Further, let us denote the standard deviation of each individual pulse by Δt and that of each broadened spectral line by Δf. Then it can also be shown, as is well known, that

$$\delta t \,.\, \Delta f = \Delta t \,.\, \delta f = 1/4\pi, \qquad (31)$$

so that the Heisenberg relation is an equality for the wrong measurements! One may further show that the structural time constant is

$$T=\frac{4\pi}{a}\delta t\,.\,\Delta t, \qquad (32)$$

where a is the time separation of the pulses, and that the frequency constant is

$$F=4\pi a\,\delta f\,.\,\Delta f, \qquad (33)$$

where $1/a$ is the separation of the spectral "lines". Consequently, as will be seen by comparing equations (31), (32) and (33), we have

$$TF=1. \qquad (34)$$

Fig. 4.

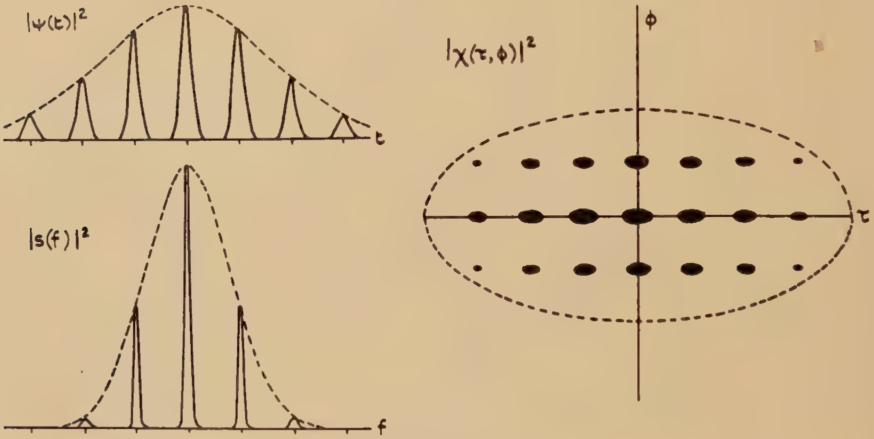

Gaussian pulse-train.

The reason for this is that the time-frequency auto-correlation function χ is separable as a product

$$\chi(\tau,\phi)=g(\tau)G(\phi), \qquad (35)$$

as also in the case of a single real Gaussian pulse. The special characteristic of frequency modulation is that χ is not separable without a rotation of axes.

Shaded areas for $|\chi|^2$ are shown in fig. 4: the function is made up of a lattice of elliptical Gaussian peaks having amplitudes which vary according to a Gaussian envelope indicated by the dotted contour. The enveloping distribution has the same eccentricity as the cellular peaks, since from equation (31) we have

$$\frac{\delta t}{\delta f}=\frac{\Delta t}{\Delta f}, \qquad (36)$$

and the area of each unit lattice cell is unity.

It should be clear from these examples that it is an easy matter to make the product of δt and δf, which occur in the Heisenberg relation, greatly exceed $1/4\pi$. Provided, however, that the time-frequency auto-correlation function remains separable, the product of the structural time and frequency constants remains equal to unity. Whether TF can ever exceed unity is not yet known, but the absolute structural constant defined by equation (16) remains equal to unity invariably.

§ 6. ACKNOWLEDGMENT.

Acknowledgment is made to the Chief Scientist, Ministry of Supply for permission to publish this paper, which is reproduced by permission of the Controller, H.M. Stationery Office (Crown copyright reserved).

§ 7. REFERENCES.

GABOR, D., 1946, *Jour. Inst. Elect. Eng.*, **93**, Pt. III, 429.
VILLE, J., 1948, *Câbles et Transmission*, No. 1, p. 61.

XCI. *The Beta Spectrum of Tritium.*

By G. M. INSCH and S. C. CURRAN,
Department of Natural Philosophy, Glasgow University*.

[Received May 21, 1951.]

ABSTRACT.

The beta-spectrum of tritium, H^3, has been carefully examined by the proportional counter method down to energies ∼1 KeV. In the present work it has been more thoroughly explored using improved techniques designed to permit accurate measurements of the spectrum shape down to a lower energy limit ∼200 eV. The improvements consisted chiefly in employing a counter which was made " end-free " by means of field-adjusting tubes and the use of an electronic method of measuring the pulse distribution in addition to the moving film technique. The intensity of the spectrum below 1 KeV. was found to be definitely less than theoretically predicted.

§ 1. INTRODUCTION.

THE beta-decay of tritium is an allowed transition. The recent work of Curran *et al.* (1949 a) has shown that between ∼1 KeV. and the upper energy limit, the spectrum is in good agreement with Fermi theory. A tentative suggestion of some deficiency in the number of beta-particles in the low energy region was made by these authors. Theoretically, the intensity of the spectrum (particles per unit energy interval) at zero energy should be about 86 per cent of the intensity at the maximum of the distribution. Cooper and Rogers (1950) have constructed a composite of the various published spectra and have concluded that all work on the spectrum indicates an excellent agreement with Fermi theory from 2·5 KeV. to 18 KeV. The introduction of the improvements to the technique makes it possible to examine the spectrum shape to lower energy limits than in the past without appreciable uncertainties arising from spuriously small pulses. These small pulses are those which have their origin in the part of the counter near the ends of the wire, since in this region the gas multiplication is reduced below the normal value unless field-adjusting tubes (Cockroft and Curran 1951) are employed.

§ 2. APPARATUS.

A diagram of the counter normally used in this work is seen in fig. 1 (*a*). The field-adjusting tubes were held at the potential appropriate to their diameter, thus ensuring a minimum of " end-effect ". The value of this potential was checked by ensuring that pulses from a homogeneous beam of X-radiation, fired through both windows W_1 and W_2, were of equal size at the centre and end of the counter. The counter was lined with a thin sheet of aluminium to minimize secondary effects at the cathode. The lining was perforated at the window positions to prevent any ionization in the window " neck " from being recorded at the central wire.

---

* Communicated by the Authors.

The pulses from the counter after amplification, were recorded on a 35 mm. film. Using this technique, it was found difficult to examine the spectrum shape accurately below ∼300 eV. The thick stems of the higher energy pulses and the brightness of the baseline itself caused a fogging of the film in the very low energy region. To overcome this limitation, the pulses were measured using a single-stage pulse analyser. This consisted essentially of two scaling units type 1009A. The discriminator of one unit was used to control the first stage of both units. The insertion of a steady source of potential difference (V volts) between the grids of the first stages in each scaling unit supplied a channel width of V volts ± the small difference in the triggering potentials of each unit. To measure the shape and width of the channel, homogeneous pulses were fed into the analyser. Graphs of the difference in the counting

Fig. 1.

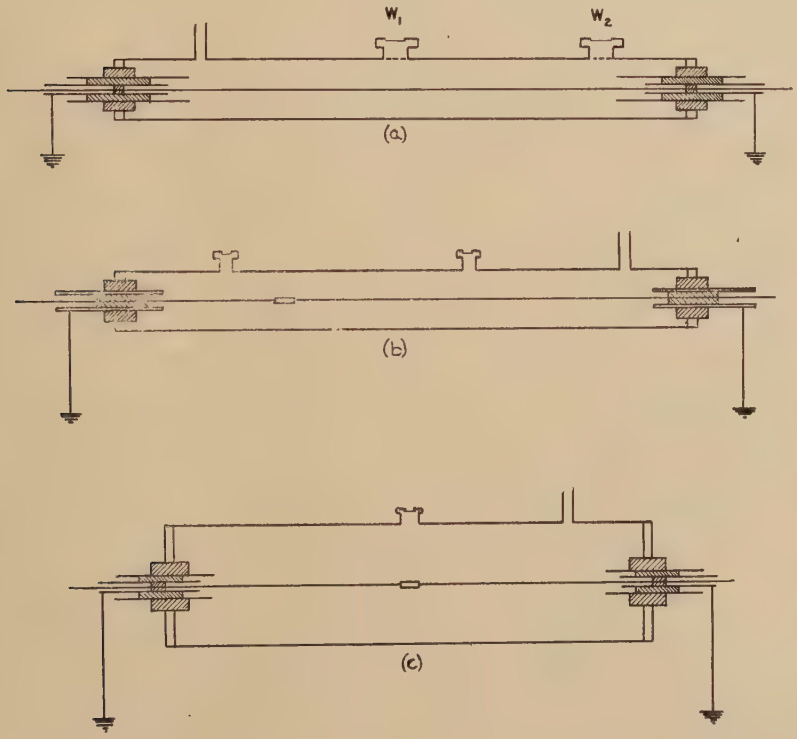

rate between the two scalers against the discriminator setting were plotted (fig. 2) at various points throughout the range of the discriminator, and it was found that the channel width was constant and that the channel had " rectangular " shape.

The tritium source had argon associated with it to act as a carrier. Before the gas was introduced into the counter its temperature was reduced to about −40° C. to remove tritiated water vapour. Measurements proved that no tritium stuck to the walls of the counter after this treatment.

Fig. 2.

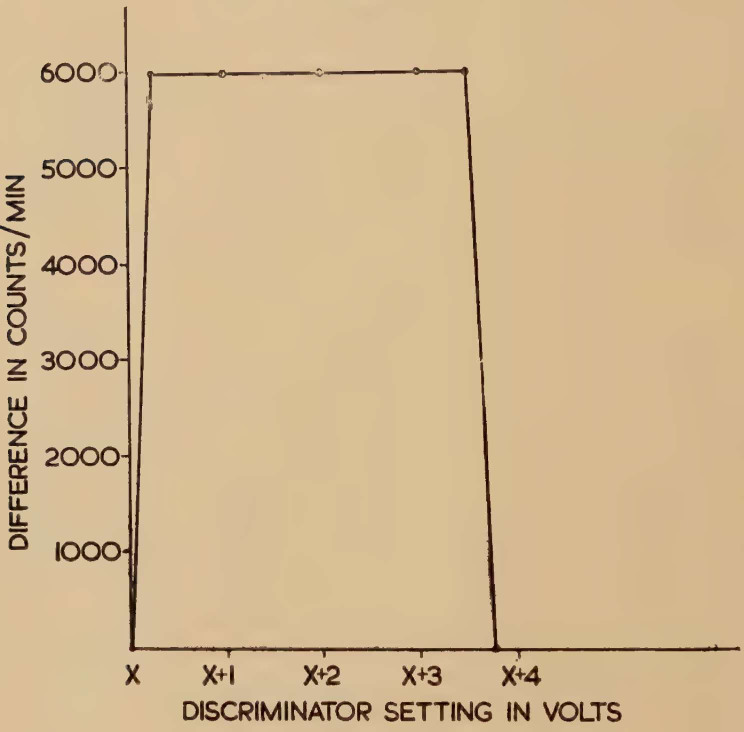

§ 3. Pulse Distribution at Low Energies.

It will be noted that all the above precautions, both in counter design and handling of the source, were introduced to eliminate the possibility of affecting the true spectrum shape, particularly in the direction of moving higher energy particles towards the lower energy region.

Three separate measurements were made on the spectrum with the counter already described. In the first a small quantity of H^3, giving a counting rate of ∼17,000 c./m. (the background counting rate was ∼300 c./min.), together with a mixture of methane at a pressure of 16 cm. Hg. and argon at slightly more than 3 atmospheres, was introduced into the counter, fig. 1 (*a*). The spectrum shape between ∼200 eV. and

2 KeV. was examined, the pulses being recorded on 35 mm film. The energy scale was calibrated by superimposing on the spectrum the fluorescence Kα X-rays of Gallium (energy 9·2 KeV.) arising from the K-capture of Ge^{71}. The amplifier gain was reduced by a factor of 4 to achieve this calibration. The pulse distribution from this measurement on the spectrum is seen in fig. 3, and the intensity below about 1 KeV. appears to be much less than expected on theoretical grounds. We have already mentioned the uncertainty of the curve below ~300 eV.

The experiment was repeated under almost identical conditions, using the pulse analyser to record the spectrum shape. Two measurements were made, one with a counting rate ~6000 c./min. and the other with a counting rate ~20,000 c./min. (fig. 3). It was found that the various points repeated satisfactorily after several hours. In the case of the low counting rate, it was not possible to obtain readings below about 300 eV. because of poor statistics. The channel width was kept at 100 eV. throughout the experiments, and the energy scale was calibrated in the same manner as before. Since the results obtained from these determinations with different counting rates agree, it seems unlikely that the apparent lack of low energy pulses is due to any limitation of the amplifier. The particular limitation in mind was the possibility of affecting pulse amplitudes when the pulses occurred within too sort an average interval.

Fig. 3.

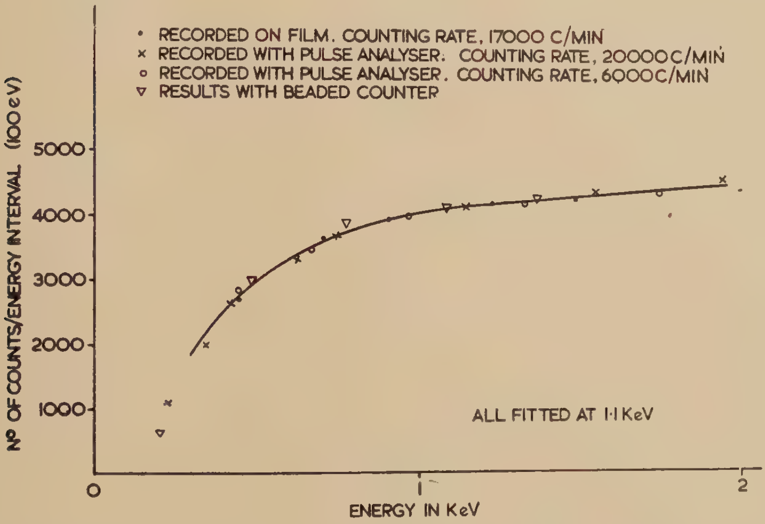

In all the above measurements, the field-adjusting tubes were held at the potential appropriate to their diameters, thus ensuring a counting tube free from " end-effect ". Curran *et al.* (1949 a) have published a result obtained using a counter which was not " end-free " and their experimental curve did not demonstrate any tendency to fall steeply at low energies. To achieve a result comparable with theirs, the field-adjusting tubes were earthed and the spectrum shape examined (fig. 4) in a manner similar to the two previous measurements. The counting mixture giving a counting rate of 20,000 c./min. was used. The result obtained is in fairly good agreement with that of Curran *et al.*

A " beaded " counter was built for further examination of the spectrum. This additional step was deemed advisable in view of the somewhat surprising result obtained. This counter consisted of a tube $2\frac{1}{4}$ in. in diameter and 24 in. in length (fig. 1 b). The central wire was divided into two sections, one 6 in. long and the other 14 in. long, insulated electrically from each other by a glass bead, 1 cm. long and 1 mm. in diameter. This provided two independent counting volumes having similar " end-effects ", and the difference between the spectrum in the long and short ends represents the distribution which would be obtained from a counter of length 8 in. free from " end-effect ". Tritium was introduced into the counter, together with a mixture of methane at a pressure of 16 cm. Hg. and argon at 2 atmospheres. The counting rates were about 20,000 c./min. in the long end and 8000 c./min. in the short end, compared with background counting rates of 600 c./min. and 200 c./min. respectively. The spectrum shape obtained from this examination is also seen in fig. 3. The pulse analyser was again used, and the calibration was carried out in the same manner as previously.

Fig. 4.

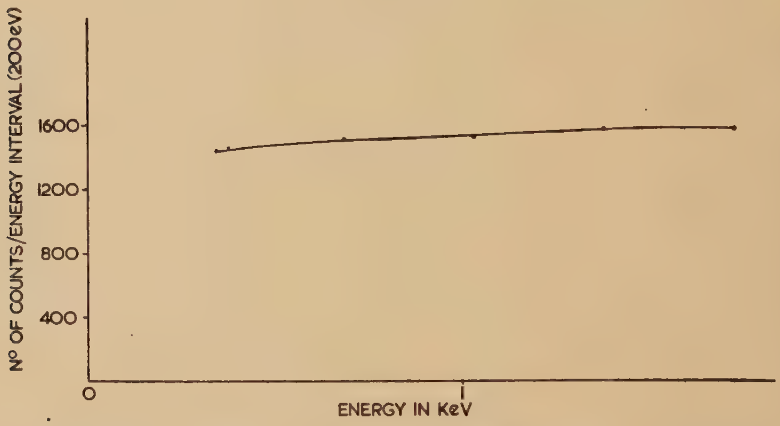

§4. Discussion.

The very good agreement between the results achieved by the differing methods employed is striking. We believe that the curves shown are accurate to within 10 per cent down to an energy value of 400 eV. and that even below this energy the shape of the curve is significant. The results obtained are in disagreement with Fermi theory in the low energy region, since the theory predicts that the curve should meet the ordinate at an intensity value about 86 per cent that of the maximum.

There are two possible explanations of the experimental results which remove disagreement with Fermi theory. (1) If the counter were not 100 per cent efficient for detection of very low energy electrons or if the energy lost by the particles per ion pair produced varied with the energy of the ionizing particles, the true shape of the spectrum could possibly be distorted into a shape similar to that obtained. (2) If there were present, in coincidence with the β-particles, quanta or particles of low energy, the results could again be explained.

Fortunately, sufficient data is at hand to discuss the first possibility. The work of Kirkwood *et al.* (1948) together with that of Curran *et al.* (1949 b) seems to establish that in argon, the energy expended on the production of an ion pair is constant down to very low energies. Additional work carried out in these laboratories with the counter shown in fig. 1 (*a*) has confirmed this result. The K and L X-rays of chlorine (energy 2·6 KeV. and 200 eV., respectively) resulting from K- and L-capture in A^{37} are largely converted by Auger effect. It is found, by using a source of A^{37} that the energy expended per ion pair by slow electrons in argon is constant down to 200 eV. It has also been found that the relative intensities of the two peaks are in agreement with the results of Pontecorvo *et al.* (1949). The low energy peak consists of two unresolved peaks, one due to the K-quantum escaping from the counter, involving the L_{II} or L_{III} shell (200 eV.) and due to nuclear L capture involving L_I electrons (280 eV.). From these results, it seems most unlikely that the counter used is failing to act proportionally down to the lowest energy values.

In connection with the second possibility, a homogeneous quantum radiation of energy $\sim$400 eV. in coincidence with the β-particles would explain the spectrum shape. Such a radiation would give a peak (Curran, Cockcroft and Angus 1949) of shape approximately represented by $x^{20} \exp(-x)$, and this radiation, together with the β-rays, would give a distribution similar to that observed. The origin of such radiation, however, is difficult to explain theoretically. We know that quanta of total energy about 60 eV. will be released in the de-excitation of the He^3 ion following β-emission from H^3. These quanta could give rise to about 3 ion-pairs per disintegration, but we require about 13 ion-pairs on the supposition that radiation is responsible for the shape of the spectrum observed. It is extremely improbable that the radiation has its origin in nuclear excitation of He^3 in the normal sense of the term. It is also possible that a number of low energy quanta (energy $\sim$50 eV.) released in coincidence with each other and the β-particles could account for the results.

§5. COINCIDENCE MEASUREMENTS.

The presence of quanta of energy $\leqslant$400 eV. is extremely difficult to establish in a coincidence measurement due to the extreme absorbability of the radiations. However, the following method was adopted in an endeavour to ascertain whether or not such radiations were present. A counter of 5½ in. diameter and 16 in. in effective length (fig. 1 (*c*)) was divided into two similar but independently operating volumes by a very thin glass bead (~½ mm. in diameter and 1·5 cm. long). The counting tube was lined with aluminium sheet. Tritium was introduced into the counter with a trace of He to act as carrier and methane was added to give a total pressure of 1 cm. Hg. The counting rate was ~10,000 c./min. in each volume, and the counter operated satisfactorily at this low pressure with about 1·5 KV. on the case, giving a high gas gain sufficient to detect pulses due to radiation of energy as low as 40 eV. The value for the mass absorption coefficient of methane for low energy quantum radiations does not appear to be accurately known, but from the data available it seemed likely that if quanta of energy 400 eV. were present, coincidences would be obtained. On the other hand, if the quanta had an energy value much less than 400 eV. no coincidences would be recorded. The counter was placed with its axis perpendicular to a magnetic field of sufficient strength to ensure that there were no β-β coincidences due to an electron travelling from one counting volume to the other. The results obtained from this investigation were indecisive. As the counting tube volts were increased the two counting volumes lost their independence and coincidences due to "mutual firing" were recorded. This phenomenon increased in frequency as the gas gain was increased. A curve giving the ratio R of the coincidence counting rate to the total counting rate in terms of the case voltage was plotted (fig. 5). This curve rose steeply at high gas gain. Kα fluorescence X-rays of copper were fired through the central window, resulting in an approximate doubling of the counting rate in each volume. An exactly

Fig. 5.

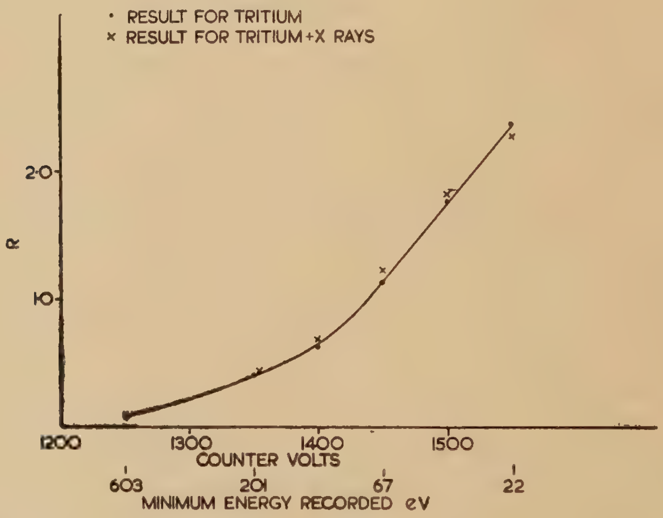

similar coincidence curve was again plotted (also fig. 5), and it was found that the points on this curve overlapped the points of the previous curve to within the accuracy of the experiment. The X-rays of copper gave pulses of average size roughly the same as those produced by the tritium β-rays. The close similarity of the two sets of observations shows that very few, if any, of the coincidences, observed with tritium alone, can be ascribed to the hypothetical β-quantum decay process. It is unfortunate that this coincidence technique fails to give definite results in the region of 400 eV. Clearly, it makes the technique quite inadequate for testing the hypothesis of much softer quanta ($\ll$400 eV.).

We are, thus, forced to conclude that the spectrum of H^3, as observed in a proportional counter, is not in accordance with Fermi theory at energies below about 1 KeV. We are unable to establish experimentally the reason for the discrepancy, although it seems possible that it might have its origin in the simultaneous emission of a quantum or quanta of total energy about 400 eV. This value is considerably higher than the expected energy release ($\sim$60 eV.) in the de-excitation of the He^3 ion.

REFERENCES.

COCKROFT, A. L., and CURRAN, S. C., 1951, *Rev. Sci. Instrum.*, **22**, 37.
COOPER, E. P., and ROGERS, F. T., 1950, *Phys. Rev.*, **77**, 402.
CURRAN, S. C., ANGUS, J., and COCKROFT, A. L., 1949 a, *Phil. Mag.*, **40**, 53; 1949 b, *Ibid.*, **40**, 36.
CURRAN, S. C., COCKROFT, A. L., and ANGUS, J., 1949, *Phil. Mag.*, **40**, 929.
KIRKWOOD, D. H. W., PONTECORVO, B., and HANNA, G. C., 1948, *Phys. Rev.*, **74**, 497.
PONTECORVO, B., KIRKWOOD, D. H. W., and HANNA, G. C., 1949, *Phys. Rev.*, **75**, 982.

XCII. *A Theoretical Investigation of the Compression of a Ductile Material between Smooth Flat Dies.*

By A. P. GREEN,
British Iron and Steel Research Association, Sheffield,
Mechanical Working Division*.

[Received May 18, 1951.]

[Plate XXIV.]

SUMMARY.

A theory is suggested to describe the distribution of stress and velocity in a block of ductile material symmetrically indented on opposite sides by two smooth flat dies. The theory is two-dimensional and an ideal plastic-rigid material is assumed. Slip-line fields are proposed for all ratios of width of dies to height of block greater than one. It is found that the velocity field transforms into its corresponding slip-line field. Other plane plastic problems where this correspondence occurs are cited. Since the velocities are known along only one slip-line boundary, the usual numerical procedure for calculating the field has to be modified and the use of influence coefficients is introduced. Solutions are computed for width/height ratios between one and two, and it is observed that simple analytical relations hold between these ratios and the corresponding velocity discontinuities in the field. The calculated mean pressures on the dies are compared with upper and lower bound curves derived by Hill on the basis of extremum principles. The deformation after different finite indentations is illustrated by photographs of experiments using (*a*) plasticine models, and (*b*) aluminium alloy strip.

Similar fields are proposed for extrusion or drawing through a wedge-shaped die with large reductions, but no solutions have been computed.

§1. INTRODUCTION.

THE plane stress–strain curve of a strip, before or after rolling, can conveniently be obtained by symmetrically indenting the strip on opposite sides by two flat dies completely spanning its width. The test was suggested by Orowan and is described by Ford (1948). Provided that the indented area is sufficiently long and narrow, the constraint of the non-plastic material on both sides of the dies inhibits lateral spread, and the deformation of the strip is essentially plane-strain, with the exception of narrow regions near the edges (Hill 1950 a). In this paper the theory of plane plastic strain due to Hencky and Geiringer is applied to analysing the stress and velocity distribution during the course of the indentation when the dies are smooth and their width, $2w$, is greater than the thickness, $2h$, of the material (fig. 2).

---

* Communicated by the Author.

When the dies are smooth and $w/h<1$, a complete solution has already been found and the pressure on the dies for different values of w/h has been calculated (Hill 1950 b, p. 256). For perfectly rough dies and $w/h>3{\cdot}64$, a complete solution was first obtained by Hill, Lee and Tupper (1945 or 1951; for a shorter account see Hill and Lee 1946). When $3{\cdot}64>w/h>1$ a solution has been suggested by Hill (1950 b, p. 230) which is only valid when there is friction on the dies; but it is uncertain for what range of frictional conditions the solution is appropriate.

In all these theoretical solutions the material under test is supposed to be rigid up to the yield-point; after which the maximum shear stress retains a constant value during plane plastic strain. Such a plastic-rigid body cannot deform until the plastic region attains a certain critical size (depending on the problem); the load-indentation curve has a discontinuity in slope at the yield-point and the load when distortion begins is called the yield-point load. When a real material is indented by rigid dies the bend in the load-indentation curve is well defined if the work-hardening is small. The bend marks the initiation of large plastic strains; at lower loads the amount of indentation is restricted by the elastic resistance of the non-plastic material and all plastic strains are of an elastic order of magnitude. The mean load in the interval corresponding to the bend should approximate closely to the yield-point load of the plastic-rigid material. If the material is annealed, it is not possible to define a load which may be compared with that calculated by the theory. The solution presented here can therefore be applied to the *initial* yielding of a material with a fairly well defined yield-point and to the continued indentation of a non-hardening material.

§2. BASIC EQUATION OF PLANE–STRAIN PLASTIC FLOW.

The theory of plane plastic strain and the slip-line field is set out most clearly by Hill (1950 b) who has considerably simplified and improved the original presentation by Hencky and Geiringer. Only a brief résumé of the basic theory will be given here.

Since the volume of an element of plastic-rigid material does not alter, each incremental distortion in a state of plane strain consists of a pure shear. Hence, for the ideal isotropic material, the state of stress at each point is a pure shear stress k, assumed constant, together with a hydrostatic pressure p. If Tresca's yield criterion is used, k is equal to $\mathrm{Y}/2$, while for von Mises' criterion it is equal to $\mathrm{Y}/\sqrt{3}$, where Y is the yield stress in uniaxial tension. It is assumed that inertial stresses are negligible compared with k and that the problem can therefore be treated as quasi-static. The plastic stress equations in the plane of flow, consisting of the yield criterion and the two equations of equilibrium, prove to be hyperbolic. The velocity equations in the plastic region express the condition for zero volume change and the fact that for an isotropic material the principal axes of stress and plastic strain-increment must coincide. These equations are also hyperbolic and their characteristics coincide with those of the stress equations. There are two orthogonal characteristic directions at any point in the plastic field ; they are the directions of maximum shear stress or shear strain-rate. The two orthogonal families of curves whose directions at every point coincide with those of the maximum shear stress are known as slip-lines and will be labelled α- and β-lines. By convention, if the α- and β-lines are regarded as a pair of right-handed curvilinear axes, the line of action of the algebraically greatest principal stress falls in the first and third quadrants. The equations governing the variation of p along a slip-line, which were first derived by Hencky (1923), are

$$\left.\begin{aligned} p+2k\phi&=\text{constant, along an } \alpha\text{-line,} \\ p-2k\phi&=\text{constant, along a } \beta\text{-line,} \end{aligned}\right\} \quad . \quad . \quad . \quad . \quad (1)$$

where ϕ is the anticlockwise angular orientation of a slip-line with respect to some fixed direction. These relations are completely equivalent to the equilibrium equations.

The equations of Geiringer (1930) for the components of velocity u, v, along the α and β slip-lines, are

$$\left.\begin{aligned} du-vd\phi&=0 \text{ along an } \alpha\text{-line,} \\ dv+ud\phi&=0 \text{ along a } \beta\text{-line.} \end{aligned}\right\} \quad . \quad . \quad . \quad . \quad . \quad (2)$$

They state that the rate of extension along any slip-line is zero.

It can be shown that the normal components of velocity may be arbitrarily prescribed without inconsistency along two intersecting slip-lines. It follows that it is possible to have a discontinuity in the tangential component of velocity across a slip-line. This implies a momentarily infinite rate of shear ; but this is permissible since work-hardening is neglected and a slip-line is a direction of maximum shear strain-rate. The discontinuities correspond to what in a real material would be a narrow transition region, where the shear strain-rate is large. It is evident that such transition regions will tend to be less sharp in a metal with a high rate of work-hardening, which emphasizes the fact that this theory is not applicable to such a material.

Hencky's first theorem, which is a direct consequence of equations (1), is the geometrical expression of the fact that the pressure difference between two points, calculated by proceeding along either of the two slip-line paths between the points, is the same. If we consider a curvilinear quadrilateral APBQ (fig. 1) bounded by two α-lines, QA and BP, and two β-lines, QB and AP, we deduce from (1) that

$$\phi_A-\phi_P=\phi_Q-\phi_B \quad . \quad . \quad . \quad . \quad . \quad . \quad . \quad . \quad . \quad (3)$$

Any two families of orthogonal curves satisfying this condition constitute a possible slip-line field for a plastically deforming mass under certain boundary conditions. In general the plastic region is divided into two parts by one or more slip-lines: a part where deformation is occurring, and a part which is rigid. The plastically deforming part consists of a number of subsidiary domains bounded by slip-lines across which the curvature of the slip-lines and/or the tangential components of velocity change discontinuously. The plastic material in the rigid part is prevented from deforming by the constraint of surrounding non-plastic material. In order to solve any problem the slip-line field must be found in the plastically deforming zone. The probable approximate location of this zone is first suggested by physical intuition, aided when possible by experiment. The slip-line field is then constructed to satisfy all the stress and velocity conditions that directly concern the zone, as well as the condition that the rate of plastic work should be everywhere positive. Finally, the solution is valid if the associated stress distribution in the rigid material is such that the yield limit is nowhere exceeded.

Fig. 1.

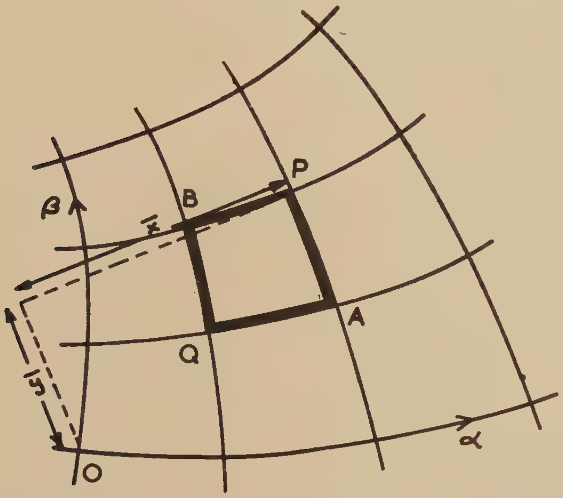

Slip-line field network showing $(\bar{x}, \bar{y})$ coordinates.

The most convenient coordinates for defining a point in a slip-line field are the quantities $(\bar{x}, \bar{y})$. They are the coordinates of the point P under consideration, referred to axes passing through some fixed origin 0, and parallel to the respective slip directions at P (fig. 1). It is easy to show that for *any* two orthogonal families of curves

$$\left.\begin{aligned} d\bar{y}+\bar{x}d\phi=0 &\text{ along an } \alpha\text{-line},\\ d\bar{x}-\bar{y}d\phi=0 &\text{ along a } \beta\text{-line}.\end{aligned}\right\} \quad . \quad . \quad . \quad . \quad . \quad (4)$$

In applying these conditions to a slip-line field the geometrical property (3) is introduced which determines ϕ at all points of a network of slip-lines.

The stress and velocity boundary conditions are particularly easy to deal with when the material is in contact with either a smooth or a perfectly rough rigid surface. The slip-lines meet a smooth surface at 45°, whereas a perfectly rough surface is cut orthogonally by one family of slip-lines since the frictional stress is equal to k. These conditions are independent of the normal pressure and we can therefore proceed with the solution of the slip-line field without specifying beforehand the value of p at any point. The only other simple frictional condition is that the shear stress on the surface has some constant value less than k. Each slip-line then intersects the surface at the same angle. This condition implies, however, that the coefficient of friction decreases with increasing normal pressure on the surface, which is an artificial condition not likely to occur in practice. If the coefficient of friction is constant, the angle of intersection varies with normal pressure along the surface of contact. This is a difficulty inherent in the solution of problems involving intermediate frictional conditions.

§3. Finding the Slip-Line Fields.

In this indentation problem geometric similarly is not maintained, and therefore we have to follow, from the very beginning, the progressive changes in the configuration. At each stage of the indentation there will be a different slip-line field, with its corresponding stress and velocity solution. The initial shape of the overhang does not affect the plastic problem, but for convenience we shall discuss the symmetrical indentation of a rectangular block.

The development of the plastic zones and the momentary boundary between the rigid and the plastically deforming material has been discussed in general terms for indentation by rough dies (Hill and Lee 1946). The present problem is similar in many respects. It may be expected that plastic zones will be initiated at the sharp edges of the dies and will spread inwards until they meet in the geometric centre of the block. Since, however, in this problem there are no frictional stresses, it does not seem possible that there should be a non-plastic area left in contact with the dies at the centre. For the solution presented here, no deformation consistent with Geiringer's equations is possible until the plastic zone has spread completely through the block. Plastic deformation is also restricted by the overhang, part of which must be non-plastic since its surfaces are stress free. It will be assumed that the overhang, even if partly plastic, moves out as a rigid whole. This was the assumption made by Hill and Lee, and it is confirmed by experiment (Nye 1947 ; see also the plasticine experiments described in this paper). It follows that the external plastic-rigid boundary must pass through the edges of the dies.

For integral width-height ratios the solution, suggested by Hill (1950 b, p. 232), is very simple. The block deforms momentarily, as a number of independent rigid units, which slide along a criss-cross of straight slip-lines, which meet the smooth dies at 45°. If the dies move with unit speed, there is a constant tangential velocity discontinuity of $\sqrt{2}$ initiated at the block centre and propagated by successive reflection from the dies along the whole length of the block. The solution is only valid for integral values of w/h because for all other dimensions the discontinuity terminates on the exist slip-lines, which is incompatible with the rigid body motion of the overhang. The solution for intermediate values of w/h must be such that it passes continuously into the simple straight line criss-cross as w/h approaches an integral value.

Consider first the general form of the field in the upper left-hand quadrant of the block, as determined by the boundary conditions (fig. 2). Velocity conditions at the plastic-rigid boundary, OB, determine that this boundary must be a slip-line, and the sense of the relative straining on either side of OB requires that it should be an α-line. Once the position of OB is chosen, the slip-line configuration is uniquely determined by equation (3) and the stress boundary conditions. These are that the slip-lines cut the axes of symmetry, DE and EB, at 45°, and that along OD they meet the smooth surface at 45°.

Assume for the moment that there is a stress singularity at O, and that the radius of curvature of OB does not change sign along its length. OB must then be convex towards the overhang, and the α-lines within a certain angular span pass through O. The field defined by OB and the singularity at O can be continued round O until the α-line that meets the surface of the die at 45° is reached. To avoid ambiguity, the point singularity will in future be denoted by O, or A, according to whether the point is considered to lie on the plastic-rigid boundary or on the surface of the die. Let the difference in ϕ be equal to ψ between O and A. The geometry of the boundary conditions on AD and BE determines that the angle turned through by OB is also ψ. These boundary conditions also make it possible to build up successive domains of the field, the boundaries of which meet the surface of the die at D_1, D_2, etc., and the horizontal axis of symmetry at E_1, E_2, etc. (fig. 3). The angle turned through by each domain boundary is equal to ψ. The vertical axis of symmetry must, clearly, be one of the domain diagonals D_1E_1, D_2E_2, etc. The number of domains through which the field must be extended depends on the value of w/h. For reasons of symmetry, velocity discontinuities can only take place along either $AE_1D_2E_3$ . . . or $OBD_1E_2D_3$ . . . This distinguishes two types of field, I. and II., with their velocity discontinuities, V_1 and V_2, ending at A and O respectively.

Fig. 2.

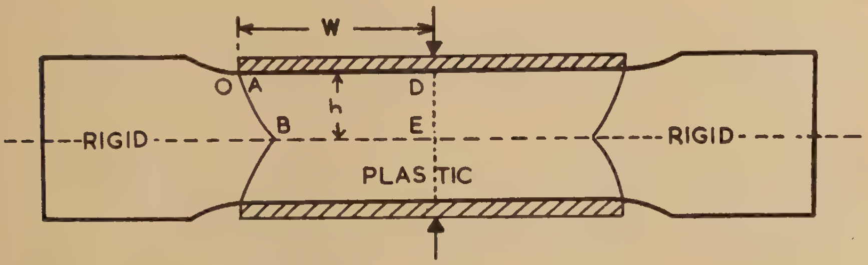

Rectangular block during indentation.

Fortunately, it is not necessary to obtain a complete solution of the velocity field in order to verify that the form of the slip-line field developed above is compatible with the velocity boundary conditions. The verification depends on the fact that, in this instance, the velocity field can be transformed into its corresponding slip-line field by means of the relations

$$u=\bar{x}, \quad v=\bar{y}\,; \quad \alpha\to\beta. \qquad \text{. . . . . . .} \quad (5\,a)$$

It can be seen, by comparing equations (2) and (4), that the variation of u along an α-line corresponds to the variation of $\bar{x}$ along a β-line, provided that the direction of change of ϕ is the same; v and $\bar{y}$ correspond in a similar manner. The normal boundary velocities u along a β-line transform into the x values along an α-line boundary. Now consider a tangential velocity discontinuity Δu across an α-line, which means that along any β-line as it crosses the discontinuity v and ϕ remain constant, and u increases by Δu. Upon transformation, this becomes a straight α-line region in the $(\bar{x}, \bar{y})$ field of length Δu. Similarly as we travel along any straight α-line through the region, $\bar{y}$ and ϕ remain constant and $\bar{x}$ increases by Δu. The velocities along a plastic-rigid boundary transform into a singularity in the slip-line field provided that the rigid part is not rotating; in addition, if there is a velocity discontinuity along the boundary, it becomes a circular arc with the singularity as its centre of curvature.

To make the correspondence exact in the present problem, the scales and origins of the two fields must first be adjusted. Let the outward speed of the rigid overhangs be U, corresponding to unit speed of the dies. The upper left hand quadrant is given a velocity U parallel to the dies towards the centre of the specimen so that the speed of the overhang is reduced to zero. The scale of the slip-line field is adjusted so that the half thickness, h, is always unity. The width of the dies will then be equal to 2U. We choose O as the $(\bar{x}, \bar{y})$ origin. The boundary conditions for the velocity and slip-line fields can then be written as follows :—

Boundary condition	Slip-line field	Velocity field
OA, β-line, $(\bar{x}, \bar{y})$ origin.	$\bar{x}=\bar{y}=0$	—
OB, α-line, velocity of rigid overhang is zero.	—	$u=v=0$
AD, slip-lines meet die at 45° ; vertical velocity is unity.	$\bar{x}=\bar{y}$	$u-v=\sqrt{2}$
BE, axis of symmetry ; vertical velocity is zero.	$\bar{x}-\bar{y}=\sqrt{2}$	$u=v$
DE, axis of symmetry (AD=U) ; horizontal velocity is U.	$\bar{x}+\bar{y}=\text{U}\sqrt{2}$	$u+v=\text{U}\sqrt{2}$

It is clear that if the relations (5 a) are applied, the velocity boundary conditions transform into those of the $(\bar{x}, \bar{y})$ field, except that certain boundaries are interchanged. The zero boundary velocities v and u on OB, which is an α-line, correspond to the $(\bar{x}, \bar{y})$ origin OA, a β-line. The points O, A, B, D_1, E_1, . . . D_n, E_n, in the velocity field correspond to the points O, B, A, E_1, D_1, . . . E_n, D_n, respectively, in the $(\bar{x}, \bar{y})$ field. The directions of change of ϕ are the same at all corresponding points. It is reasonable to expect, therefore, that the solutions of both fields are identical. This implies that there are straight line regions in the $(\bar{x}, \bar{y})$ field corresponding to the velocity discontinuity. The two types of slip-line obtained by transforming the two types of velocity field, I. and II., are shown in fig. 3. Although it has not been proved that the rate of work is positive everywhere in the field, it is reasonable to assume that this is so since the directions of shearing across all the velocity discontinuities imply positive work. An examination of the already existing solution for $w/h < 1$ shows that here also the two fields are equivalent. Discussion of the transformation of fields is continued later in the paper; for the moment, we confine our attention to the indentation problem.

Fig. 3.

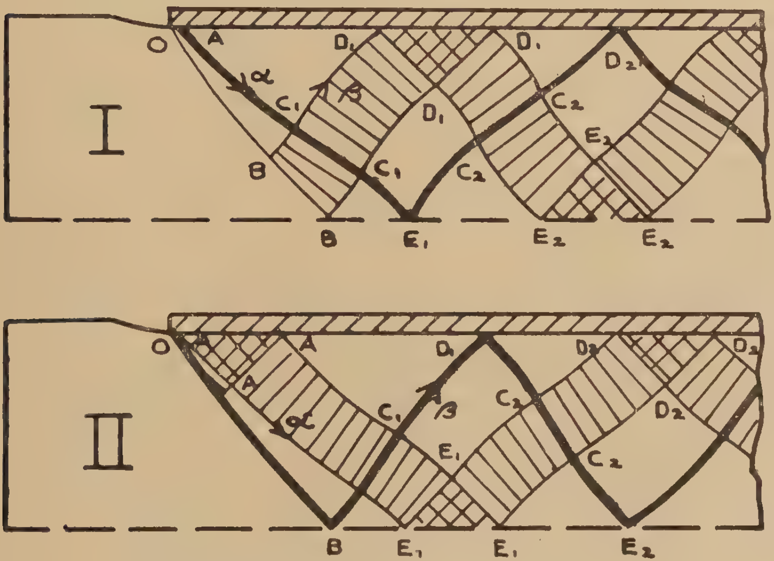

Two types of slip-line field (not to scale).

§4. NUMERICAL CALCULATION OF THE FIELDS.

The basis of the usual numerical method of solution is the replacing of the differential form of equations (2) by linear difference relations across a network of slip-lines. In the present problem we are able to choose the network so that the increments of slope $\Delta\phi$, between consecutive points, is the same throughout the field. This is possible because the angles turned through by the boundaries of all domains are equal to ψ. The field is thus split into an assembly of equal unit cells of which a typical one is shown in fig. 1. In order to calculate the velocities at P in terms of those at A and B, equations (3) are replaced by

$$\left.\begin{aligned} u_{\mathrm{P}}-u_{\mathrm{B}}&=\tfrac{1}{2}\lambda\Delta\phi(v_{\mathrm{P}}+v_{\mathrm{B}}),\\ v_{\mathrm{P}}-v_{\mathrm{A}}&=-\tfrac{1}{2}\mu\Delta\phi(u_{\mathrm{P}}+u_{\mathrm{A}}),\end{aligned}\right\} \quad . \; . \; . \; . \; . \; . \quad (6)$$

where $\Delta\phi$ denotes the *numerical* value of the change in angle, and λ and μ must be assigned the values of 1 or -1, according to whether ϕ increases or decreases in travelling towards the point P along the respective slip-lines from A and B. Solving for u_{P} and v_{P}, and retaining powers of $\Delta\phi$ only up to the third, there results

$$\left.\begin{aligned} u_{\mathrm{P}}&=(1-\tfrac{1}{4}\lambda\mu\Delta\phi^2)u_{\mathrm{B}}+\tfrac{1}{2}\lambda\Delta\phi(1-\tfrac{1}{4}\lambda\mu\Delta\phi^2)(v_{\mathrm{A}}+v_{\mathrm{B}})-\tfrac{1}{4}\lambda\mu\Delta\phi^2u_{\mathrm{A}},\\ v_{\mathrm{P}}&=(1-\tfrac{1}{4}\lambda\mu\Delta\phi^2)v_{\mathrm{A}}-\tfrac{1}{2}\mu\Delta\phi(1-\tfrac{1}{4}\lambda\mu\Delta\phi^2)(u_{\mathrm{A}}+u_{\mathrm{B}})-\tfrac{1}{4}\lambda\mu\Delta\phi^2v_{\mathrm{B}}.\end{aligned}\right\} \quad . \quad (7)$$

If the normal components of velocity are known at net points along two intersecting slip-lines, the velocities at all net points within the domain defined by these slip-lines can be calculated by repeated application of equations (7).

We shall now consider how these equations can be used to obtain numerical solutions of the velocity field for width/height ratios between one and two. The boundary velocities are known initially only on OB, the outer slip-line on the rigid side of which u and v are zero. Neither ψ, nor the velocity discontinuities that correspond to different values of U, are known in advance ; and before solutions over the whole range of U have been completed, even the range of ψ can be guessed only approximately. There is, clearly, not sufficient information to calculate the velocities *directly* through the field, in the same way that the velocity solution was calculated, for example, in the rough die indentation problem. It is necessary first to try normal components of velocities on a slip-line adjacent to OB. OA was chosen because the velocities along this slip-line correspond to the $(\bar{x}, \bar{y})$ coordinates along OB, which are needed when calculating the stress distribution. OA and OB were divided into five equal arcs so that $\Delta\phi$ throughout the field was equal to $\psi/5$.

The normal component of velocity on OA at O, within the plastic region, is either zero, or V_2, according to whether a solution of type I. or II. is being considered. At the five successive net points on OA after O, the normal components of velocity, u, were taken as a, b, c, d and e. Using the second of equations (6) and the condition that $v=0$ at O, a step integration along OA gives the values of v at the net points on this boundary. Since the equations (7) are linear in u and v, the calculated velocities at all net points are linear functions of the normal boundary velocities on the starting slip-lines OA and OB.

Therefore, groups of boundary velocities containing the different unknowns can be integrated through the field *separately* and the results superposed at each net point. We require a number of solutions in the selected range in order to be able to draw a graph of the mean pressuse on the dies against 1/U. Therefore, instead of repeating the computation several times for chosen values of $\Delta\phi$, it is more convenient to compute in terms of $\Delta\phi$, using equations (7), and neglecting powers of $\Delta\phi$ higher than the third. This can be done fairly rapidly provided an efficient method of tabulating the results is used.

The velocities on AC_1 and BC_1 are first calculated by integrating through the domain OAE_1B. The boundary conditions on the diagonals AD_1 and BE_1 enable the calculation to be continued through AC_1D_1 and BC_1E_1. It should be noticed that the boundary condition on AD_1 introduces a numerical term which must be integrated separately from the terms involving the various unknown velocities. The field in the domain $C_1D_1E_1C_2$ is defined by the calculated velocities on C_1D_1 and C_1E_1 and is computed as far as the six diagonal points on D_1E_1. The velocities on this diagonal must satisfy the condition, $u+v=U\sqrt{2}$, and the velocities at A, in contact with the die, must satisfy the condition, $u-v=\sqrt{2}$. We thus have seven equations for seven unknowns, a, b, c, d, e, U and either V_1 or V_2, which are solved numerically, substituting a definite value for $\Delta\phi$.

Fig. 4.

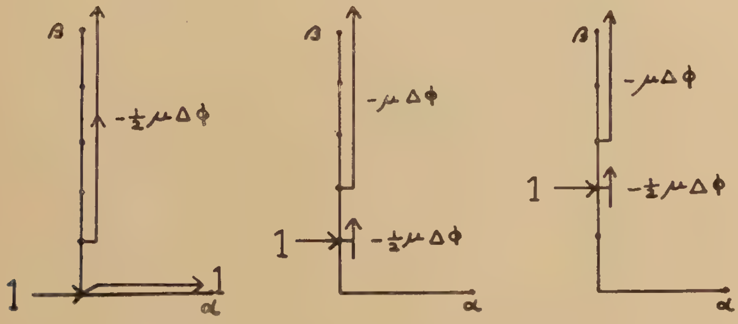
β
$-\frac{1}{2}\mu\Delta\phi$
1
1
α
β
$-\mu\Delta\phi$
1
$-\frac{1}{2}\mu\Delta\phi$
α
β
$-\mu\Delta\phi$
1
$-\frac{1}{2}\mu\Delta\phi$
α

(a) (b) (c)

The process of integrating through the different domains of the field is considerably shortened by the use of " influence coefficients ". These coefficients are the calculated velocities at net points of a domain, due to a unit normal velocity at a single net point on the initial boundary. The tangential velocities on the initial boundary are found in the usual manner by applying one of the equations (6). Three typical groups of initial boundary velocities are shown in fig. 4. The integrations of grounds (*b*) and (*c*) of this figure are clearly similar. The field of (*c*) is the same as that of (*b*) shifted one step along the network. All the influence coefficients for the network can therefore be obtained by integrating groups (*a*) and (*b*). As we have already observed, the linearity of the velocity equations enables any group of velocity boundary values to be "integrated" through the domain by simple super-position of their individual effects. We can, if we wish, proceed directly from the initial to any final boundary chosen in the domain, without having to calculate the velocities at any intermediate net points; all we need to know are the influence coefficients on the final boundary, corresponding to each net point on the initial boundary.

For the solution of the present problem influence coefficients were worked out in terms of $\Delta\phi$ (retaining powers of $\Delta\phi$ only up to the third), for integration between the following boundaries:—OA to AC_1, and BC_1; BC_1 to BE_1, and C_1E_1; AC_1 to C_1D_1; C_1D_1 to D_1E_1; C_1E_1 to D_1E_1. The reason for calculating the velocities on the diagonal BE_1, where $u=v$, is that this corresponds to the surface of the die AD_1 in the slip-line field, along which $\bar{x}=\bar{y}$. The coordinates are required along AD_1 in order to calculate the mean pressure on that surface. The use of influence coefficients reduced the labour of computing the field by about a half. For a problem in which one fixed value of $\Delta\phi$ is sufficient, it would probably be more convenient to calculate the influence coefficients numerically, and the proportion of time saved would probably be greater than in this problem.

Fig. 5.

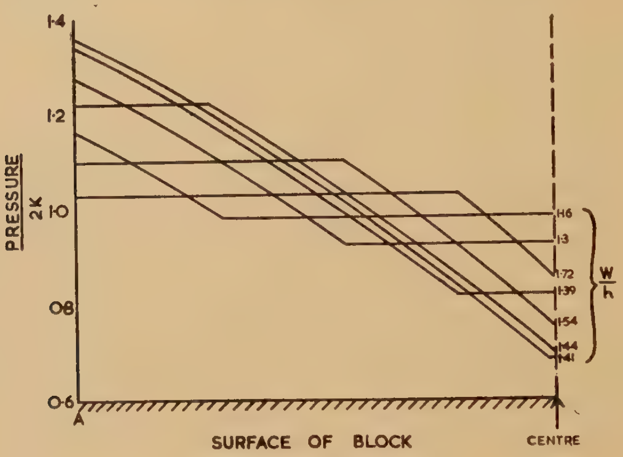

Pressure distributions.

When the slip-line configuration has been completed the values of the mean compressive stress p at all net points can be found from Hencky's equations (1), provided that the value p_0 at one point of the field, say, B is known. This value is provided by the condition that the horizontal component of the total force acting over OB is zero. Fig. 5 shows the distributions of pressure on the die at different stages of the indentation.

The relation between the mean pressure on the die and the ratio $h_0 w = 1/U$, is shown by the full curve in fig. 6.

§ 5. Discussion of Results.

The velocity fields, and hence the slip-line fields, of types I. and II., have been determined for values of ψ equal to 5°, 10°, 15° and 19° 30′. In fig. 7, the slip-line fields of both types, for ψ equal to 15°, are shown to scale. In order to plot these fields in detail the shapes of the initial slip-lines, OB, were found by the methods described above. The fields were then re-calculated numerically, using an equiangular network with $\Delta\phi$ equal to 5°. This was quicker than working out the coordinates of net points by substituting known values of $\Delta\phi$ and the initial boundary values in the original calculations.

Fig. 6.

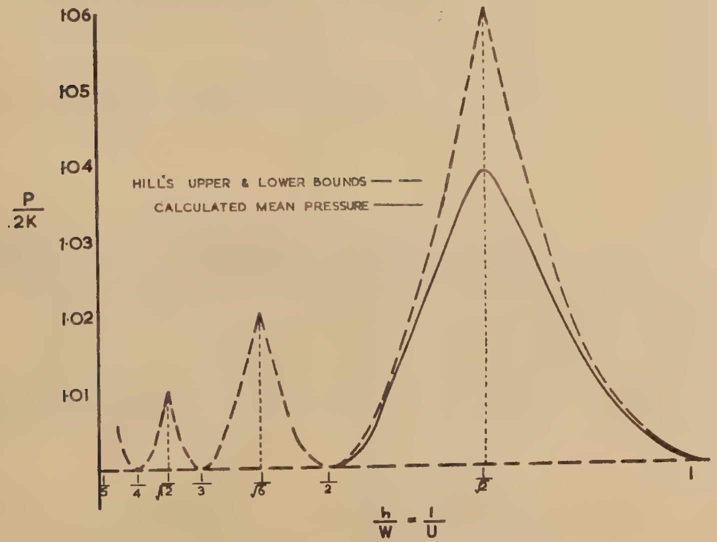

Calculated mean pressures and the two bounds.

The following simple relations are found empirically from an examination of the numerical results :—

$$U_1^2 + \tfrac{1}{2}V_1^2 = U_2^2 - V_2^2 = 2\,;$$

$$\left.\begin{aligned} U_1U_2 &= 2 \\ \text{and}\quad P_1 &= P_2 \end{aligned}\right\} \text{ if } \psi_1 = \psi_2 \quad . \quad . \quad . \quad . \quad . \quad . \quad . \quad . \quad . \quad . \quad . \quad (8)$$

The suffixes 1 and 2 refer to the two types of solution, I. and II., respectively. The accuracy with which these relations are satisfied by the calculated values is shown in Table I. It can be seen that the discrepancy is nowhere greater than 0·02 per cent. This is a useful check on the accuracy of the calculations. It seems likely that fairly accurate results would have been obtained even if the cube powers of $\Delta\phi$ had been neglected throughout the solution. The change over from the solution of type I. to that of type II. takes place smoothly when

Fig. 7.

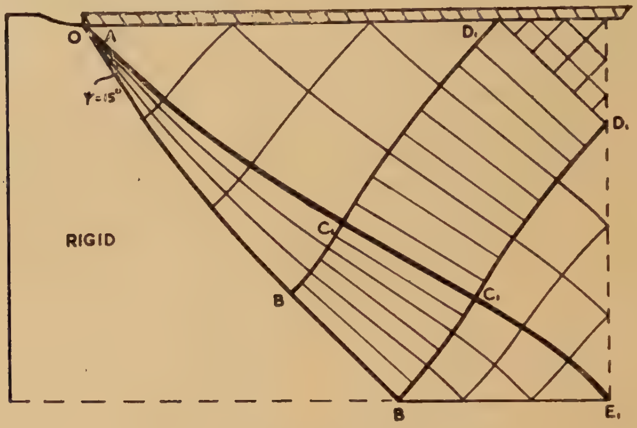

I. $\frac{w}{h}=1{\cdot}386$.

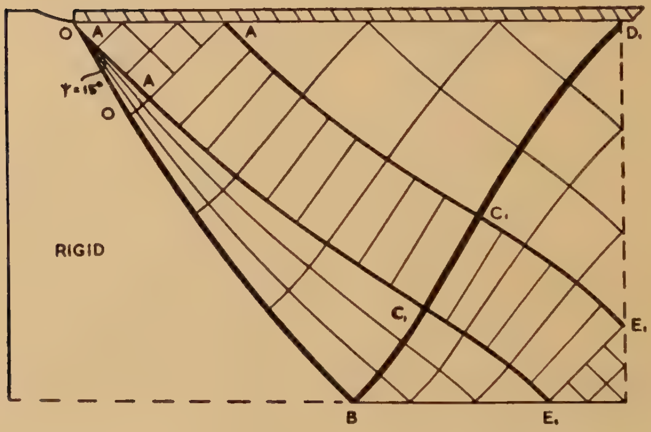

II. $\frac{w}{h}=1{\cdot}443$.

Slip-line fields to scale.

$U_1=U_2=\sqrt{2}$ and $V_1=V_2=0$. Since the last two equations of (8) express U_2 and P_2 separately in terms of U_1 and P_1, it appears that only one type of field need be solved to obtain the variation of P over the whole range considered.

PLASTICINE EXPERIMENTS.

Fig. 8.

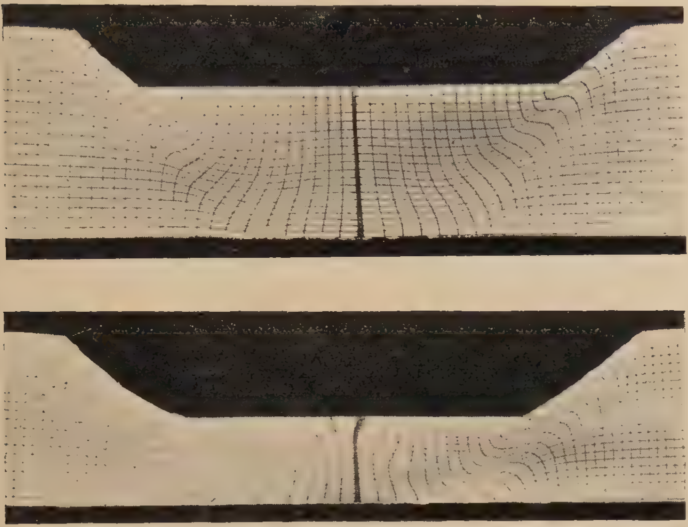

(a) $w/h=1\rightarrow\sqrt{2}$.

(b) $w/h=1\rightarrow2$.

Fig. 9.

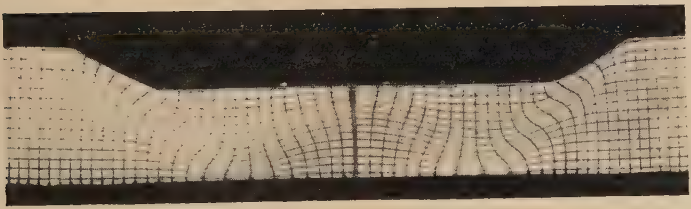

$w/h=\sqrt{2}\rightarrow2$.

Fig. 10.

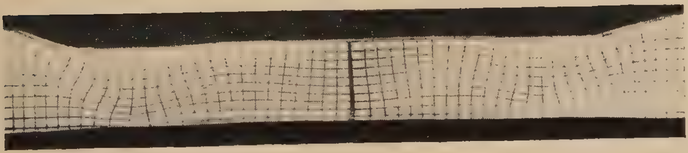

$w/h=\sqrt{6}\rightarrow\sqrt{12}$.

METAL EXPERIMENTS (Al 7% Mg).

Fig. 11.

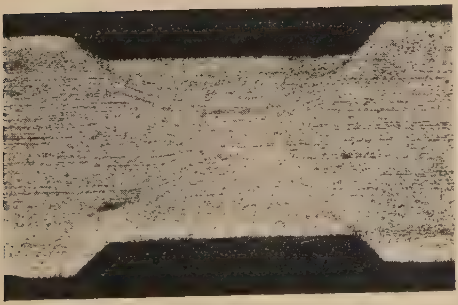

$w/h=1\rightarrow1{\cdot}34$.

Fig. 12.

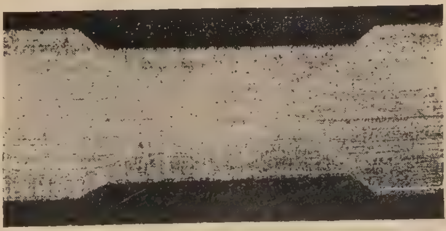

$w/h=\sqrt{2}\rightarrow1{\cdot}86$.

A theoretical explanation of equations (8) is not yet known. It seems probable that the general forms of these relations, valid for all U greater than unity, are

$$\left.\begin{array}{ll} U_1^2+\frac{m}{2}V_1^2=m(m+1), & \text{where } m\leqslant U_1\leqslant\sqrt{[m(m+1)]}, \\ U_2^2-\left(\frac{m+1}{2}\right)V_2^2=m(m+1), & \text{where } \sqrt{[m(m+1)]}\leqslant U_2\leqslant m+1\,; \end{array}\right\}$$

$$\left.\begin{array}{r} U_1U_2=m(m+1), \\ P_1=P_2, \end{array}\right\} \begin{array}{l} \text{for the same } m, \text{ if } \psi_1=\psi_2 \\ m=1, 2, \ldots \end{array} \quad \ldots\ldots \quad (9)$$

It should also be noted that when U is less than unity but greater than 1/8·74

$$U^2-\tfrac{1}{2}V^2=0,$$

which is in agreement with the second of equations (9) when $m=0$.

Table I.

ψ	U_1	V_1	U_2	V_2	$U_1^2+\frac{1}{2}V_1^2$	$U_2^2-V_2^2$	U_1U_2	$P_1/2k$	$P_2/2k$
0	1	2	2	2	2	2	2	1	1
5°	1·1646	1·1348	1·7174	0·9744	2·0002	2·0000	2·0001	1·0106	1·0108
10°	1·2985	0·7922	1·5400	0·6098	1·9999	1·9993	1·9997	1·0277	1·0279
15°	1·3859	0·3977	1·4429	0·2858	1·9998	2·0003	1·9997	1·0376	1·0377
19° 30′	1·4140	0·0118	—	—	1·9997	—	—	1·0389	—

§ 6. UPPER AND LOWER BOUNDS FOR THE MEAN PRESSURE.

It is interesting to compare the calculated mean pressure on the block with upper and lower bounds derived by Hill†; they were obtained by the application of two extremum principles for a plastic-rigid body (Hill 1950 c), extended to the case where part of the body is non-plastic by Drucker, Greenberg and Prager (1950).

The lower bound is

$$P\geqslant 2k, \quad \ldots\ldots\ldots\ldots \quad (10)$$

which expresses the otherwise obvious fact that it is not possible for the mean pressure to be less than it is in uniform compression. The upper bound is obtained by applying the inequality

$$\int F_i u_i^* \, dS \leqslant k\{\int \gamma^* \, dV + \int [u^*] \, ds\}. \quad \ldots\ldots \quad (11)$$

---

† Private communication.

F_i is the actual distribution of external stresses on the surface S. The asterisks denote a fictitious velocity distribution, u_i^*, which satisfies the boundary conditions and the conditions of no volume change ; γ^* denotes the corresponding maximum shear strain-rate in a volume element dV ; $[u^*]$ is the absolute value of the velocity discontinuity, and the corresponding integral is taken along it. The fictitious velocity solution used to obtain the upper bound of P is as follows :—the block is divided symmetrically into a number of independent rigid units, which slide along a criss-cross of lines inclined at the same angle θ to the faces of the dies. For integral values of U this is, of course, the actual manner of deformation with $\theta=45°$. The integral involving γ^* is now zero, and $[u^*]$ is equal to $1/\sin\theta$ between the rigid units. Assuming that there are m units in contact with each die, it follows from (10) that

$$\int F_i u_i^* dS = PU \leqslant k\int\frac{ds}{\sin\theta}=\frac{km}{\sin^2\theta}, \text{ where } \cot\theta=\frac{U}{m}.$$

Hence the least upper bound is defined by

$$\frac{P}{2k}\leqslant\frac{1}{2}\left(\frac{m}{U}+\frac{U}{m}\right), \quad \ldots\ldots\ldots \quad (12)$$

where $[m(m-1)]\leqslant U\leqslant[m(m+1)]$; $m=1, 2, \ldots$

The two bounds (10) and (12) are shown as dashed lines in fig. 7. The closer the similarity between the fictitious and the real velocity fields, the nearer the upper bound approaches to the actual mean pressure. Peak values of both the upper bound and the calculated mean pressure occur when $U=\sqrt{2}$, and here the discrepancy between the two curves is greatest. This might be expected since the actual velocity field for this value of U involves no velocity discontinuity and is therefore very different from the fictitious field. The peaks of the upper bound are closely approximated by the expression

$$\frac{P}{2k}\sim 1+\frac{1}{8U^2}$$

which rapidly approaches unity as U increases. There is no need, therefore, to extend the accurate solution of this problem beyond $U=2$, since for all U greater than 2, $P/2k$ differs from unity by less than 2 per cent.

§7. INDENTATION EXPERIMENTS.

(a) *Plasticine.*

The instantaneous velocities can be found at net points of the slip-line field for any chosen value of w/h, but it would clearly be a very laborious process to calculate the distortion of a square grid after a finite indentation. It is comparatively easy, however, to obtain an approximate picture of the deformation by the use of plasticine models : for it has been shown, by comparing plasticine model experiments with calculations made on the basis of the theory for a non-hardening plastic-rigid material, that in plane strain plasticine deforms in a similar manner to such an ideal material (Green 1951).

Rectangular plasticine blocks were made in two halves, $\frac{1}{4}$ in. thick. On the inner face of one-half a 1/10 in. square grid was lightly stamped in ink. The two halves were clamped between parallel glass plates lubricated with vaseline to ensure plane strain conditions, and French chalk was used to prevent the two halves sticking together. The blocks were indented from one side only, the horizontal plane of symmetry BE being replaced by a plane lubricated base. The photographs of the deformed grids after indentation between different initial and final values of w/h are shown in figs. 8, 9 and 10 (Pl. XXIV.). For $1 < w/h < \sqrt{2}$ the deformation is mainly confined to regions of intense shear radiating from the edges of the die (fig. 8*a*). As indentation continues, the mode of deformation clearly changes from type I. to type II., as shown by three relatively undeformed triangular regions in fig. 8*b*, where w/h has reached the value 2. This is also illustrated in fig. 9 where the formation has been of type II. throughout. Fig. 10 shows a block which has been compressed from $w/h \sim \sqrt{6}$ to $w/h \sim \sqrt{12}$; there are five triangular regions in which the deformation has been small, which is what we should expect from the theory.

(b) *Metal*†.

The deformation of metal strips symmetrically indented on opposite sides by two flat dies is illustrated in figs. 11 and 12 (Pl. XXIV.). Aluminium 7 per cent magnesium alloy was used because the deformation can be clearly demonstrated with this metal. When it is rolled the segregated impurities in the metal are strung out in straight lines along the length of the strip. The distortion of such lines by indentation was shown up by polishing the central longitudinal section of the strip, and etching it with acid ferric chloride. The width of the strip was five times the width of the dies, which were made of tungsten carbide and lubricated with calcium oleate. Since the metal had been cold worked by rolling it to the required thickness, the rate of work-hardening during indentation was small. If the non-dimensional quantity H is defined as the mean slope of the stress–strain curve over the range of strain during indentation, divided by the mean stress in uniaxial compression over the same range of strain, then H was equal to approximately 0·4 and 0·25 for the indentations shown in figs. 11 and 12 respectively. The flow patterns are in qualitative agreement with the theory and are similar to those shown in figs. 8*a* and 9, the corresponding plasticine experiments, though in the metal the regions of intense shear are more sharply defined.

It will be noticed that experiment confirms the assumption made in the theory, that the overhang moves out as a rigid whole: the material outside the initial area of deformation remains undisturbed and the general shape of this region agrees with the theory. All the photographs demonstrate the inhomogeneous nature of the deformation. It is clear, therefore, that severe work-hardening will modify the nature of the flow. For example, in similar experiments with annealed metal strip the regions of large shear were much more diffuse, though the type of deformation was similar.

---

† Metal experiments carried out by the Metallurgy Section of the Metal Flow Research Laboratory, Sheffield, under the supervision of Mr. L. Bourne.

§ 8. TRANSFORMATION OF FIELDS—DISCUSSION AND APPLICATION.

In addition to equation (5*a*) alternative relations for transforming the velocity field are :

$$\left.\begin{array}{llll} u=\bar{y}', & v=-\bar{x}', & \alpha\rightarrow\alpha', & \phi=\phi' \ (b), \\ u=\bar{x}', & v=-\bar{x}', & \alpha\rightarrow\beta', & \phi=-\phi' \ (c), \\ u=\bar{y}', & v=\bar{y}', & \alpha\rightarrow\alpha', & \phi=-\phi' \ (d). \end{array}\right\} \quad . \quad . \quad . \quad (5)$$

Starting with the velocity field of any quadrant in the present problem, these transformations all result in an $(\bar{x}, \bar{y})$ field of the same shape as that of the original quadrant. However, either the α- and β-lines are interchanged, in effect reversing the directions of the maximum shear stress throughout the field so that the work of distortion would be negative (*b* and *c*); and/or the field is the mirror image in an axis of symmetry of the field in the original quadrant (*c* and *d*).

The relations (5) can be used to transform any velocity or slip-line field. In general, the velocity field cannot be expected to transform into its own slip-line field; but it may transform into a slip-line field which has already been computed, thus saving a considerable amount of labour. For example, the transformed velocity fields for symmetrical steady motion problems, such as drawing or extrusion, sometimes involve the field defined by equal circular arcs; this is a standard field that has already been computed and which can also be found analytically. In certain problems with particularly simple stress and velocity boundary conditions the two fields will be equivalent. This occurs, for example, in the following plane strain problems :—symmetrical indentation of a block on opposite sides by two rough flat dies for w/h greater than unity; extrusion or drawing through a smooth square or wedge-shaped die (Hill 1948 a, Hill and Tupper 1948); indentation by a smooth wedge of the plane surface of a semi-infinite block (Hill, Lee and Tupper 1947); expansion of a semi-cylindrical cavity in the surface of a semi-infinite block (Hill 1948 b). The last two are rather trivial examples of this equivalence.

An interesting example is the problem of sheet-drawing through a smooth wedge-shaped die. The solution which is valid for lower reductions fails for certain higher reductions, when the velocity discontinuity terminates on the exit slip-line (Hill and Tupper 1948). The situation is analagous to that encountered in the smooth die indentation problem when w/h has non-integral values greater than unity; the slip-line configuration which overcomes the difficulty is similar in form (fig. 13). The $(\bar{x}, \bar{y})$ and velocity solutions are again identical if the origin of the $(\bar{x}, \bar{y})$ field, O, is taken on the axis of symmetry at the point of intersection of the tangent to the die faces. No numerical calculations of the field or of the corresponding upper bound have yet been made.

The importance of considering the velocity field associated with a slip-line field is emphasized by the solutions presented in this paper. The transformation of fields, and the existence of equivalent fields do not appear to have been discussed in the same manner previously. Geiringer (1937) speaks of " conjugate " solutions, but these involve the correspondence between one complete solution (velocity and slip-line field) and another. The transformation equations of the two kinds of conjugate solution which she discusses can be written

Fig. 13.

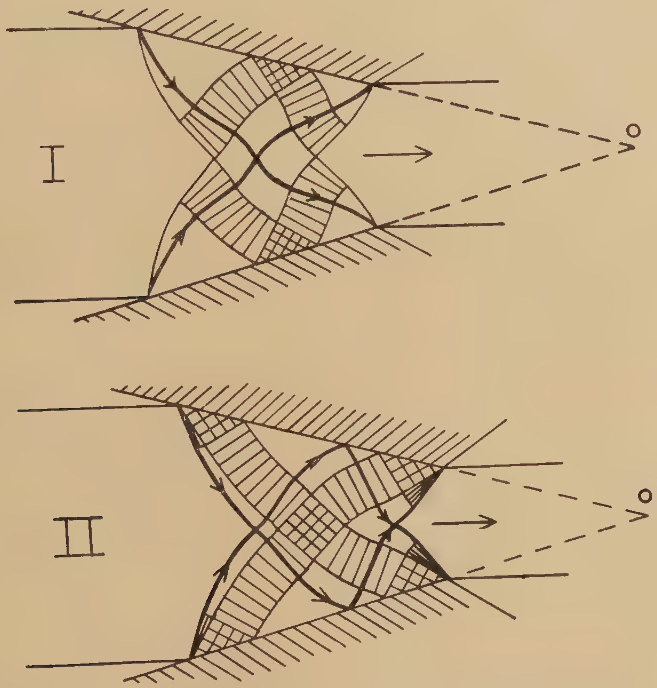

Slip-line fields for wedge-shaped die (not to scale).

$$\left.\begin{aligned}\bar{x}' &= -v \;;\; u' = \bar{y},\\ \bar{y}' &= -v \;;\; u' = \bar{x},\end{aligned}\right\}\quad \text{1st kind,}$$

$$\left.\begin{aligned}\mathrm{R}' &= -v \;;\; u' = \mathrm{S},\\ \mathrm{S}' &= u \;:\; v' = -\mathrm{R},\end{aligned}\right\}\quad \text{2nd kind,}$$

(she actually uses cartesian coordinates for both position and velocity). R and S are the radii of curvature of the α- and β-lines at a point. They satisfy the relations

$$d\mathrm{S}+\mathrm{R}\,d\phi=0 \text{ along an } \alpha\text{-line},$$

$$d\mathrm{R}-\mathrm{S}\,d\phi=0 \text{ along a } \beta\text{-line}.$$

The particular conjugate solutions which she derives are mainly of academic interest. Transformation relations exist, similar to those expressed by equations (5), but involving (R, S) coordinates. These, however, are not likely to prove so useful in practice, since the stress boundary conditions can usually be expressed more easily in terms of $(\bar{x}, \bar{y})$ coordinates.

§9. CONCLUSIONS.

The value of the investigation presented in this paper, apart from the interest of the new solutions presented, lies in the formulation of new methods for solving plane plastic problems. The transformation of velocity fields and the use of influence coefficients will often save considerable computational labour. Provided that initially the form of the field can be tentatively built up, the possibility of integrating unknown boundary values from an initial to a final boundary overcomes the difficulty which arises when insufficient boundary values are known for a direct solution. The element of trial and error is thus reduced though not eliminated. The method due to Hill for obtaining upper and lower bounds for mean applied loads is likely to prove most useful in some of the many problems of which the exact solution cannot be found or would be extremely laborious to calculate.

ACKNOWLEDGMENTS.

I am grateful to the Director of the British Iron and Steel Research Association for permission to publish the paper ; to Dr. R. Hill for helpful advice and criticism ; and to Mr. G. Douglass of the Solid Mechanics Section of B.I.S.R.A. for his valuable assistance in the numerical computations and the photography.

REFERENCES.

Ford, H., 1948, *Proc. Inst. Mech. Eng.*, **159** 115.

Geiringer, H., 1930, *Proc. 3rd Int. Cong. App. Mech., Stockholm*, **2,** 185 ; 1937, *Mem. Sci. Math.*, **86.**

Green, A. P., 1951, *Phil. Mag.*, **42,** 365.

Hencky, H., 1923, *Zeits. ang. Math. Mech.*, **3,** 241.

Hill, R., 1948 a, *Journ. Iron & Steel Inst.*, **158,** 177 ; 1948 b, *Proc. 7th Int. Cong. Appl. Mech., London* ; 1950 a, *Phil. Mag.*, **41,** 733 ; 1950 b, *The Mathematical Theory of Plasticity* (Oxford : Clarendon Press) ; 1950 c, *J. App. Mech.*, **17,** 64.

Hill, R., and Lee, E. H., 1946, *Proc. 6th Int. Cong. App. Mech., Paris.*

Hill, R., Lee, E. H., and Tupper, S. J., 1945, *Ministry of Supply, Armament Research Dept., Theoretical Research Rep.* 28/45 ; 1947, *Proc. Roy. Soc.* A, **188,** 273 ; 1951, *Journ. App. Mech.*, **18,** 46.

Hill, R., and Tupper, S. J., 1948, *Journ. Iron & Steel Inst.*, **159,** 353.

Nye, J. F., 1947, *Ministry of Supply, Armament Research Dept., Rep.* 39/47.

XCIII. *The Development of Deformation Textures in Metals.—*
Part III. *Hexagonal Structures.*

By E. A. Calnan, B.Sc., and C. J. B. Clews, Ph.D.,
National Physical Laboratory*.

[Received May 11, 1951.]

§ 1. Introduction.

Hexagonal close-packed metals slip on a single crystallographic plane and not on a system of equivalent planes as is the case for cubic metals. Due in part to this simple slip mechanism, considerable attention was devoted to the deformation of the hexagonal metals, notably zinc and magnesium, by the German school during the decade 1925–1935 (Schmid and Boas 1950). There is, however, an additional factor important in the deformation of these metals, namely, the frequent occurrence of deformation twins. The crystallography of the slip and twinning processes has been well established, and the main features of the deformation textures observed have been explained in general terms, but there appears to have been no completely systematic treatment on the basis of slip rotations and twinning re-orientations. Mathewson and his co-workers have attempted to rationalize deformation textures as a whole, but their method is not applicable to hexagonal metals (see for example, Hibbard and Yen 1948).

The purpose of the present paper is to show how the effect of twinning may be introduced into the treatment already developed for face-centred and body-centred cubic metals (Calnan and Clews 1950, 1951, subsequently referred to as Parts I. and II.), and how this treatment may be applied to the prediction of the deformation textures in hexagonal metals.

§ 2. Deformation Mechanisms.

Slip. All hexagonal close-packed metals deformed at room temperature slip on basal planes, (0001), in the $<11\bar{2}0>$ directions. Approximate resolved shear stress contours are shown in fig. 1. It will be noted that the shear stress varies from the maximum possible value, 0·50 of the applied stress, at 45° from the pole of the slip plane and the slip direction, to zero at 0° and 90° from the pole of the slip plane. The calculation of accurate values of the $\cos\chi\cos\lambda$ function, where χ and λ are the angles which the slip plane normal and the slip direction make with the applied stress direction, was not necessary owing to the simplicity of the system. The rotations under stress are of the usual kind leading under tension towards the slip direction and under compression towards the pole of the slip plane. Tension rotations are shown in fig. 4. Most of

---

* Communicated by the Authors.

the rotations are those associated with single crystal slip, but at those orientations for which the effective stress, T_e, as defined in Parts I. and II., may reach the boundary [0001] to $[10\bar{1}0]$ duplex slip can occur. There is no position corresponding to multiple slip.

Twinning. The orientation of a twin relative to the matrix may be considered as the result of rotation through 180° about a specific axis, the twinning plane normal. This does not, of course, imply a bodily rotation of the lattice, for the atomic movements correspond to a shear of each atom layer parallel to the twinning plane together with, in many cases, atomic movements perpendicular to this plane. The macroscopic effect of these movements is one of simple shear in the twinning direction. The twinning planes in hexagonal close-packed metals are of the form $\{10\bar{1}2\}$, and for the $(10\bar{1}2)$ plane the twinning direction is the intersection of this plane with the $(1\bar{2}10)$.

Fig. 1.

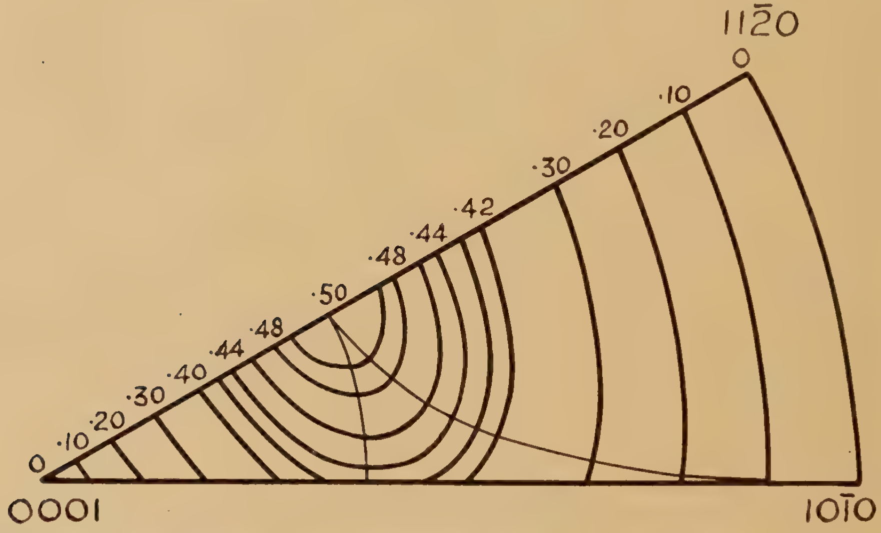

Unit triangle of standard hexagonal stereographic projection showing resolved shear stress contours and some lines of quickest descent for slip on (0001) planes in the $[11\bar{2}0]$ direction.

In establishing the conditions under which twinning occurs, it is necessary to take account of the fact that some metals have axial ratios, c/a, less than the ideal close-packed value of $\sqrt{3}$, *e. g.* magnesium, beryllium and titanium, while for others c/a exceeds this value, *e. g.* zinc and cadmium. Figs. 2 (*a*) and 2 (*b*) show the geometry of twinning for these two cases. For convenience, the positive sense of the twinning direction is taken as that lying on the opposite side of the *c*-axis from the twin plane normal. For $c<\sqrt{3}a$, fig. 2 (*a*), it is obvious that twinning will occur under tension only when the stress is so oriented as to give a component in the positive sense of the twinning direction, OD. The

Fig. 2.

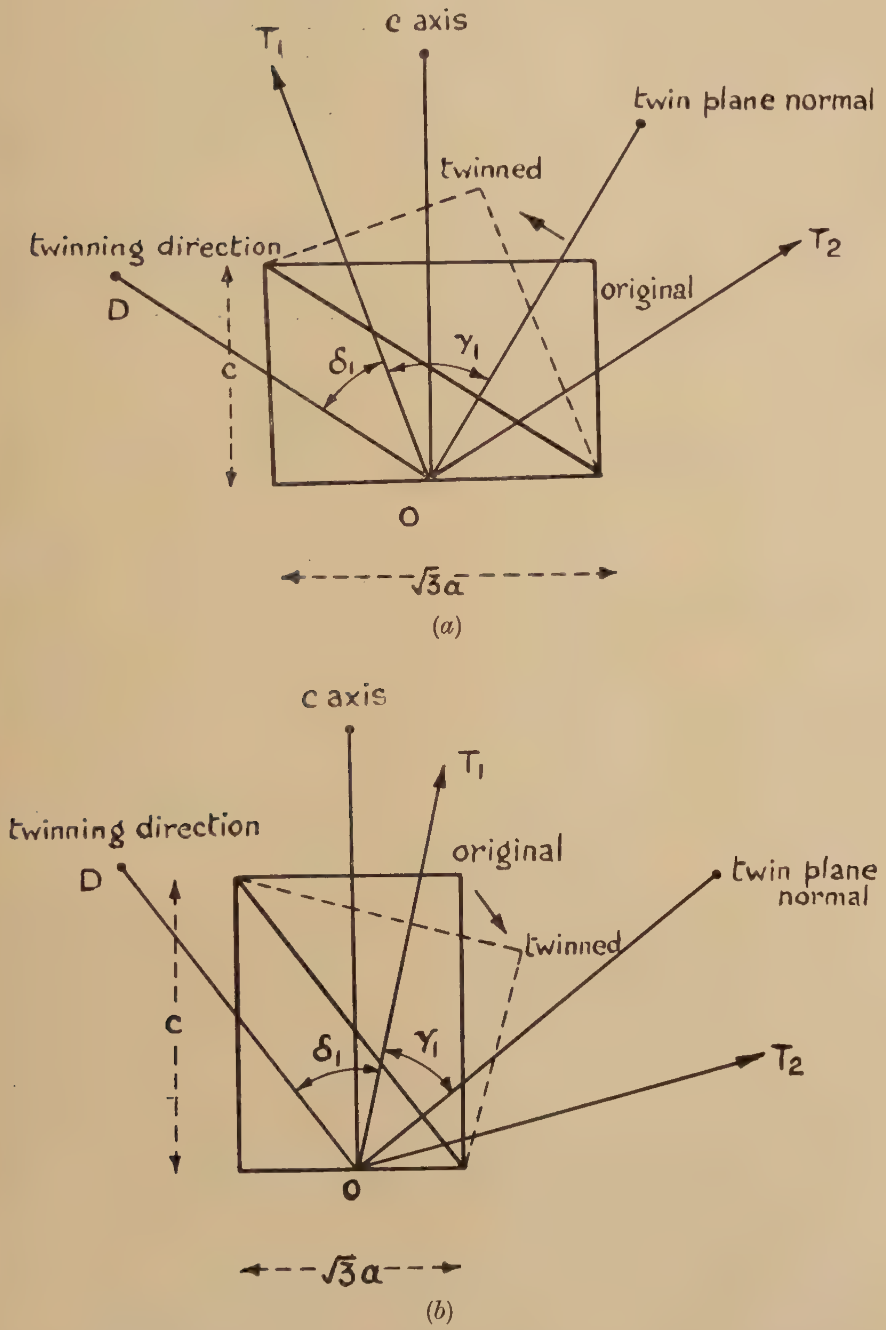

Diagrams illustrating the geometrical conditions for twinning, (*a*) for $c<\sqrt{3}a$, and (*b*) for $c>\sqrt{3}a$. The twinning direction, the twin plane normal, and the *c*-axis are all in the plane of the diagram.

resolved shear stress for twinning is T $\cos\gamma\cos\delta$ where γ and δ are respectively the angles which the stress makes with the twin plane normal and the positive sense of the twinning direction. Thus for twinning T $\cos\gamma\cos\delta$ must be positive. A tension of sufficient magnitude in the direction T_1 will produce twinning, but one in the direction T_2 can never do so. Consideration of fig. 2*b* for $c>\sqrt{3}a$ shows that the condition for twinning under tension is that T $\cos\gamma\cos\delta$ shall be negative. Conversely, under compressive stresses these two conditions are interchanged.

Boundaries between regions of slip and twinning. The boundaries between regions of slip and twinning are the loci of points at which the ratio of the resolved shear stress to the critical stress for slip is equal to the corresponding ratio for twinning, *i. e.*

$$T\cos\chi\cos\lambda/C_s=T\cos\gamma\cos\delta/C_t,$$

where T is the applied stress and C_s and C_t are the critical stresses for slip and twinning. The equation to the boundary is thus

$$\cos\gamma\cos\delta=n\cos\chi\cos\lambda, \quad . \quad . \quad . \quad . \quad . \quad . \quad . \quad . \quad (1)$$

where $n=C_t/C_s$. Inserting now the sign conditions for twinning, (1) becomes

$$\cos\gamma\cos\delta=+n\cos\chi\cos\lambda \quad . \quad . \quad . \quad . \quad . \quad (1\,a)$$

for $c<\sqrt{3}a$ under tension,

and $c>\sqrt{3}a$ under compression,

and

$$\cos\gamma\cos\delta=-n\cos\chi\cos\lambda \quad . \quad . \quad . \quad . \quad . \quad (1\,b)$$

for $c<\sqrt{3}a$ under compression,

and $c>\sqrt{3}a$ under tension.

In the calculations n has been chosen to be unity, the reason for which will be considered later. This choice was not made merely to simplify calculation. The intersections of the boundaries with the sides of the 30° unit triangle were determined for each of the six twinning systems with the most favourable slip system by appropriate substitution in equations (1 *a*) and (1 *b*). The angular distances of these intersections from the [0001] direction for the tension and compression cases of both zinc and magnesium are listed in Table I. The most favourable twinning system is that which has its boundary nearest to the maximum of the resolved shear stress contours for slip; these are marked with an asterisk in the Table and shown in fig. 3.

Reorientation due to twinning. The new orientation resulting from twinning may be found easily on a stereographic projection. For magnesium under tension twinning takes place from the area M_T on the twinning system *3* (Table I. and fig. 3 (*a*)). The original and twinned orientations are equidistant from the operative twin plane normal on the

Fig. 3.

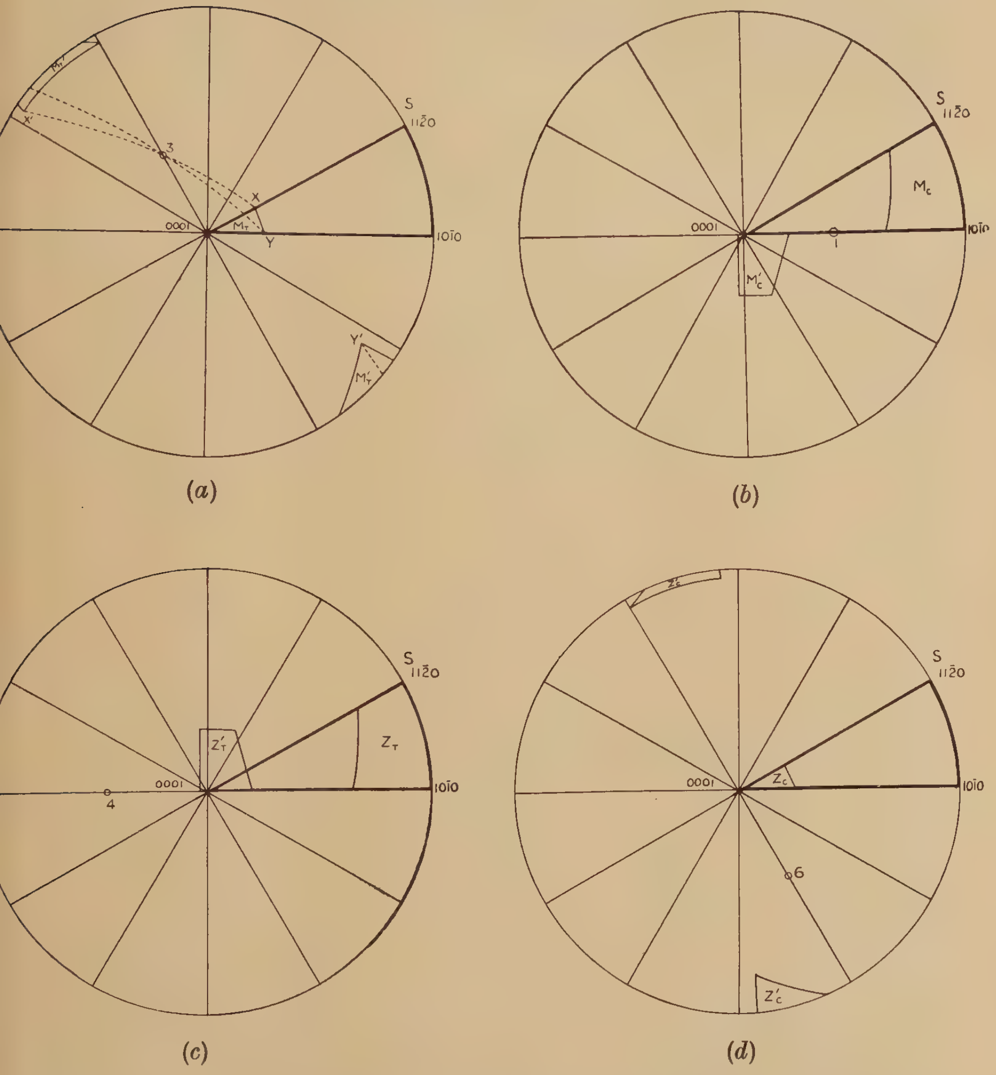

(a) (b) (c) (d)

Hexagonal standard stereographic projection, S is the most favourable slip direction for the reference unit triangle in heavy outline.

(*a*) Magnesium under tension. Showing the re-orientation from the twinning area M_T to the twinned area M'_T. The operative twin plane normal is the point *3*.

(*b*) Magnesium under compression. Twinning area, M_C, re-orients to the twinned area, M'_C. Operative twin plane normal, *1*.

(*c*) Zinc under tension. Twinning area, Z_T; twinned area, Z'_T; twin plane normal, *4*.

(*d*) Zinc under compression. Twinning area, Z_C; twinned area, Z'_C; twin plane normal, *6*.

great circle, through these three points. Thus, to obtain the twinned orientation X′ corresponding to the point X a great circle is drawn through X and the twin plane normal *3*; the angular distance between X and *3* along this great circle is measured, and an equal angular distance beyond *3* is marked off to give the point X′. Similarly the points Y′ and 0001′ may be obtained. The twinning areas and the regions into which they twin are shown in fig. 3 for magnesium and zinc under tension and compression.

TABLE I.

Intersections of Twin-Slip Boundaries.

Magnesium : $c/a=1{\cdot}624$; $n=1$.

Twinning system	Tension		Compression	
	Angles from [0001] along		Angles from [0001] along	
	$[0001]$–$[10\bar{1}0]$ side	$[0001]$–$[11\bar{2}0]$ side	$[0001]$–$[10\bar{1}0]$ side	$[0001]$–$[11\bar{2}0]$ side
1	23·4°	22·4°	64·4°	71·3°*
2	28·4°	22·4°	82·1°	71·3°
3	28·9°*	26·5°*	82·5°	90°
4	25·4°	24·2°	65·5°	72·8°
5	28·9°	24·2°	82·5°	72·8°
6	28·4°	26·5°	82·1°	90°

Zinc : $c/a=1{\cdot}858$; $n=1$.

Twinning system	Tension		Compression	
	Angles from [0001] along		Angles from [0001] along	
	$[0001]$–$[10\bar{1}0]$ side	$[0001]$–$[11\bar{2}0]$ side	$[0001]$–$[10\bar{1}0]$ side	$[0001]$–$[11\bar{2}0]$ side
1	66·5°	72·9°	25·7°	24·1°
2	82·7°	72·9°	29·0°	24·1°
3	82·1°	90°	27·4°	26·5°
4	64·4°*	71·3°*	23·5°	22·2°
5	82·1°	71·3°	27·4°	22·2°
6	82·7°	90°	29·0°*	26·5°*

* Most favourable twinning system. That the values for magnesium under tension and compression are equal respectively to those for zinc under compression and tension is fortuitous.

§ 3. TENSION AND COMPRESSION TEXTURES.

Magnesium under Tension. In the region AK$[10\bar{1}0][11\bar{2}0]$ of fig. 4 the only deformation mechanism is slip, which causes rotation leading to the $[11\bar{2}0]$ direction. It is now necessary to consider what happens in the neighbourhood of the twin-slip boundary XY. In accordance with the general concepts developed in Parts I. and II., it is visualized that if deformation occurs when the effective stress is at a boundary such as XY, then both slip and twinning will occur simultaneously in the small part of a grain under discussion. Since, however, the slip and twinning mechanisms are not necessarily initiated at the same point in this region both may begin. Whether one or both processes are halted by mutual interference is not important here, for the effect may be stated in general terms as producing some material which has slipped and some which has twinned. In a like manner, deformation occurring when the effective stress has reached a point such as Y, where two twin and two slip systems are equally favourable, will produce material of both twinned orientations and some of the orientation resulting from duplex slip rotation. For all the orientations in the area AXY the path of the effective stress leads to the slip-twin boundary XY and thence to Y. Thus, corresponding to the first part of the path of T_e, single slip rotation towards $[11\bar{2}0]$ results ; to the second part along XY, the same single slip rotation together with twinning on twin plane *3* ; and lastly, to deformation at Y, twinning on planes *3* and *5* and duplex slip rotation towards $[10\bar{1}0]$. For the adjacent region AKY also, T_e may reach Y and the same twinning and slip may occur. The further the original orientation from the boundary XY, the greater the path length of T_e during which there may be single or duplex slip, and consequently the more probable are these modes of deformation. As every element of slip rotation moves the original orientation away from the boundary the probability of twinning decreases fairly rapidly across the regions AXY and AKY until it is zero at the boundary AK. Similarly, there is some probability of slip for orientations within the twinning area [0001]XY. It will be seen, therefore, that in a polycrystalline aggregate, even assuming a unique value of the ratio of critical shear stresses for slip and twinning, there is no sharply defined boundary between orientations which twin and those which slip, but that the boundary XY defines the regions in which these processes predominate.

In specifying the fibre textures it is sufficient to consider only a single unit triangle of the standard projection, and the orientation after twinning, M'_T of fig. 3, is equivalent to the area M''_T in fig. 4. That is to say, material from the area [0001]XY twins to M''_T. Thus, after considerable deformation, all the orientations will have moved by slip and twinning to the edge of the unit triangle near to the $[11\bar{2}0]$–$[10\bar{1}0]$ boundary. This corresponds to a texture with all directions in the basal planes parallel to the tension axis. As further deformation can occur only by slip, giving rotation towards the $[11\bar{2}0]$ direction, in final texture with this direction parallel to the stress axis might be expected. However, on the $[11\bar{2}0]$–$[10\bar{1}0]$ edge the resolved shear stress on the slip system is zero, and the result of T_e reaching here can only be fracture of the grain or part of a grain under consideration. When this occurs early in the deformation process, fracture of the whole specimen may or may not follow, but in the later stages when it has occurred at a number of places, failure of the whole specimen is practically certain. The probability of fracture is highest for orientations near the [11$\bar{2}$0]–[10$\bar{1}$0] edge, and so the development of a very strongly marked [11$\bar{2}$0] tension texture is unlikely.

Magnesium under Compression. The magnesium compression texture is equally simple. The slip rotations lead towards the pole of the operative

Fig. 4.

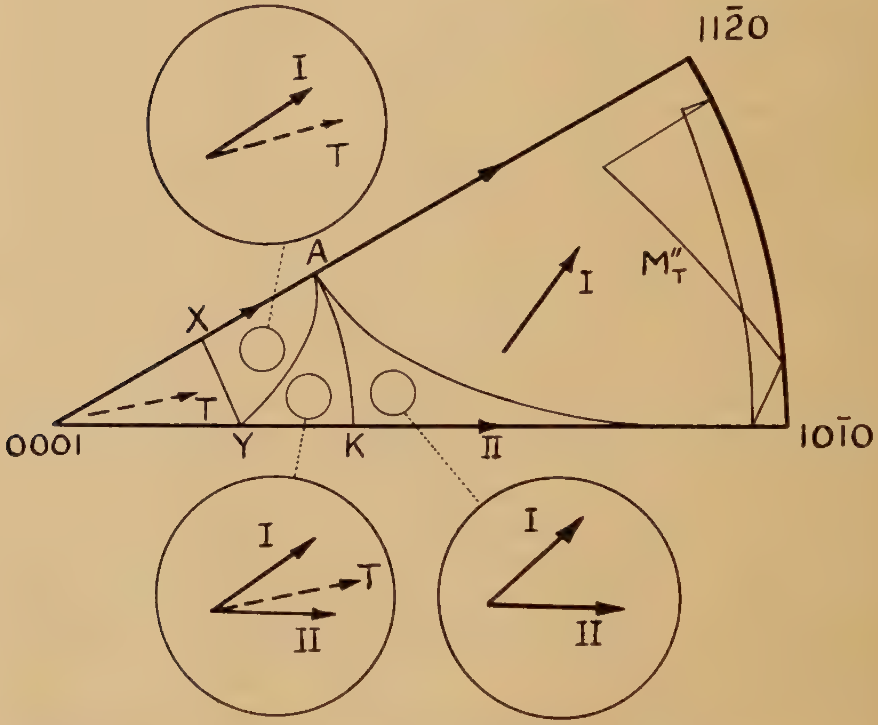

Stereographic Unit triangle showing the slip rotations and twinning re-orientations for magnesium under tension. I and II indicate directions of single and duplex slip rotations ; T is the general direction of twinning re-orientation.

slip plane, namely the basal plane, and the twinning takes place from a region near the [11$\bar{2}$0]–[10$\bar{1}$0] edge to new orientations also near the pole of the basal plane, M'_C in fig. 3. The texture is thus specified as [0001] parallel to the direction of compression.

Zinc under Tension. In zinc the different geometry of the twinning, typical of axial ratios $c/a>\sqrt{3}$, gives an interesting dynamical equilibrium of texture instead of the usual end points. Under tension the slip rotations lead towards the [11$\bar{2}$0] direction, but orientations within the twinning area Z_T of fig. 3 and all those which rotate by slip to this area twin back to a region near the pole of the basal plane, Z'_T. The ensuing cycle of slip and twinning is not, however, endless, for local fracture occurs whenever T_e reaches the [0001] position where the resolved shear stress on the slip system is zero. Thus, there will be a concentration of orientations in the neighbourhood of the slip-twin boundary, more marked near its intersection with the [0001]–[11$\bar{2}$0] edge. In the case of $n=1$, this corresponds to [11$\bar{2}$0] directions at not less than 20° from the tension axis. For higher values of n this angle decreases. Due to the twinning of material back to Z'_T, there will be a continuous spread of orientation from the [0001] pole towards the slip-twin boundary.

Zinc under Compression. Here the twinning region is near the pole of the basal plane, which is also the end point of the slip rotations. Again there may be a cycle of slip and twinning, and the resulting texture, defined by the slip-twin boundary, is, with $n=1$, that of [0001] directions not less than 25° from the direction of compression. In addition, there is a spread of orientation across the unit triangle.

§ 4. Rolling Textures for Magnesium and Zinc.

The stresses associated with sheet rolling may be simulated by compression parallel to the rolling plane normal and subsidiary tension parallel to the rolling direction. The development of the rolling texture in terms of the basal plane pole figure will now be considered.

For magnesium, the compression twins all grains having orientations with (0001) poles more than about 68° from the compression axis the centre of the pole figure in fig. 5. This twinning brings the (0001) poles to the centre of the figure to which point also the slip rotations lead. This corresponds to a texture in which the basal planes lie in or near the rolling plane. At the same time, the tension tends, somewhat weakly, to line up [11$\bar{2}$0] with the rolling direction. These orientations are mutually consistent, but there is some departure from circular symmetry in the pole figure due to further twinning effects. In the region less than 28° from the rolling direction characterized by the point a, only tension twinning occurs to new orientations in the vicinity of the transverse direction. These then twin under compression to the centre of the pole figure. This twinning of the region around a leaves less material to rotate by slip to the centre and gives a corresponding contraction in the intermediate contours of the texture, fig. 5.

In the rolling of zinc the compression gives slip rotations bringing basal plane poles to within 25° of the centre of the pole figure, fig. 6. Inside this circle twinning occurs to orientations near the circumference of the pole figure. The tension causes twinning of all material with basal plane poles more than 70° from the rolling direction, the new orientations being around the rolling direction. Since the tension removes the material from the central band the compression twinning is principally that from orientations such as C. These twin to positions near the transverse direction and thence under tension to near the rolling direction. Thus, the twinning gives some concentration of orientations in the neighbourhood of the rolling direction rather than at other points around the circumference. From these considerations the semi-quantitative pole figure in fig. 6 was drawn.

§ 5. DISCUSSION.

In magnesium and zinc it can be shown that the texture for cold-drawn wires predicted from a consideration of basal plane slip and twinning on the $\{10\bar{1}2\}$ planes is the same as that for pure tension. This is because the textures produced by longitudinal tension and radial compression are mutually consistent. Schmid and Wassermann (1929) have shown that in magnesium wire all directions in the (0001) planes are parallel to the wire axis in complete accord with the texture predicted here. It is found, however, with cold-drawn magnesium alloy, Dowmetal, that only the $<10\bar{1}0>$ directions lie parallel to the wire axis (Morell and Hanawalt 1932). This texture is not predicted by the present treatment but it is consistent with the incidence of pyramidal slip, *i. e.* slip on the $\{10\bar{1}1\}$ planes in the close-packed direction, $<11\bar{2}0>$. Since this deformation mode is not accepted as playing a principal role in

Fig. 5.

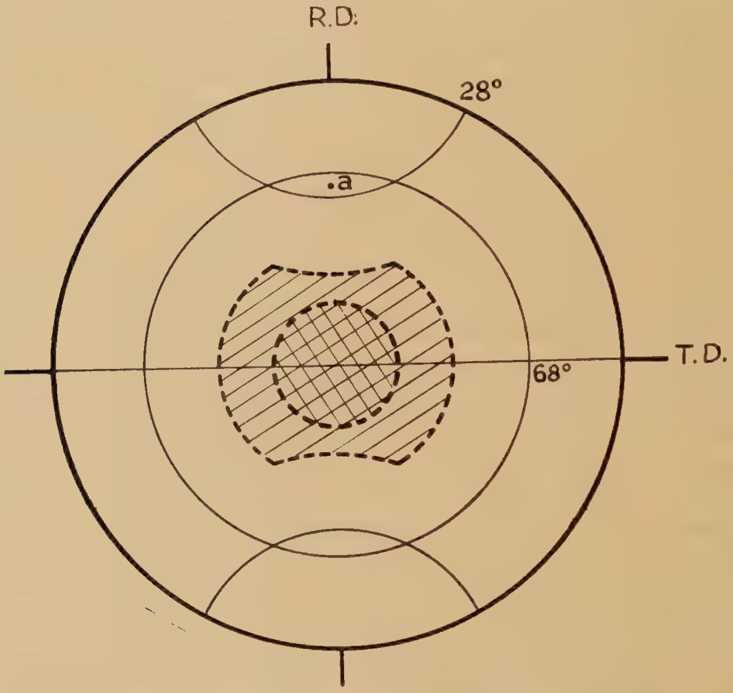

(0001) pole figure for rolled magnesium sheet.

hexagonal metals at room temperatures it has not been considered here, but it may be profitably introduced at some future time. Zinc wires in the early stages of deformation show [0001] directions parallel to the wire axis, while at later stages the hexagonal axis lies at about 70° from the wire axis, Barrett (1943). This latter texture is predicted and the early [0001] texture is no doubt due to the augmentation of this orientation by the initial twinning.

The simple compression texture derived for magnesium in the previous section is confirmed by the experiments of Tsuboi (1928) who found [0001] directions parallel to the axis of compression. There appear to be no experimental data on the pure compression texture of zinc or other hexagonal metals.

Fig. 6.

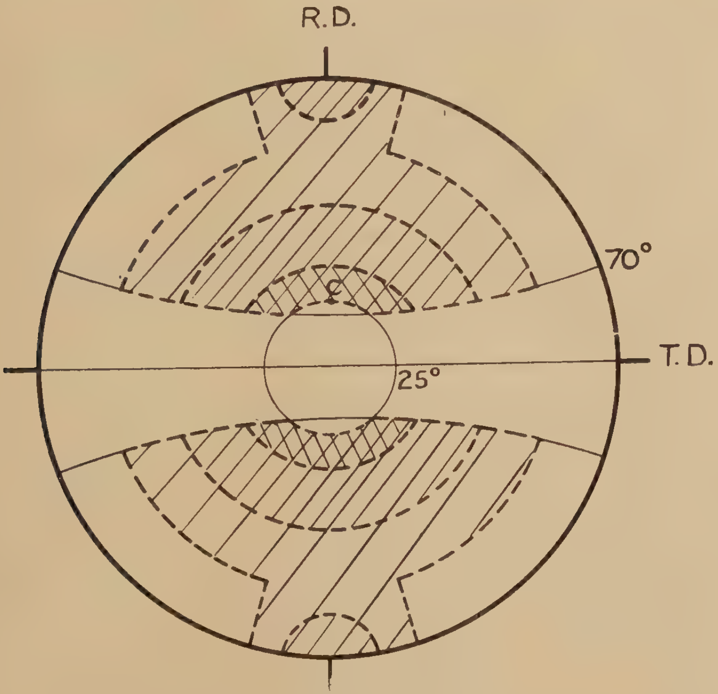

(0001) pole figure for rolled zinc sheet.

The general features of the rolling texture of magnesium, basal planes in or near the rolling plane and <11$\bar{2}$0> tending towards the rolling direction, are in agreement with the experimental pole figures of Schmid and Wassermann (1930), Caglioti and Sachs (1932) and Bakarian (1942). There are, however, some minor differences in the results of these investigations. It has been shown that some of these differences may be due to changes in composition of rolling technique, Hanawalt (1936), or to inhomogeneity of texture through the sheet, Fuller and Edmunds (1934) and Hargreaves (1945). The other metals titanium, beryllium and zirconium which have axial ratios less than $\sqrt{3}$ have the same general texture of basal planes lying in or near the rolling plane, but there is definite evidence of a spread of basal plane normals towards the transverse direction (Clark 1950, Smigelskas and Barrett 1949, Burgers and Jacobs 1935). There is also a tendency for the $[10\bar{1}0]$ directions rather than the $[11\bar{2}0]$ directions to lie parallel to the rolling direction. These observations appear to be consistent with the operation of pyramidal slip. It is felt that a detailed consideration of this deformation mode will be justified when the textures have been determined more accurately with the aid of X-ray Geiger counter methods.

The pole figure for zinc, fig. 6, is in good agreement with the pole figures of Caglioti and Sachs (1932) and Valouch (1932). In addition, the increase in density of [0001] directions around the rolling direction found by Fuller and Edmunds (1934) is explained.

All the textures have been derived on the assumption that $n=1$, *i.e.* that the ratio of critical shear stresses for slip and twinning is unity. This assumption must be examined in the light of the experimental observations on these stresses and the agreement obtained between the observed and the predicted textures. There are few experimental determinations of the critical shear stress associated with the twinning process, and even these are not conclusive. They indicate, however, that in the earliest stages of deformation the critical stress for twinning is several times that for slip, although the twinning stress appears to decrease after slip has taken place (Miller 1936). The ratio of the stresses therefore may well approach unity after the severe deformations required to produce the degree of preferred orientation considered in the foregoing sections. The textures themselves provide further evidence that the effective value of the ratio is near to unity. Cold-drawn zinc wires have the hexagonal axis at about 70° from the wire axis, the predicted angle with $n=1$ being about 69°. Again, in the sheet rolling texture of zinc the hexagonal axes lie at 20–25° from the rolling plane normal towards the rolling direction, compared with the predicted value of about 27°. These results suggest that n is slightly greater than unity.

§ 6. Conclusions.

The manner in which the process of twinning may be incorporated into the treatment of the development of deformation textures described in Parts I. and II. has been demonstrated. Good agreement with the observed textures has been obtained for both magnesium and zinc, hexagonal metals characteristic of those having axial ratios respectively less and greater than the ideal close-packed value.

The method is capable of refinement in the prediction of details of the hexagonal textures by the introduction of the effects of pyramidal slip, and of a more careful consideration of twinning re-orientations should a particular problem arise or more accurate experimental observations become available to justify this course.

ACKNOWLEDGMENTS.

The work described above has been carried out as part of the general research programme of the National Physical Laboratory, and this paper is published by permission of the Director of the Laboratory.

REFERENCES.

BAKARIAN, P. W., 1942, *Trans. A.I.M.E.*, **147,** 267.

BARRETT, C. S., 1943, *Structure of Metals*, 1st Ed., p. 383 (New York : McGraw-Hill).

BURGERS, W. G., and JACOBS, F. M., 1935, *Metallwirt*, **14,** 285.

CAGLIOTI, V., and SACHS, G., 1932, *Metallwirt*, **11,** 1.

CALNAN, E. A., and CLEWS, C. J. B., 1950, *Phil. Mag.* [7], **41,** 1085 ; 1951, *Ibid.*, **42,** 616.

CLARK, H. T., 1950, *Trans. A.I.M.E.*, **188,** 1154.

FULLER, M. L., and EDMUNDS, G., 1934, *Trans. A.I.M.E.*, **111,** 146.

HANAWALT, J. D., 1936, *Symposium on Radiography and X-ray Diffraction*, (Philadelphia : A.S.T.M.).

HARGREAVES, A., 1945, *J. Inst. Metals*, **71,** 73.

HIBBARD, W. R., and YEN, M. K., 1948, *A.I.M.E.*, T.P. 2334.

MILLER, R. F., 1936, *Trans. A.I.M.E.*, **122,** 176.

MORRELL, L. G., and HANAWALT, J. D., 1932, *J. Appl. Phys.*, **3,** 161.

SCHMID, E., and WASSERMANN, G., 1929, *Naturwiss.*, **17,** 312 ; 1930, *Metallwirt*, **9,** 698.

SCHMID, E., and BOAS, W., 1950, *Plasticity of Crystals*, (English Translation of *Kristallplastizität*), (London : F. A. Hughes & Co.).

SMIGELSKAS, A., and BARRETT, C. S., 1949, *Trans. A.I.M.E.*, **185,** 145.

TSUBOI, S., 1928, *Mem. Coll. Sci. Kyoto Imp. Univ.*, **A11,** 375.

VALOUCH, M. A., 1932, *Metallwirt*, **11,** 165.

XCIV. *Observations on the Multiple Scattering of Ionizing Particles in Photographic Emulsions.*—Part II. *The Scattering of Positrons at* 105 *and* 185 *MeV.*

By M. G. K. MENON, C. O'CEALLAIGH*, and O. ROCHAT,
H. H. Wills Physical Laboratory, University of Bristol.†

SUMMARY.

The coordinate method has been used to measure the multiple scattering in Ilford G5 emulsions of positrons of nominal energy 113 and 196 MeV. The energies of the positrons corrected for loss by ionization and radiation are calculated to be 105 and 185 MeV. respectively. The experimental distributions of second differences have been compared with those predicted by the theory of Molière (1947, 1948) and the agreement found to be very satisfactory. Methods of minimizing the effects of spurious scattering and of taking into account the influence of distortion are discussed. Values are found for the scattering constant which are in good agreement with those calculated from the theory of Molière. A discussion of these results has been given in a previous paper of this series (Gottstein *et al.* 1951). A mathematical treatment is given in the Appendices: (I.) the correlation existing between successive second differences, (II.) the distribution of second differences when measured in the presence of spurious scattering, and (III.) a possible method for correcting second differences which have been affected by a large angle scattering.

§ 1. INTRODUCTION.

THE multiple scattering of positive electrons has been measured for two energies in Ilford G5 nuclear research plates. They had been exposed in the Cornell Synchrotron to a beam of positrons selected by a magnetic spectrometer, and have been made available to us through the courtesy and cooperation of Professor Dale R. Corson. He has also supplied us with the following information. Deducting 1 MeV. to allow for loss in the 2·4 mm. of aluminium which the particles traversed before entering the plates, the nominal energies of the positrons were 113±4 MeV. and 196±5 MeV. The uncertainties quoted represent, not probable errors, but limits of uncertainty. It will be shown later that these nominal figures must be corrected for ionization and radiation loss. The final energy values adopted for the purposes of this experiment are 105±4 and 185±5 MeV. respectively.

---

[*] On leave of absence from the University College, Cork.
[†] Communicated by Prof. C. F. Powell, F.R.S.

§ 2. EXPERIMENTAL METHOD.

The scattering has been measured by the coordinate method of Fowler (1950). Two Cooke, Troughton and Simms M4000 nuclear research microscopes were employed. The plates 1 in. × 3 in. with emulsions 100 μ thick, were mounted so that the paths of the electrons appeared approximately parallel to the x-axis of motion of the stage. The particles entered the plates near one of the shorter edges and followed a path approximately parallel to the longer edges. In order to minimize the effect of errors due to possible distortion of the emulsion, no measurement of scattering was made on any portion of track which was less than 2 mm. from an edge of the plate. This distance has been found adequate, having regard to the magnitude of the multiple scattering and the thickness of the emulsion.

A line 2 mm. from the edge through which the electrons entered the emulsion, and approximately parallel to the y-axis of motion of the stage, was traversed, and particles which crossed this line were selected for measurement if they satisfied the following criteria :

(1) The angles between the trajectory of the particle and the stage x-axis must be less than 0·04 radians.

(2) The path length visible in the emulsion must exceed a minimum of 1500 μ for the 105 MeV., and 3000 μ for the 185 MeV. positrons.

By imposing these conditions, it was hoped to exclude both stray particles and such cases of radiation loss as were accompanied by scattering of appreciable magnitude. Each selected track was then traced back to the point at which it entered the emulsion, so that due allowance could be made for such energy loss by ionization and radiation as occurred between the magnetic spectrometer and the point from which measurement of the multiple scattering was carried out.

The measurements were made using oil-immersion objectives × 95 with eyepieces × 15, one of which was furnished with a scale of 120 divisions. This was set perpendicular to the direction of motion of the stage.

The stage was advanced in equal steps by a micrometer screw. These steps will be referred to as the primary cell size. The position of the track was read on the eyepiece scale as shown in fig. 1. We draw in imagination, a mean line passing through the mass centres of such grains as lie within a suitable distance, on either side of the scale. The position of the track is then defined as the point of intersection of this line with the scale axis. In fig. 1 this distance is shown as 10 μ, since the tracks are of minimum grain density and the grains rather widely spaced ; in the case of tracks of higher grain densities, the distance used will be smaller.

This procedure results in a smoothing ; and we may no longer set the "smoothing factor" $(\langle\Phi\rangle_{\text{chord}}/\langle\Phi\rangle_{\text{tan}})^2=2/3$ as would be valid if dealing with chords measured between two points on a continuous curve, The smoothing factor applicable to our case was calculated to be $(2/3)(1-\gamma^2+3r^3/5)$ (following Molière 1951) where $\gamma=0{\cdot}1/s$ and s=cell size in units of 100 μ. For cells of 50 μ or greater this correction will be negligible.

For each track the second differences of the coordinate readings D_j were evaluated for the primary cell-size in the way described by Fowler (1950), and also for other cell-sizes using varying degrees of overlap. A definition of "degree of overlap", and a detailed discussion of its influence on the measurements, is given in the following paper (III.) of this series (O'Ceallaigh and Rochat 1951). The mean of these values of second difference taken without regard to sign we denote by the symbol $\bar{D}$. We have $\bar{D}=(1/n)\sum_{j=1}^{n}|D_j|$ where n is the number of individual values of second difference in the track. Physically, this statistic is a measure of the mean value of the angle between successive chords of track segments defined by the cell-size. The symbol "s" will be used to denote the cell-size in units of 100 μ and $\bar{D}_s$ the value of the corresponding statistic. The following Table summarizes the relevant information.

Fig. 1.

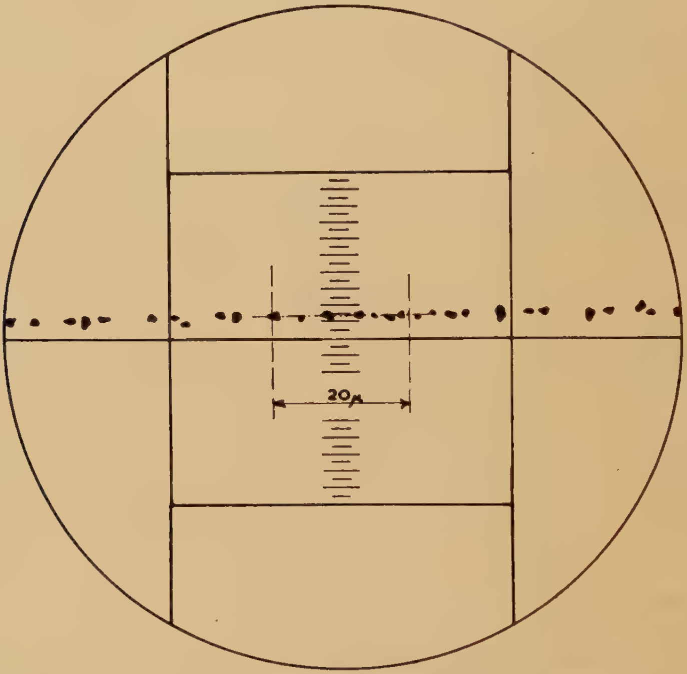

Diagram showing the method of reading the position of the track on the eyepiece scale. For clarity, only 40 divisions are shown on the scale in the diagram. A mean line is drawn in imagination passing through the mass centres of the grains lying about 10 μ on either side of the scale axis. The intersection of this line with the scale axis is read off.

TABLE I.

Energy	185 MeV.	105 MeV.
Total number of tracks	56	57
Total length (cm.)	24·0	15·2
Average length per sample (mm.)	4·30	2·67
Prime cell-size (s)	0·5	0·25
Other cell-sizes employed (s)	1, 2, 4, 6, 8	0·5, 1, 2, 3

§ 3. SELECTION OF TRACKS SUITABLE FOR MEASUREMENT.

Among the tracks selected, and included in Table I., there may still be some which have lost energy or which may be unrepresentative. Such tracks have been rejected in accordance with the following systematic procedure.

The value of $\bar{D}$ was evaluated for each track using cell-size 100 μ for the 105 MeV. and 200 μ for the 185 MeV. positrons. A value $\bar{\Delta}=\frac{1}{n}\sum_{j=1}^{n}\bar{D}_j$ was also obtained by adding together the results for all the individual tracks to obtain a single composite track. $\bar{\Delta}$ will be an unbiased estimate of the $\bar{D}$ of the tracks provided that no track had suffered large energy loss.

The distributions of $\bar{D}$ obtained from the individual tracks are shown in the upper quadrants of fig. 2. Because the tracks are of finite length, the occasional large deviations due to plural or single scattering will be reflected in the sampling histogram by the occurrence of a few unrepresentative tracks with large values of $\bar{D}$. In order to avoid this inconvenience, it has been usual, before evaluating $\bar{D}$ for any track, to remove from it all values of $D_j \geqslant 4\bar{D}$. The distributions indicated by single hatching are those of the tracks which contained no signals $D_j \geqslant 4\bar{D}$. They are exhibited in both upper and lower quadrants, and are thus distinguished from those tracks which contained such excessive values. The unshaded portions show the latter. In the upper quadrants they refer to the tracks before removal of all $D_j \geqslant 4\bar{D}$ and, in the lower quadrants, to the distribution of $\bar{D}$ after these had been excluded.

Certain tracks remain which exhibit values of $\bar{D}$ so high that it is improbable that they have been observed merely as a matter of chance, but rather, that they are those of electrons, the energy of which has become degraded below that of the beam. Let us assume that $\bar{\Delta}$, the value of $\bar{D}$ obtained from the composite track is that of the universe from which the sample has been drawn, and that this universe is normal. Both assumptions are sufficient approximations. We evaluate for each suspect track in turn, starting with that of greatest $\bar{D}$, the quantity $\chi^2=n\bar{D}^2/\bar{\Delta}^2$ where n is the number of statistically independent cells in the chosen track. The probability of chance occurrence of χ^2 may be found from the well-known tables. In the present case, rejection was fixed at $2\frac{1}{2}$ per cent level. After rejection of each track which failed to satisfy the test, the amended value of $\bar{\Delta}$ was calculated before applying the test to the next suspect. The probability of chance occurrence of the low values of $\overline{D}$ was examined in a similar way. In all, twelve tracks were excluded, seven for the 185 MeV., and five for the 105 MeV. series. They are represented by cross-hatching in the lower pair of histograms.

Fig. 2.

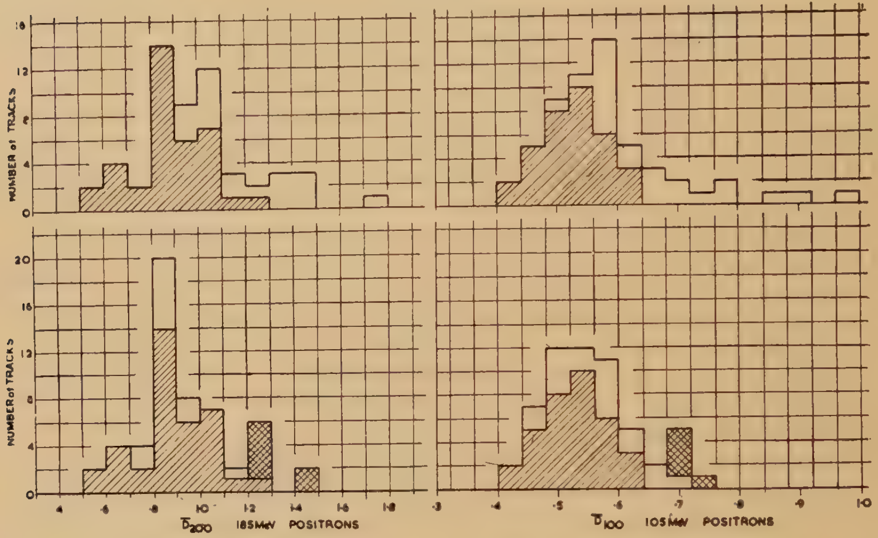

Distribution of $\overline{D}$ obtained from individual tracks. The effect of removing values of $D_j \geqslant 4\overline{D}$ and of eliminating tracks of certain unrepresentative electrons is shown as follows.

Upper quadrants: Before elimination of large angles.

Single-hatching-tracks containing no signals $\geqslant 4\overline{D}$. Unshaded-tracks containing one or more signals $\geqslant 4\overline{D}$.

Lower quadrants: After elimination of large angles.

Single-hatching-tracks unaffected by the elimination procedure. Unshaded+cross-hatching-tracks to which the elimination procedure had been applied.

Tracks represented by cross-hatchings in the lower quadrants are those which have been excluded since they are suspected of having suffered Bremsstrahlung loss.

§ 4. INFLUENCE OF DISTORTION.

The precautions taken to exclude distorted tracks have already been touched upon. Since the emulsion was only $100\,\mu$ thick, distortion is likely to be inappreciable, except in the immediate neighbourhood of corners and edges. Nevertheless, certain further precautions were taken. Histograms were drawn for the composite track, showing the distribution of the individual D_j's for different cell-sizes. One such histogram is reproduced in fig. 3. The value of the true (algebraic) mean, computed for the $100\,\mu$ and $200\,\mu$ cell-sizes, did not differ significantly from zero at any statistical level less than 10 per cent. Further, the distribution of D_j was examined for each individual track. The calculated value of the algebraic mean was checked by Student's t-Test in order to ascertain the probability that the sample could have been drawn from a universe of mean equal to zero. No track yielded a value which was significant at the 5 per cent level. The observed distributions of the algebraic means for 200 μ cells, both for the 105 and 185 MeV. positrons, are plotted in fig. 4. The histogram shown in fig. 4(a) is found to compare satisfactorily with the normal distribution of means for samples of track of average length. The histogram of fig. 4(b), on the other hand, shows some evidence of representing a bimodal distribution. It would appear reasonable to suppose that it is due to the superposition on a normal distribution, of values of algebraic mean derived from a few tracks affected by slight positive or negative distortion. Even though the tracks have been selected from a region 2 mm. away from any edge, it is not unlikely that such slight distortion exists in the fringing regions. It may be seen from the histogram, however, that such distortion as may exist in individual tracks cannot have any significant influence on the experimentally determined value of $\bar{D}$.

Fig. 3.

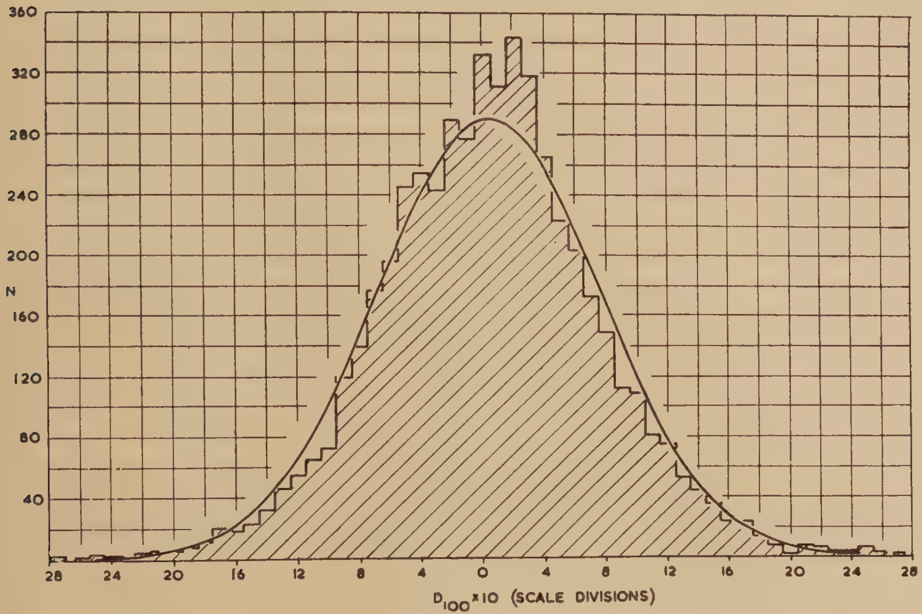

Distribution of 5249 individual values of D_j in overlapping 100μ cells for the 105 MeV. positrons. The curve in full is the normal error curve, the algebraic mean, and standard deviation of which have been chosen to agree with that of the sample.

§ 5. CORRECTIONS TO THE NOMINAL ENERGY OF THE TRACKS.

The energy of the electrons, known on emergence from the magnetic spectrometer, must be corrected for loss by ionization and radiation, first in an aluminium sheet of 2·4 mm. thickness, and then in passing through the glass and emulsion of the plates. It was found that the average electron travelled 1 mm. through glass and 1 mm. through emulsion before reaching the point from which the scattering was measured.

The correction for energy loss by ionization and radiation has been computed for the various absorbers, taking into consideration the following facts. Particles which had suffered large radiation losses ($\gtrsim$50 per cent) up to the point from which the measurements started, have been excluded by the systematic procedure of selection ; those in which such losses occurred along the measured path could be recognized from the trend of scattering along the course of each track.

Fig. 4 (*a*).

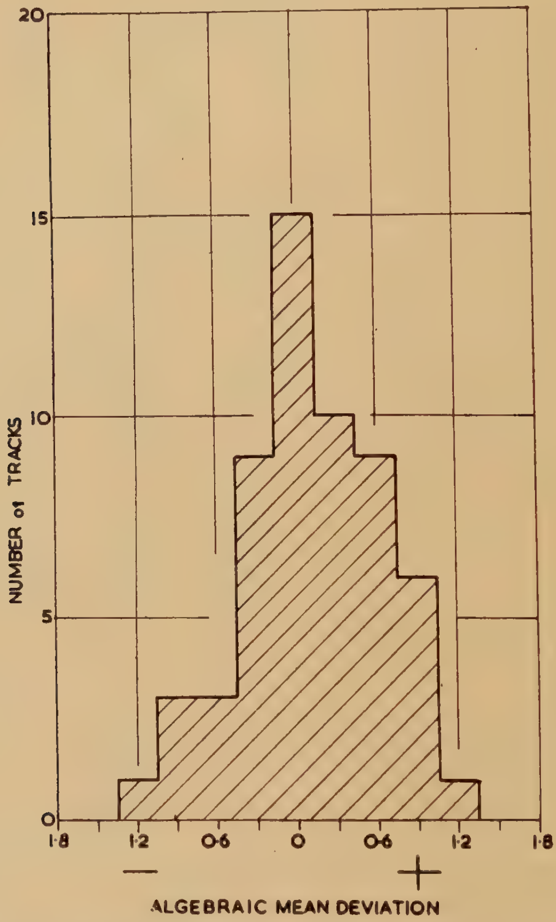

Distribution of the algebraic means in 200 μ cells for individual tracks. 105 MeV. positrons.

Energy loss along the measured portion of the tracks was allowed for. The energy chosen as appropriate was that corrected to the mid-point of the track of average length. The energies adopted were 105 MeV. and 185 MeV. for the electrons of nominal energy 113 and 196 MeV., and were used both for the purpose of comparison with theory, and for obtaining a value of the scattering constant.

§ 6. Experimental Results.

The value of $\overline{\mathrm{D}}$ for the 105 MeV. electrons was determined for cell-sizes 25, 50, 100, 200 and 300 microns.

As each track was being scattered the readings were plotted on squared paper. This proved a useful method of avoiding gross errors. A smooth curve drawn through the readings was assumed to be a good representation of the course of the track. There is less likelihood of a background grain being mistaken for one belonging to the track when this technique is used, and uncertainties arising from the random distribution of developed grains about the true trajectory of the particle are to some extent smoothed out.

Fig. 4 (*b*).

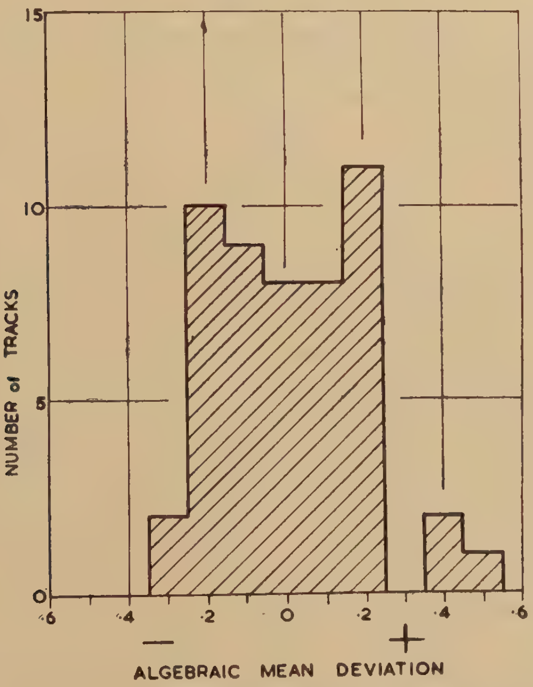

Distribution of the algebraic means in 200 μ cells for individual tracks. 185 MeV. positrons.

The experimental results are summarized in Table II. In column 2 are listed the experimental values of $\overline{\mathrm{D}}$ for the various cell-sizes. The third column gives the value of $\overline{\mathrm{D}}_{c.o.}$ which is the mean value of $\overline{\mathrm{D}}$ when all values of $D_j \geqslant 4\bar{D}$ are excluded and corresponds to the truncated distributions discussed previously (Gottstein *et al.* 1951, henceforth referred to as I.).

TABLE II.

105 MeV. Electrons.

Cell-size (μ)	$\bar{D}$ Scale Divisions	$\bar{D}$ cut-off
25	—	0·1425
50	0·243	0·234
100	0·556	0·537
200	1·50	1·47
300	2·59	2·55

Corresponding figures for the 185 MeV. electrons are given in Table III.

TABLE III.

185 MeV. Electrons

Cell-size (μ)	$\bar{D}$ Scale Divisions	$\bar{D}$ cut-off
50	0·220	0·210
100	0·410	0·400
200	0·910	0·870
400	2·24	2·16
600	3·81	3·73
800	5·90	5·76

Since the magnifying power of the instruments is slightly dependent on the interocular distance, the factor for converting scale divisions to microns will vary with different observers. The magnification was found by using a standard object engraved in 10 μ divisions, and by means of the stage micrometer. An extreme variation between observers was $2\frac{1}{2}$ per cent and a weighted mean factor of 0·48 was calculated for conversion of scale divisions to degrees/100 μ.

The values of the scattering constant given in Table II. and fig. 1 of Gottstein *et al.* (1951), have been calculated from the results shown in Tables II. and III. The values obtained for the scattering constant (K) are :—

(1) 105 MeV. positrons, 200μ cells :

$$K_{\text{without cut-off}}\ 26{\cdot}7 \pm 0{\cdot}6, \quad K_{\text{with cut-off}}\ 26{\cdot}2 \pm 0{\cdot}6.$$

(2) 185 MeV. positrons, 400μ cells :

$$K_{\text{without cut-off}}\ 24{\cdot}9 \pm 0{\cdot}8, \quad K_{\text{with cut-off}}\ 24{\cdot}0 \pm 0{\cdot}8.$$

The influence of noise on these results is very small for these cell-sizes, as will be shown later on in this paper, and has therefore been neglected.

§ 7. DISTRIBUTION OF SECOND DIFFERENCES AND COMPARISON WITH THEORY.

Histograms of the distribution of the individual values of the second difference (D_j) have been studied for different cell-sizes. Fig. 3 gives the results of plotting 5249 values of D_j obtained from overlapping

100 μ cells for the 105 MeV. positrons. The curve in full line is the normal error curve, of which the algebraic mean and standard deviation have been chosen to agree with those of the sample.

Judged by the χ^2 test, the fit is satisfactory. The appearance of the histogram, however, suggests that the universe from which the values of D_j have been drawn is more peaked than normal. This accords with theory, and receives further support from the fact that the " noise " present in the measurements on 100 μ cells will tend to flatten the experimental distribution. Hence, if the central region is fitted to a normal curve of smaller dispersion, the distribution of the larger values of D_j will appear as a " tail " to this normal curve in the manner envisaged by Williams.

The experimental distributions compared with the theory of Molière are shown in fig. 5(*a*) (105 MeV. 100 μ cells), and fig. 5(*b*) (185 MeV. 200 μ cells). All the curves have been drawn for the energies stated above, using figures for the composition of the emulsions supplied by the manufacturers. The curves drawn in dotted lines represent the " normal approximations " defined in I., p. 712. Since the experimental results contain " noise " they may be expected to present a less peaked appearance than the theoretical distributions. We have found it possible, however, to calculate an expected distribution which takes account of the effect of noise. The detailed working is given in Appendix II., and yields the modified theoretical distribution shown by the curves in full line. The agreement with experiment appears to be very satisfactory.

In the experimental distribution of D_j for cell-sizes in excess of 300 μ the " tail " is less in evidence than for the smaller cell sizes, and the distributions tend towards the normal more rapidly than might be expected from the change of L with cell-size (I., p. 714). Since the emulsions used were only 100 μ in thickness, it seems reasonable to suppose that this effect is due to what has been termed by Molière the " Flache Kammer " effect (Molière 1948). Briefly, in evaluating functions $P(\phi)$ it was tacitly assumed that no restriction need be placed on the magnitude of the projected deflection on a plane at right angles to that of the emulsion. For thin emulsions, however, this assumption becomes invalid, especially when measurements are made on large cell-sizes. In these circumstances the tracks selected as being of length sufficient for measurement will tend to be those deficient in large signals.

The distribution functions must be modified so as to take account of this bias. Molière has considered the limiting case of vanishing thickness, and obtains a distribution which differs little from the " normal approximation ". Calculations have already been published which apply to cloud chamber measurements where a similar restriction exists because of the finite depth of the illuminated region (O'Ceallaigh and MacCarthaigh 1944, Barker 1948, O'Ceallaigh 1950). It is intended to examine the general case for the photographic emulsion using similar methods.

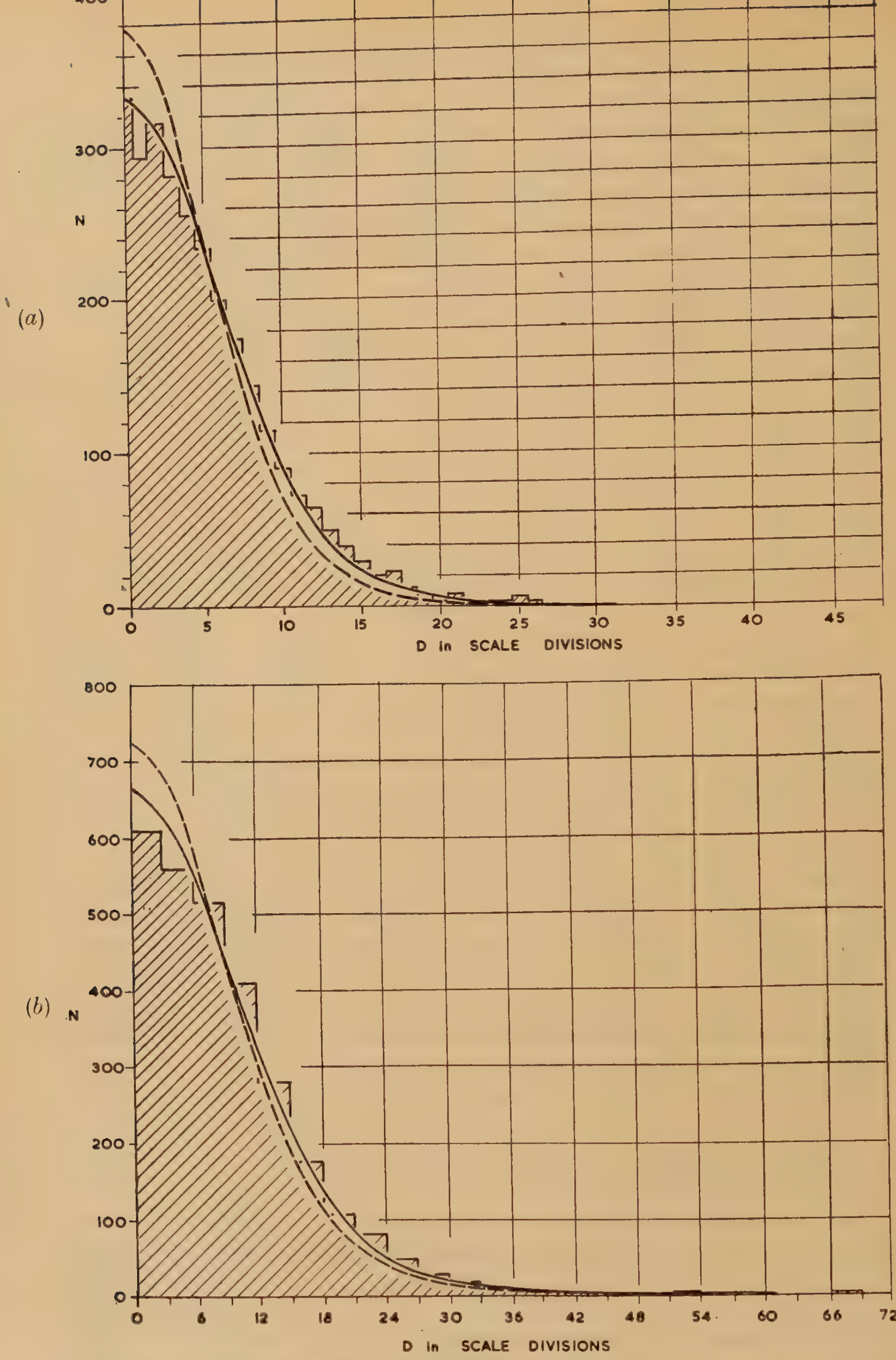

Comparison of the experimental distribution of the absolute values of second difference with the distribution functions of Molière's theory :

dotted lines : " normal approximations " considering only genuine scattering (Molière 1948).

full lines : distribution function of genuine + spurious scattering calculated in the manner shown in Appendix II.

(*a*) 105 MeV. positrons, 100 μ cells (1 scale division = 0·048°).

(*b*) 185 MeV. positrons, 200 μ cells (1 scale division = 0·024°).

The distribution of second differences D_j shown in fig. 5(*b*) for the 185 MeV. positrons (200 μ cells) may be compared with that of fig. 6 obtained after applying the procedure shown in Appendix III. This correction results in a cut-off of the " tail " of the distribution at a value corresponding to $4\bar{D}$ without altering the shape of the distribution to any appreciable extent.

Fig. 6.

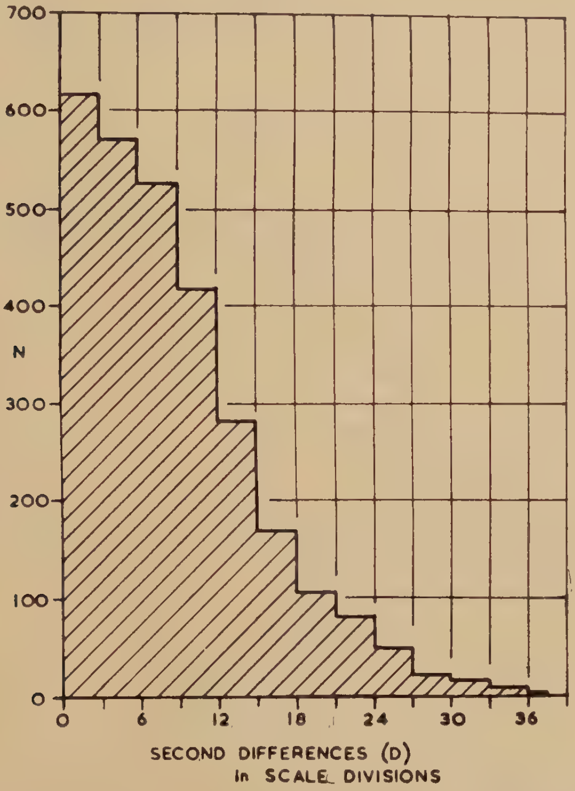

Histogram showing the distribution of the absolute values of second difference in 200 μ cells for 185 MeV. positrons after correcting "single" scattering in the manner shown in Appendix III.

§ 8. Elimination of " Noise ".

Because of the presence of various sources of uncertainty all the values of $\bar{D}$ listed in Tables II. and III. will be greater than the true value. The chief causes of this excess are (*a*) reading errors (ϵ_1), (*b*) errors (ϵ_2) due to the grains being distributed at random about the true path of the particle, (*c*) errors (ϵ_3) caused by random departures from linearity in the motion of the microscope stage. The resultant effect of such errors is usually termed " noise ". Recently, they have been most carefully studied by members of the Brussels group (Goldschmidt-Clermont 1950, Levi Setti 1950), as well as by members of this laboratory. Various methods of eliminating such errors or neutralizing their effect have been suggested.

An approximate method suggested by Fowler (unpublished) assumes that the various sources of error are statistically independent, and that the resultant quadratic mean noise level is given by

$$\epsilon=(\epsilon_1^2+\epsilon_2^2+\epsilon_3^2)^{1/2}. \quad . \quad . \quad . \quad . \quad . \quad . \quad . \quad . \quad . \quad (1)$$

Since we shall have to deal with mean absolute deviation, we denote by $\langle\epsilon\rangle$ the mean absolute value of the resultant noise level. Using equation (16) of (I.) and assuming that L remains independent of cell-size, we may show

$$\bar{D}^2=K_2^2s^3+\langle\epsilon\rangle^2. \quad . \quad . \quad . \quad . \quad . \quad . \quad . \quad . \quad . \quad (2)$$

This implies that the graph of $\bar{D}^2$ as a function of s^3 is a straight line having slope K_2^2. Taking the experimental figures $\bar{D}_1$ and $\bar{D}_2$ found for cell-sizes s_1 and s_2, we may eliminate $\langle\epsilon\rangle^2$ and obtain the value of $\langle\Phi\rangle_{100\mu}$ by substitution in the expression

$$\langle\Phi\rangle_{100\mu}=R\sqrt{\left(\frac{\bar{D}_2^2-\bar{D}_1^2}{s_2^3-s_1^3}\right)}. \quad . \quad . \quad . \quad . \quad . \quad . \quad . \quad (3)$$

R is the constant which reduces the readings of $\bar{D}$ expressed in scale-divisions to degrees/100 μ.

Setting $K_2=GL_{(s)}$ where G now depends only on the properties of the emulsion, and $L_{(s)}$ is given by I(8), we may correct this formula to take account of the variation of L with cell-size. This correction is particularly important for small cell-sizes where the rate of change is most rapid. We find the more accurate expression

$$\langle\Phi\rangle_{100\mu}=RL_{100\mu}\sqrt{\left(\frac{\bar{D}_2^2-\bar{D}_1^2}{L_2^2s_2^3-L_1^2s_1^3}\right)}. \quad . \quad . \quad . \quad . \quad . \quad . \quad (4)$$

There is, however, ample evidence that $\langle\epsilon\rangle$ does not remain constant but, on the contrary, that it tends to increase markedly with cell-size due to the increase of the stage noise component $\langle\epsilon_3\rangle$ (Camerini and Fowler unpublished, Levi-Setti 1950).

Its order of magnitude may be found by measuring in different cell-sizes the scattering of the tracks of relativistic particles, which are the primaries of large cosmic ray showers. The results of such measurements for our microscopes are incorporated in I, fig. 3. Great variations are found in the performances of individual instruments.

The presence of stage noise in the present experiments is shown by a departure of the plot $\bar{D}^2$ *vs* s^3 from the form predicted by theory. Since the scattering constant increases as the square root of the logarithm of the cell-size (I. (15)), this plot should appear slightly concave when viewed from above. Experimentally, however, it appears convex when so viewed, especially for cell-sizes less than 100 μ. This behaviour may be explained if we assume that the noise increases directly as the cell-size, in such manner that we must replace equation (2) by

$$\overline{D}^2 = K_2^2 s^3 + \eta_0^2 (1+Qs) \quad . \quad . \quad . \quad . \quad . \quad . \quad . \quad . \quad (5)$$

where η_0^2 represents the square of the mean absolute noise level due to ϵ_1 and ϵ_2, and Q is a pure number of the order of unity.

The assumption that stage noise varies linearly with s agrees with the experimental results of Levi Setti (1950) to which we have already referred.

Q varies widely from instrument to instrument, and also, unfortunately, with the position and the condition of the stage. For this reason it is desirable, as far as is practicable, to confine the measurements to the same region of the stage coordinates, and also to maintain the guides in a clean condition. The magnitude of the stage-noise should be checked at intervals by measurements on a long straight primary track.

Direct evidence for increase of stage-noise with cell-size will be given by noise elimination, on cell-sizes less than 100 μ using Fowler's formula, or its modified form (4). It will then be found that the highest value of $\langle \Phi \rangle_{100\mu}$ is obtained by elimination between the pair of smallest cells, because, as we have seen, the plot of $\overline{D}^2$ as a function of s^3 will be convex when viewed from above.

Taking account of the variation of stage-noise with cell-size, we may obtain from (5) the elimination formula

$$\langle \Phi \rangle_{100\mu} = RL \sqrt{\left(\frac{\overline{D}_2^2 (1+Qs_1) - \overline{D}_1^2 (1+Qs_2)}{L_2^2 s_2^3 (1+Qs_1) - L_1^2 s_1^3 (1+Qs_2)} \right)} . \quad . \quad . \quad (6)$$

By suitable choice of Q, noise elimination between the various pairs of cell-sizes may be made to yield the same value of $\langle \Phi \rangle_{100\mu}$. These points are illustrated in Table IV. which gives for 105 MeV. electrons, the values for $\langle \Phi \rangle_{100\mu}$ found by using the various methods of elimination.

TABLE IV.

Method	Cell-size (μ) 50–25	100–25	100–50	200–25	200–50	200–100
Fowler (3)	0·266	0·250	0·248	0·248	0·248	0·248
Fowler (4)	0·279	0·250	0·246	0·238	0·238	0·236
Present work Q=5	0·236	0·235	0·236	0·234	0·234	0·234

The adopted value of Q=5 was found to be consistent with the magnitude and variation with cell-size of the stage-noise found directly by using the track of a heavy primary particle of great energy (I., fig. 3).

From the results given in the third row of Table IV., we deduce values of the scattering constant *for* $100\,\mu$ *cells* based essentially on the experimental results for the following cell-sizes :—

$$50\ \mu = 24{\cdot}9 \pm 0{\cdot}4,$$

$$100\ \mu = 24{\cdot}9 \pm 0{\cdot}6,$$

$$200\ \mu = 24{\cdot}7 \pm 0{\cdot}7.$$

The uncertainties are standard deviations and are calculated from the theoretical sampling distribution of mean deviation (III., Eqn. 10). These results are to be compared with that predicted by Molière's theory for particles for which $\beta^2 \sim 1$, I(13), diminished by 10 per cent to take into account the truncation of the distribution caused by excluding all signals $\geqslant 4\overline{D}$, namely,

$$K_{\text{chord},\, \beta^2 \sim 1} = 23{\cdot}0 \text{ degrees} \times \text{MeV.}/(100\,\mu)^{1/2}.$$

The agreement would appear to be satisfactory, taking into consideration possible uncertainties in the value of the energy.

The influence of noise on the values of $\langle \Phi \rangle$ will be seen by comparing the second and third rows of Table IV. For $200\,\mu$ cells the difference of about 1·5 per cent justifies the neglect of noise in the comparison of theory with experiment described in I and illustrated in fig. 1 of that paper.

ACKNOWLEDGMENTS.

We are indebted to Professor C. F. Powell, F.R.S., for his continued interest and encouragement during the course of this work. Our best thanks are due to Professor Dale R. Corson, who has very kindly put at our disposal plates exposed to a beam of positrons in the Cornell Synchrotron, without which this investigation could not have been carried out. We also wish to thank Mrs. M. O'Ceallaigh and Miss R. Mitchell for their valuable assistance with the measurements.

APPENDIX I.

CORRELATION COEFFICIENTS.

In a recent paper Molière (Part IV., 1951) has shown that when the scattering parameter observed (Merkmal) is composed of two parts, genuine and spurious, the correlation coefficient of two successive parameters x_i and x_{i+1} (two successive second differences in the present case), is a quantity which depends upon the ratio of signal to noise *e. g.* the ratio of the mean absolute values (or standard deviations) of the genuine and spurious scattering.

By definition the correlation coefficient is

$$\frac{\overline{x_i x_{i+1}}}{\overline{x_i^2}} = \frac{\frac{1}{4} - \frac{2}{3}\mu}{1+\mu}, \quad . \quad . \quad . \quad . \quad . \quad . \quad . \quad . \quad . \quad (1)$$

where

$$\mu=\left(\frac{\text{noise}}{\text{signal}}\right)^2=\left(\frac{\bar{\Delta}_n}{\bar{\Delta}_s}\right)^2;\quad \Delta_{n,s}=\text{mean value of}\begin{cases}\text{noise}\\ \text{signal.}\end{cases}$$

One way of finding μ and then $\bar{\Delta}_n$ or $\bar{\Delta}_s$ (which is *not* the solution of the variational problem of maximum likelihood, but involves a much simpler calculation) consists in equating the right hand side of the relation (1) to the experimental quantity (2)

$$\frac{(1/(n-1))\Sigma\Delta_i\Delta_{i+1}}{(1/n)\Sigma\Delta_i^2}. \qquad (2)$$

Then

$$\bar{\Delta}_s=\sqrt{\left(\frac{2}{\pi}\right)}\sqrt{\left(\frac{1}{\frac{1}{4}+\frac{2}{3}}\right)}\sqrt{(\tfrac{2}{3}\overline{\Delta^2}-\overline{\Delta_i\Delta_{i+1}})}. \qquad (3)$$

$$\bar{\Delta}_n=\sqrt{\left(\frac{2}{\pi}\right)}\sqrt{\left(\frac{1}{\frac{1}{4}+\frac{2}{3}}\right)}\sqrt{(\tfrac{1}{4}\overline{\Delta^2}+\overline{\Delta_i\Delta_{i+1}})}. \qquad (4)$$

The variance of these two quantities is also calculated. A preliminary attempt to apply this method has been made using the tracks of 185 MeV. electrons.

Two hundred and sixty-six angles measured between successive chords (cell-size 200 μ) gave the following results expressed in divisions of the eyepiece scale :

$$\overline{\Delta_i^2}=1{\cdot}115,$$

$$\overline{\Delta_i\Delta_{i+1}}=+0{\cdot}0673.$$

Using formulae (3) and (4) this yields :

$$\bar{\Delta}_s=0{\cdot}736,$$

$$\bar{\Delta}_n=0{\cdot}383.$$

Transforming into degrees, we obtain :

$$|\bar{\alpha}|=0{\cdot}177\pm{\cdot}0054 \text{ in } 200\,\mu \text{ cells,}$$

$$|\bar{\alpha}|_{\text{noise}}=0{\cdot}092\pm{\cdot}0011.$$

The value of the scattering constant then obtained is 23·1 ± 1·1 in close agreement with the theoretical value after cut-off (24·05).

APPENDIX II.

The distribution function of the second differences measured in the presence of spurious scattering is derived from Molière's theory as follows :

We may write $$x=x_{\text{sp}}+x_{\text{gen}}, \qquad (1)$$

where x is the value of the quantity observed, x_{sp} the contribution due to spurious scattering and x_{gen} the contribution due to genuine scattering. We assume the normality of the distribution of x_{sp} and the statistical independence of x_{sp} of x_{gen}.

The exponent of the Fourier transform of the distribution function of x_{gen} is then

$$\frac{x_c^2\xi^2}{4}\log\left(\frac{\gamma^2x_a^2\xi^2}{4e}\right), \quad . \quad . \quad . \quad . \quad (2)\ \text{(Molière)}$$

whereas the corresponding quantity for the distribution function of x_{sp} is

$$-\frac{(x_0^{\text{sp}})^2}{4}\,\xi^2, \quad . \quad . \quad . \quad . \quad . \quad . \quad . \quad . \quad . \quad . \quad (3)$$

(where $x_0^{\text{sp}}=\sqrt{2}$ standard deviation of x_{sp}).

The sum of (2) and (3) gives the exponent of the Fourier transform of the distribution function of x.

Introducing

$$\left(\frac{x_0^{\text{sp}}}{x_c}\right)^2=\mu' \quad . \quad . \quad . \quad . \quad . \quad . \quad . \quad . \quad . \quad . \quad . \quad (4)$$

and

$$\Omega^*_{b,x}=\left(\frac{x_c^2}{x_a^2}\right)e^{\mu'} \quad . \quad . \quad . \quad . \quad . \quad . \quad . \quad . \quad . \quad (5)$$

together with

$$\mathrm{B}^*_x-\log\mathrm{B}^*_x=\log\left(e\Omega^*/\gamma^2\right) \quad . \quad . \quad . \quad . \quad . \quad . \quad . \quad (6)$$

as well as the new variable $\eta=x_c\sqrt{(\mathrm{B}^*)}\xi$ in place of ξ, the d.f. of x takes the form

$$f(|x|)\,d|x|=\frac{d|x|}{x_c\sqrt{(\mathrm{B}^*)}}\cdot\frac{2}{\pi}\int d\eta\cos\left(\frac{|x|}{x_c\sqrt{(\mathrm{B}^*)}}\eta\right)\exp\left(-\frac{\eta^2}{4}+\frac{\eta^2}{4\mathrm{B}^*_x}\log\frac{\eta^2}{4}\right) \quad . \quad . \quad . \quad (8)$$

which, after development in powers of $1/\mathrm{B}^*$ yields the well known formula

$$f(\phi)d\phi=d\phi\left[\frac{2}{\sqrt{\pi}}\,e^{-\varphi^2}+\frac{1}{\mathrm{B}^*_x}f^{(1)}(\phi)+\frac{1}{\mathrm{B}^{*2}_x}f^{(2)}(\phi)+\ .\ .\ .\right], \quad . \quad . \quad (9)$$

where now

$$\phi=|x|/x_c\sqrt{(\mathrm{B}^*_x)}.$$

When the values of B and Ω for the case of pure scattering are known, the new values B* and Ω^* are obtained from the relation (6) together with

$$\Omega^*=\Omega e^{\mathrm{B}\mu}, \quad . \quad . \quad . \quad . \quad . \quad . \quad . \quad . \quad . \quad . \quad (10)$$

where $\mu=\frac{\mu'}{\mathrm{B}}=\left(\frac{\text{noise}}{\text{signal}}\right)^2.$

APPENDIX III.

CORRECTION OF "SINGLE" SCATTERING.

The following has been found a convenient procedure for correcting a group of second differences obtained by the method of overlapping cells in a region where the particle has suffered a sharp deflection. It consists in subtracting from each second difference involved a certain quantity which represents the contribution to it due to the "single scattering".

Let

$$\ldots y_{p-4},\ y_{p-3},\ y_{p-2},\ y_{p-1},\ y_p,\ y_{p+1},\ y_{p+2},\ y_{p+3},\ y_{p+4},\ \ldots\ y_j\ \ldots$$

be the measured coordinates of points of the track, namely, their distance from an arbitrary line of reference. The intervals between two points are s_1/λ where λ=coefficient of overlap, s_1=cell-size in microns.

Suppose that the "single scattering" of Φ radians occurs between the points of which the coordinates are y_{p-1} and y_p at a distance x from the latter. The second difference D_j in cell-size s_1 will be

$$D_j=y_j-2y_{j-\lambda}+y_{j-2\lambda}. \qquad (1)$$

Let

$$D_j=a_j+s_j, \qquad (2)$$

where S_j=contribution due to the single scattering,

a_j=contribution due to the multiple scattering.

Simple geometrical considerations show that a "block" of 2λ such second differences are influenced by the single scattering, corresponding to values of j ranging from $j=p$ to $j=p-1+2\lambda$ and we find readily

$$\left.\begin{aligned}
s_p&=x\Phi,\\
s_{p+1}&=\left(\frac{s_1}{\lambda}+x\right)\Phi,\\
s_{p+2}&=\left(2\frac{s_1}{\lambda}+x\right)\Phi,\\
s_{p+3}&=\left(3\frac{s_1}{\lambda}+x\right)\Phi,\\
&\vdots\\
s_{p-1}&=\left(\frac{\lambda-1}{\lambda}s_1+x\right)\Phi,\\
s_{p+\lambda}&=(s_1-x)\Phi,\\
s_{p+1+\lambda}&=\left(\frac{\lambda-1}{\lambda}s_1-x\right)\Phi,\\
&\vdots\\
s_{p-1+2\lambda}&=\left(\frac{s_1}{\lambda}-x\right)\Phi.
\end{aligned}\right\} \qquad (4)$$

A knowledge of Φ and x, which can often be measured, allows us to correct the second differences, by subtracting from them the quantity S_j

$$a_j=D_j^*=D_j-S_j. \qquad (5)$$

Approximation.

It can be seen that the quantities $x\Phi$ and $(s_1/\lambda-x)\Phi$ may be obtained approximately in the following manner :—

Let us write

$$\left.\begin{aligned}
\delta_1&=y_p-2y_{p-1}+y_{p-2},\\
\delta_2&=y_{p+1}-2y_p+y_{p-1}.
\end{aligned}\right\} \qquad (6)$$

These quantities are the pair of second differences in the prime cell-size of length s_1/λ microns which have been influenced by the single scattering. We have thus

$$\left.\begin{aligned}\delta_1&=a_1'+s_1',\\ \delta_2&=a_2'+s_2',\end{aligned}\right\} \quad . \; . \; . \; . \; . \; . \; . \; . \quad (7)$$

with

$$s_1'=x\Phi, \quad s_2'=\left(\frac{s_1}{\lambda}-x\right)\Phi.$$

The quanties a_1' and a_2' are $\lambda^{3/2}$ times smaller than $a_1 \ldots a_2 \ldots$ in (2). In many cases these contributions due to multiple scattering in the small cell-size may be neglected. We then have

$$\delta_1=x\Phi \text{ and } \delta_2=\left(\frac{s_1}{\lambda}-x\right)\Phi. \quad . \; . \; . \; . \; . \; . \quad (8)$$

Thus

$$\left.\begin{aligned}s_p&=\delta_1,\\ s_{p+1}&=2\delta_1+\delta_2,\\ s_{p+2}&=3\delta_1+2\delta_2,\\ \vdots\quad&\quad\vdots\quad\quad\vdots\\ s_{p+1-\lambda}&=\lambda\delta_1+(\lambda-1)\delta_2,\\ s_{p+\lambda}&=(\lambda-1)\delta_1+\lambda\delta_2,\\ s_{p+1+\lambda}&=(\lambda-2)\delta_1+(\lambda-1)\delta_2,\\ \vdots\quad&\quad\vdots\\ s_{p-1+2\lambda}&=\delta_2.\end{aligned}\right\} \quad . \; . \; . \quad (9)$$

The following table shows an example of the application of this correction on the track of a 185 MeV. electron, for $\lambda=4$ and $s_1=200\,\mu$.

j	y_j	y_j-y_{j-1}	$y_j-2y_{j-1}+y_{j-2}$	y_j-y_{j-4}	$D_j=$ $y_j-2y_{j-4}+y_{j-8}$	$S_j=$ Correction	D_j Corrected 2nd dif.
$p-8$	27·4	−0·3	—	—	(+0·6)		
$p-7$	27·1	−0·3	0·0	—	(+0·6)		
$p-6$	26·3	−0·8	−0·5	—	(−0·5)		
$p-5$	25·7	−0·6	+0·2	—	(−0·8)		
$p-4$	25·3	−0·4	+0·2	−2·1	(−0·8)		
$p-3$	24·6	−0·7	−0·3	−2·5	(+1·3)		
$p-2$	24·7	+0·1	+0·8	−1·6	(+0·2)		
$p-1$	23·9	−0·8	−0·9	−1·8	(+0·2)		
p	25·0	+1·1	+1·9 $=\delta_1$	−0·3	+1·8*	−1·9	−0·1
$p+1$	26·2	+1·2	+0·1 $=\delta_2$	+1·6	+4·1*	−3·9	+0·2
$p+2$	27·4	+1·2	0·0	+2·7	+4·3*	−5·9	−1·6
$p+3$	28·7	+1·3	+0·1	+4·8	+6·6*	−7·9	−1·3
$p+4$	29·9	+1·2	−0·1	+4·9	+5·2*	−6·1	−0·9
$p+5$	31·7	+1·8	+0·6	+5·5	+3·9*	−4·1	−0·2
$p+6$	33·3	+1·6	−0·2	+5·9	+3·2*	−2·1	+1·1
$p+7$	34·8	+1·5	−0·1	+6·1	+1·3*	−0·1	+1·2
$p+8$	36·2	+1·4	−0·1	+6·3	+1·4		

The values of D_j in brackets in the sixth column of the Table have been computed using values of y_j corresponding to $j<p-8$ (which are not given in the first column). These values of D_j are listed here in order to show the magnitude of the value of D_j in the region prior to the " single " scattering.

Here the " single " scattering has a visible influence on the sign of the first differences between successive y's. They are all positive for $j<p$ and become positive afterwards. Thus the point where the deviation occurs can be detected at once.

Also, it can be seen that $\delta_1=y_p-2y_{p-1}+y_{p-2}$ is equal to 1·9 div. of eyepiece scale. The eight second differences influenced by the single scattering are marked with crosses. Their absolute values average 3·8 div. All the second differences of the track (5500 μ long) including these, average 1·09 div.

After the entire block of second differences affected has been removed, this average becomes $\overline{D}=\cdot 853$ div.

The average of the corrected block is ·82 div., and the average of the track, after including the corrected values, becomes $\overline{D}=\cdot 851$ div.

REFERENCES.

BARKER, 1948, *J. Sci. Instrum.*, **25,** 65.
CAMERINI and FOWLER, 1951, (private communication).
FOWLER, 1950, *Phil. Mag.*, **41,** 169 ; 1951 (private communication).
GOLDSCHMIDT–CLERMONT, 1950, *Nuovo Cimento*, **7,** 331.
LEVI SETTI, 1950, Note No. 22, *Bull. Du. Cen. de Phys. Nuc. de L'Univ. Libre de Bruxelles.*
MOLIÈRE, 1947, *Z. f. Naturforschung.*, **2 A,** 133 ; 1948, *Ibid.*, **3 A,** 78 ; 1951, unpublished.
O'CEALLAIGH and MACCARTHAIGH, 1944, *Proc. Roy. Irish Acad.* A, **50,** 13.
O'CEALLAIGH, 1950, *Proc. Roy. Irish Acad.* A, **53,** 133.

XCV. CORRESPONDENCE.

The reaction ^{10}B (γ, d) $2\ ^4He$.

By M. J. Brinkworth and E. W. Titterton,
A.E.R.E., Harwell, Didcot, Berks.*

[Received May 23, 1951.]

The reaction

$$^{10}B + h\nu \rightarrow 2\ ^4He + ^2H - 5{\cdot}89\ \text{MeV}. \quad . \quad . \quad . \quad . \quad . \quad (1)$$

first reported by Goward, Titterton and Wilkins (1950) has been investigated with the γ-rays from the ^7Li (p, γ) 440 KeV. resonance. Ilford E_1 emulsions, some of which were loaded with boron of normal isotopic constitution and others with separated ^{10}B, were used.

The boron loading has an intensifying action at development, and as a result it is difficult to distinguish the deuteron from the α-particles by inspection, and the tracks are too short for scattering measurements. A momentum balance is carried out on each event to distinguish the ^{10}B from the ^{11}B and ^{12}C stars, and to identify the deuteron in the ^{10}B stars.

65 events due to reaction (1) have been observed, and a histogram of the γ-ray energies is given in fig. 1. The ^7Li (p, γ) radiations consist of a narrow peak at 17·6 MeV., and a second peak, about 2 MeV. wide of half the intensity of the first, at 14·8 MeV. (Walker and McDaniel 1948). Only three events fall in the 17·6 MeV. peak, indicating a much smaller value of the cross-section at this energy than at 14·8 MeV. The events

Fig. 1.

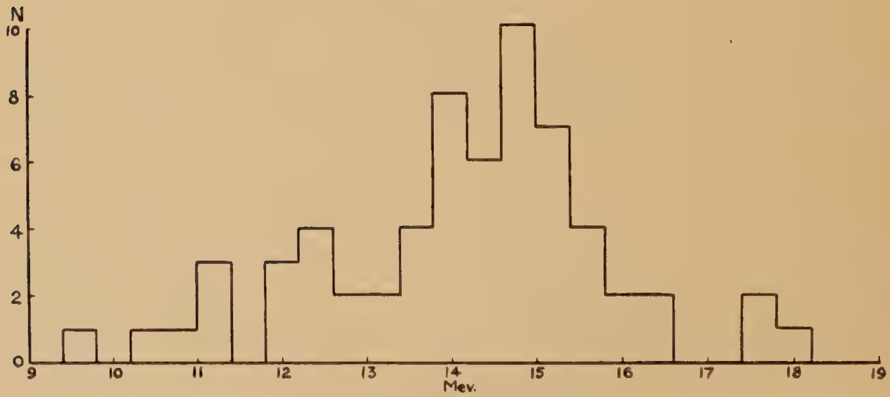

γ-ray energy distribution.

---

* Communicated by the Authors.

with $E_\gamma < 12$ MeV. are due to γ-rays which are either in the tail of the 14·8 MeV. peak or have suffered Compton scattering in the wall of the target chamber. A quantitative estimate has been made of the relative γ-ray intensity to be expected at energies less than 12 MeV. due to these causes (Brinkworth 1951) and the number of ^{10}B events obtained is approximately twice that which would be given by a uniform cross-section. This suggests that the ^{10}B (γ, d) cross-section passes through a maximum at 13 ± 2 MeV.

By normalization against the ^{12}C stars, using the cross-section measured by Wäffler and Younis (1949), the ^{10}B (γ, d) cross-section at 14·8 MeV. is estimated to be $(2{\cdot}9 \pm 1{\cdot}4) \times 10^{-28}$ cm.².

On the assumption that a three-body reaction is not occurring, the course of the ^{10}B photodisintegration is either $^{10}B\ (\gamma, d)\ ^8Be^*$; $^8Be^* \rightarrow 2\ ^4He$ or $^{10}B\ (\gamma, \alpha)\ ^6Li^*$; $^6Li^* \rightarrow {}^4He + {}^2H$.

If ^8Be is the intermediate nucleus, the energy release Q when it disintegrates is given by

$$Q = E_1/2 + E_2/2 - (E_1\, E_2)^{\frac{1}{2}} \cos \theta, \quad . \quad . \quad . \quad . \quad . \quad (2)$$

where E_1 and E_2 are the energies of the α-particles, and θ is the angle between them. Q is also given by the formula

$$Q = E_1 + E_2 - E_D/4 - p_\gamma^2/8 + (p_\gamma/4)\ (2\ E_D)^{\frac{1}{2}} \cos \phi, \quad . \quad . \quad . \quad (3)$$

Fig. 2.

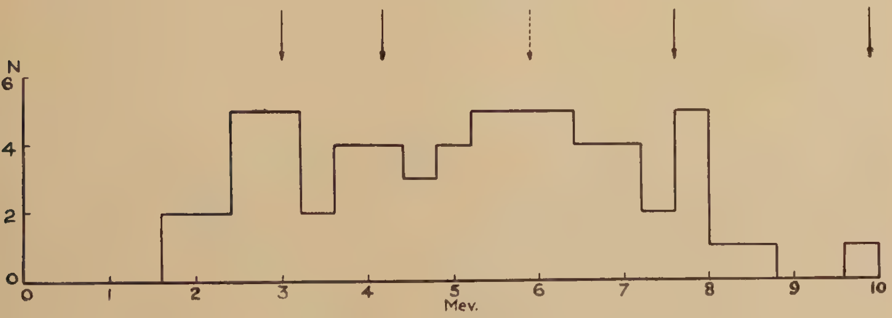

Q value histogram.

where E_D is the deuteron energy, p_γ the momentum of the γ-ray, and ϕ is the angle between the direction of emission of the deuteron and the incident γ-ray. The terms involving p_γ may be neglected with a maximum error in most of the present calculations of 6 per cent, and 9 per cent in the worst case.

The Q values calculated from the two formulæ are in approximate agreement when the tracks have been correctly identified. About 10 events which had been provisionally identified as ^{10}B (γ, d) 2α failed to give concordant Q values, indicating that these events were really ^{10}B (γ, np) 2α, a reaction which will be discussed in a later communication.

Fig. 2 shows the histogram of the Q values. It appears that if the reaction does proceed through ^{8}Be then the known excited levels of this nucleus at 2·9, 4·05, 7·5 and 9·8 MeV. may all be involved (Hornyak, Lauritsen, Morrison and Fowler 1950), the corresponding Q values being indicated by arrows in fig. 2. The resolution of the present experiment is not sufficient to establish whether the level at 4·9 MeV. decays by α-particle emission. Bennett *et al.* have reported a γ-ray from this level (Bennett, Bonner, Richards and Watt 1947).

The Q value histogram in fig. 2 suggests that there may be a broad level in ^{8}Be at about 5·8 MeV., as indicated by the broken arrow. Some indication of a level in this position has been found from the ^{11}B (γ, *t*) 2α reaction (Titterton and Calcraft 1951).

A plot of the deuteron energies cannot be used to give the ^{8}Be level scheme in this case owing to the width of the 14·8 MeV. γ-ray peak, the presence of scattered γ-rays, and the variation of cross-section with energy.

The alternative mode of disintegration to be considered is through ^{6}Li. Experiments with lithium-loaded plates have shown that the reaction $^6\mathrm{Li}+h\nu\rightarrow{}^4\mathrm{He}+{}^2\mathrm{H}$ does not occur (Titterton 1950) but this does not necessarily preclude the ^{10}B disintegration from passing through an excited state of ^{6}Li. Use of the Q formula to determine these levels is unsatisfactory, because it is not known which of the two α-particles should be taken as resulting from the break-up of the $^6\mathrm{Li}^*$.

Fig. 3.

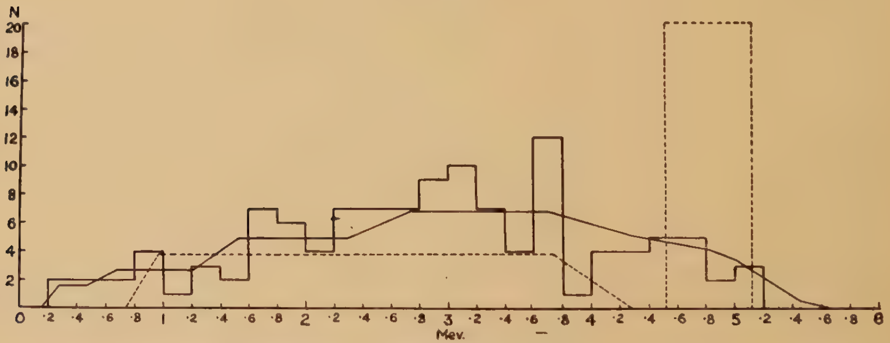

α-particle energy distribution (excluding events due to 17·6 MeV. γ-ray).

A histogram of all the α-particle energies, excluding events due to the 17·6 MeV. γ-ray, is given in fig. 3. If the reaction passes through the 2·4 MeV. level of ^{6}Li (Hornyak *et al.* 1950), half the α-particle energies should fall in a narrow peak, and the other half yield a broad, approximately uniform distribution, as shown by the broken line in fig. 3, level width and γ-ray width having been neglected. It is evident that the reaction cannot proceed exclusively through the 2·4 MeV. level, but it is possible that it proceeds partly through this and other undetermined levels of the nucleus. The α-particle energy distribution is of necessity consistent with the disintegration of B^{10} by way of Be^8, if it is assumed that the relative probabilities of the occurrence of the different Be^8 levels is given by the Q histogram in fig. 2. The full line in fig. 3 shows the approximate distribution to be expected on this assumption, the γ-ray and level widths again being neglected.

The experiments suggest that the probable mode of disintegration is through ^{8}Be, but more events are awaited to confirm this, and to provide more accurate information on the energy levels involved.

Members of the nuclear emulsions group at A. E. R. E. are thanked for microscope work.

REFERENCES.

BENNETT, BONNER, RICHARDS, and WATT, 1947, *Phys. Rev.*, **71,** 11.
BRINKWORTH, 1951, *A.E.R.E.* G/M 81.
GOWARD, TITTERTON and WILKINS, 1950, *Proc. Phys. Soc.* A, **63,** 172.
HORNYAK, LAURITSEN, MORRISON and FOWLER, 1950 *Rev. Mod. Phys.*, **22,** 291.
TITTERTON, 1950, *Proc. Phys. Soc.* A., **63,** 915.
TITTERTON and CALCRAFT, 1951, *Phil. Mag.* [7], **42,** 666.
WÄFFLER and YOUNIS, 1949, *Helv. Phys. Acta.* **22,** 614.
WALKER and MCDANIEL, 1948. *Phys. Rev.* **74,** 315.

The Disintegration of Light Nuclei by Cosmic Rays.

By P. E. HODGSON,
Imperial College of Science and Technology, London*.

[Received June 5, 1951.]

USING sandwich emulsion composed of alternate layers of C2 emulsion and pure gelatin, Harding (1949, 1951) has analysed the cosmic ray induced disintegrations of the carbon, nitrogen and oxygen nuclei constituting the gelatin. He found that the average charge emitted from the disintegrations in the gelatin was $4{\cdot}7\,e$. The average charge on the elements (excluding hydrogen) which constitute the gelatin at normal humidity is $6{\cdot}63\,e$. In order to obtain the average expected charge per star, a small correction of $\sim 0{\cdot}2$ must be added to this to allow for the proton initiated stars. A charge of about $2{\cdot}1\,e$ therefore remained to be accounted for.

As Harding pointed out, this loss of charge may be due to three causes : (1) The ejection of fast singly charged particles which are not recorded in C2 emulsion. (2) The ejection of a group of charged particles of short range, the majority of which remain in the gelatin layer. (3) The ejection of particles of charge greater than two which have been mistaken for alpha-particles.

---

* Communicated by Sir George Thomson, F.R.S.

Perkins (1950) has since shown that the number of visible particles of charge greater than two is very small for stars of the size found in gelatin layers.

In order to resolve the remaining ambiguity between (1) and (2), sandwich emulsions composed of alternate layers of G5 emulsion and pure gelatin have been exposed to cosmic rays on the Jungfraujoch.

From the thirty-six disintegrations of gelatin nuclei examined in this type of emulsion, there were emitted 140 particles making black or grey tracks and six at or near minimum ionization. Allowing for those particles which were missed because they remained wholly in the gelatin layer or emerged from it too far from the star centre to be observed, these figures become 158 ± 9 and about ten respectively.

In his analysis of gelatin stars in C2 sandwich plates, Harding found 1·50 alpha particles per star, after correcting for loss. This number of the black tracks found in G5 emulsion must therefore be due to alpha particles. Camerini *et al.* (1950) have shown that 17 per cent of shower particles are protons, and so this fraction of the minimum ionization tracks was included in the charge per star. The emitted mesons were assumed to be as often positively as negatively charged and were omitted. Owing to the small number of minimum ionization tracks, any error in estimation of the charge emitted in this way will not critically effect the final result.

The corrected value of the average charge per star emitted as singly or doubly charged particles is therefore $5{\cdot}96 \pm 0{\cdot}25\,e$.

An average charge per star of $0{\cdot}87 \pm 0{\cdot}25\,e$ is therefore emitted as short range particles which mostly remain in the gelatin layer and escape detection. On the average, emitted particles have an energy such that, if singly or doubly charged, they would have sufficient range to be observed. These short range particles must therefore have a charge greater than two. Assuming they have an average charge of $4\,e$, the number of such fragments becomes $0{\cdot}22 \pm 0{\cdot}006$ per star, or 7·9 in the group of stars examined. One such particle was observed, which is of the correct order of magnitude in view of the unfavourable conditions of observation.

Bradt and Peters (1950) have used Harding's result to calculate a value of 0·7 for $p_{\mathrm{H}}(\mathrm{B})$, the probability that a stable lithium, beryllium or boron nucleus will be produced when a relativistic carbon, nitrogen or oxygen nucleus collides with an interstellar hydrogen nucleus, which is the same physical event as that examined here, but with target and projectile interchanged. The present work shows that this value should be modified to $0{\cdot}22 \pm 0{\cdot}06$, which is close to the 0·23 actually used by Bradt and Peters in their calculations.

Since the stars analysed are mainly produced by neutrons of energies of the order of hundreds of MeV., whereas $p_{\mathrm{H}}(\mathrm{B})$ refers to relativistic collisions, this method depends on the assumption that $p_{\mathrm{H}}(\mathrm{B})$ is the same for the two types of disintegration. This uncertainty could be avoided if only those stars initiated in gelatin by a relativistic proton were analysed. Unfortunately, however, such stars constitute only a small fraction of all the stars, and in order to find a sufficient number for analysis a prohibitively large plate area would have to be scanned.

Small styles are more likely to be missed during examination of the plates than large ones. Since these have the heavier recoils, this effect will reduce the value found for $p_{\mathrm{H}}(b)$, which is consequently only a lower limit.

I should like to express my gratitude to Professor Sir George Thomson and Dr. J. B. Harding for valuable discussions, to Mr. A. J. Herz for developing the plates and to Mr. L. Mandel for assisting with their exposure.

REFERENCES.

BRADT, H. L., and PETERS, B., 1950, *Phys. Rev.*, **80**, 943.
CAMERINI, U., FOWLER, P. H., LOCK, W. O., and MUIRHEAD, H., 1950, *Phil. Mag.*, **41**, 413.
HARDING, J. B., 1949, *Nature, Lond.*, **163**, 440 ; 1951, *Phil. Mag.*, **42**, 63.
PERKINS, D. H., 1950, *Proc. Roy. Soc.*, **203**, 399.

ERRATUM

A High Precision Pulse Height Analyser of Moderately High Speed.

By G. W. HUTCHINSON, M.A., and G. G. SCARROTT (*Phil. Mag.*, **42**, 792).

The appendix of this paper was altered in proof to show the latest model of the analyser. By a printer's oversight the paper appeared with the altered diagrams but with the unaltered script of the appendix, which is no longer appropriate.

The circuit details are shown in the following diagrams. Resistances are given in kilo-ohms except where otherwise stated. The capacities of all condensers lie between 5 $\mu\mu$F. and 1 μF. and are stated in either $\mu\mu$F. or μF. since no ambiguity can arise. To avoid confusing the diagrams, many decoupling condensers have been omitted from circuit points which carry only D.C. reference potentials.

The following valves are used except where otherwise stated :—

Single diodes	EA50
Double diodes	EB91
Double triodes (cathodes connected)	ECC91
Double triodes (separate cathodes)	12 AT 7
Pentodes	EF91
Selenium rectifiers	M1

The terminal links in the resistance networks of the bias and calibration pulse circuits are provided for the insertion of an external milliammeter.

The four-position switches of figs. 2 and 3 are ganged.

The couplings to the crystals of the supersonic delay line are through matching transformers.

XCVI. *Notices of New Books and Periodicals received.*

Theory of the Interior Ballistics of Guns. By J. Corner. [Pp. 443.] (New York: John Wiley and Sons; London: Chapman and Hall, 1950.) Price 64*s*.

The theoretical study of the motion of a shot in a gun involves at least three distinct, though interrelated, aspects: (i.) the manner of burning of the propellant and its dependence on the surroundings; (ii.) the physical chemistry of the propellent gases; (iii.) the dynamics of the products of burning, the shot, and the gun. The author, who is in a Ministry of Supply establishment, specialized in interior ballistics during and after the war, and has contributed largely to recent research. He has written a clear and carefully ordered account in which the three aspects are thoroughly treated.

Interior ballistics is nowadays a distinctly applied science. The improvement of experimental techniques has shown the great complexity of the subject. The elegant theories constructed by eminent mathematicians of the past have to be augmented by numerous semi-empirical corrections. Much of the book deals with the minutiæ of these corrections, which are of concern only to the specialist. However, interior ballistics also raises problems of wider interest, for example in the hydrodynamics of the gases in the chamber of the gun before and after shot-ejection, and in the thermochemistry of propellants. The author has presented a balanced picture of his subject, both close-up and in perspective.

R. H.

Selected Topics in X-ray Crystallography, edited by J. Bouman. (Amsterdam: North Holland Publishing Company.)

This is the third volume of the series of Monographs on Theoretical and Applied Physics edited by Professors de Boer and Brinkman and Dr. Casimir. The topics dealt with comprise General Methods for Structure Analysis, Distortions in Crystals, Crystal Growth, Quantitative Determinations, and special applications of X-ray methods to the study of photographic emulsions, the amorphous state, natural rubber and some problems in the biological field. The topics discussed are brought well up to date and adequately documented, the articles provide excellent summaries of present practice and it will be seen that the scope of the articles includes features that are of interest to most laboratories dealing with pure or applied crystallographic work. The book can confidently be recommended as likely to prove a valuable addition to the more general treatises to be found in the library of any such laboratory, and will appeal particularly to workers who are commencing research work on any of the applied problems discussed.

S. H. P.

Superfluids—Macroscopic Theory of Superconductivity, Vol. I. [Pp. 161.] By Fritz London. (Chapman and Hall.) Price 40*s*.

This volume consists of a careful survey of the macroscopic electrodynamics of superconductors and its consequences. It is divided into five sections. The first deals with the thermodynamical correlations between the variables. The second is concerned with the electrodynamics of the pure superconducting state, and is based on the equations first introduced by the Londons in 1935. A section on the intermediate state is followed by one on the various effects due to surface energies. In the final section Dr. London attempts to isolate the microscopical problem, and concludes that to explain superconductivity it might suffice to prove the existence of a long range order in the momentum.

It might have been helpful to include in such a survey a discussion of the two-fluid thermodynamical model of superconductors suggested by Gorter and Casimir in *Zeit. f. Tech. Phys.*, **15,** 539, 1934. This correlates such data as the specific heat law, the parabolic relation between critical field and temperature, and the temperature dependence of the penetration depth. It would have been of special interest to compare this model of a superconductor with the somewhat similar two-fluid models of Helium II which will presumably play a considerable part in volume II. of Dr. London's work.

This is, however, but a small criticism of a book which is generally excellent alike in choice of material and mode of presentation. R.B.D.

The Identification of Molecular Spectra. By R. W. B. PEARSE and A. C. TAYLOR. Second Revised Edition. (Chapman and Hall, London, 1950.) 50*s*. net.

THIS book which has become a quite indispensable work of reference in all spectroscopic laboratories has been thoroughly revised and brought up-to-date in this new edition. The valuable table of persistent band heads which allows the emitters responsible for many diffuse " lines " to be identified has been considerably extended. This is of interest to those engaged in both analytical and astrophysical work. The identifications can usually be confirmed by reference to the more detailed data on the band systems and re-examination of the spectra. In addition to such analytical applications, the volume provides (for research workers) a most useful source-book of references to molecular spectra, particularly to spectra which have not yet been analysed in detail and which are therefore often not recorded in the standard works on the subject. This feature of the book has been fully appreciated by the authors who have included many new references in this edition.

Chemical Thermodynamics. By F. D. ROSSINI. (Chapman and Hall, London.) [Pp. 48.] Price 48s

IN this book, the subject of thermodynamics is developed along the general lines of Lewis and Randall's *Thermodynamics and the Free Energy of Chemical Substances* which has played such an important part in the training of physical chemists in the United States of America. Apart from a few minor modifications, their nomenclature is followed.

Professor Rossini has, however, given a much broader treatment of modern chemical thermodynamics and has introduced the methods of statistical mechanics whenever appropriate. In a number of modern textbooks, the fundamentals of thermodynamics are developed by elegant mathematical methods with little or no reference to practical problems, and after reading such books students are often left with an uncertain grasp of the subject. As might be anticipated from his extensive experience in this field and from his previous publications, Professor Rossini blends theoretical deduction and practical application in a thoroughly satisfactory way into an outstandingly clear presentation of the subject. The chapters are followed by well selected references for further reading and by a sound collection of numerical problems. For practical thermodynamics calculation little reference need be made to outside sources, fundamental constants and conversion factors being tabulated in an appendix.

Advanced Dynamics, Vols. I. and II. By E. HOWARD SMART. (Macmillan and Co., Ltd., 1951.) Each volume 40*s*.

THESE two volumes by the late Professor Smart cover the syllabus of a university degree course. Volume I. is primarily concerned with the dynamics of the particle ; for example orbital motion under a central force, motion in a resisting medium, and constrained motion in two or three dimensions. Volume II. proceeds, after an unusually full discussion of plane kinematics, to the dynamics of a solid body and carries the fundamental theory as far as the Hamilton–Jacobi equations and Jacobi's complete integral.

The main feature of the book is the exceptional large number of worked examples, illustrating every type of examination problem. Many points which are glossed over in most textbooks, and which frequently trouble students, are carefully explained ; an instance is the dynamics of a system with varying mass. The author has chosen not to follow the modern tendency to use vector notation indiscriminately ; indeed, he has gone to the opposite extreme and used Cartesian coordinates throughout.

In many ways the presentation of Newton's laws is quite admirable, and certainly much better than in most books, particularly in regard to the concept of an unaccelerated frame of reference. On the other hand, a discussion of mass is scarcely entered upon, while the real significance of D'Alembert's principle is not mentioned. Apart from this, the development of the theoretical basis could hardly be bettered for clarity and thoroughness. R.H.

Notice.—*Electromagnetic Theory*. By OLIVER HEAVISIDE. The English re-issues of this book is to be published by E. & F. N. Spon, Ltd., London. Price 63*s*.

NOTICE TO CONTRIBUTORS

The Symbols Committee of the Royal Society, including representatives of the Chemical, Faraday and Physical Societies, has recently issued a report giving a full list of symbols, signs and abbreviations recommended for British scientific publications.

In the interests of uniformity the Editors of *The Philosophical Magazine* hope that authors will as far as possible conform to these recommendations in the preparation of papers. Copies of the report may be obtained from the Royal Society, Burlington House, W.1, price 9*d*. per copy.

[*The Editors do not hold themselves responsible for the views expressed by their correspondents.*]